Received: Added at production | Revised: Added at production | Accepted: Added at production

DOI: xxx/xxxx

ARTICLE TYPE

Adaptive Digital PID Control of First-Order-Lag-Plus-Dead-Time Dynamics with Sensor, Actuator, and Feedback Nonlinearities

Mohammadreza Kamaldar[1] | Syed Aseem Ul Islam[1] | Sneha Sanjeevini[1] | Ankit Goel[1] | Jesse B. Hoagg[2] | Dennis S. Bernstein*[1]

[1]Department of Aerospace Engineering, University of Michigan, MI, USA.
[2]Department of Mechanical Engineering, University of Kentucky, KY, USA.

Correspondence
*Dennis S. Bernstein,
Department of Aerospace Engineering,
1320 Beal Avenue,
University of Michigan,
Ann Arbor, MI, 48109 USA.
Email: dsbaero@umich.edu

Summary

Proportional-integral-derivative (PID) control is one of the most widely used feedback control strategies because of its ability to follow step commands and reject constant disturbances with zero asymptotic error, as well as the ease of tuning. This paper presents an adaptive digital PID controller for sampled-data systems with sensor, actuator, and feedback nonlinearities. The linear continuous-time dynamics are assumed to be first-order lag with dead time (i.e., delay). The plant gain is assumed to have known sign but unknown magnitude, and the dead time is assumed to be unknown. The sensor and actuator nonlinearities are assumed to be monotonic, with known trend but are otherwise unknown, and the feedback nonlinearity is assumed to be monotonic, but is otherwise unknown. A numerical investigation is presented to support a simulation-based conjecture, which concerns closed-loop stability and performance. Numerical examples illustrate the effect of initialization on the rate of adaptation and investigate failure modes in cases where the assumptions of the simulation-based conjecture are violated.

KEYWORDS:
autotuning, integral control, nonlinear system, time delay process, process control

1 | INTRODUCTION

The enduring popularity of proportional-integral-derivative (PID) control as the most effective and widely used feedback control strategy is due to at least three reasons. First, one of the most common control objectives is to have the measured output of a process attain a setpoint while rejecting a constant disturbance. The internal model principle[1] implies that an integrator is needed to achieve this goal. Next, a PID controller—at least in its simplest form—entails only three numbers, each of which has a distinct effect on the closed-loop response, thus facilitating tuning. Finally, extensive practical experience with PID controllers helps to ensure that these controllers can be reliably implemented and maintained in applications ranging from a few PID loops to dozens or hundreds of interacting loops operating under changing and uncertain conditions.

The simplicity of PID control, however, is challenged by a multitude of real-world effects. As in all feedback applications, a PID controller must ensure closed-loop stability either by not destabilizing a stable plant or by stabilizing an unstable plant. In fact, the class of linear time-invariant continuous-time plants that can be stabilized by continuous-time PID controllers is a difficult and unsolved problem[2].

For linear time-invariant continuous-time plants, continuous-time PID controller tuning has been extensively studied, and a vast number of tuning rules have been developed based on analytical models, simulation models, or the actual plant response[3,4,5,6,7,8,9]. Since all models are erroneous to some extent and the dynamics of a real system can change unexpectedly, the challenge is to tune the PID controller for reliable performance despite model errors and unpredictable plant changes. Although integral control implies asymptotic setpoint command following, this guarantee is predicated on closed-loop stability. Therefore, for plants whose dynamics change over time, PID tuning for closed-loop stability must be maintained through continual closed-loop identification and careful gain updating. In modern applications, PID controllers are typically implemented digitally[10,11,12,13], and thus sampling (A/D) and reconstruction (D/A) effects may impact closed-loop stability and performance.

Beyond these considerations, virtually all real plants contain nonlinearities, and the problem of stabilizability by PID control is more difficult, especially in the case where the plant nonlinearities are unmodeled, unknown, or uncertain[14,15]. For example, magnitude saturation, which is universal to all control applications, is a nonlinearity that requires anti-windup techniques to avoid divergence of the integrator state and degradation of the ability to follow changing setpoints[16,17].

Adaptive PID control, also called autotuning, is an attractive extension of fixed-gain PID control. These techniques have been developed for continuous-time control in[18,19,20,21,22,23,24,25,26,27,28,29,30,31,32,33,34,35,36,37,38,39,40,41,42,43] and for discrete-time control in[11,12,44,45,46,47,48,49,50,51,52]. Adaptive PID control has the potential to allow PID controllers to continually adjust their gains due to changing plant dynamics with little or no manual intervention.

The present paper develops an adaptive digital PID controller based on the approach developed in[53]. The plant is assumed to have linear dynamics with sensor, actuator, and feedback nonlinearities, thus forming a Hammerstein-Wiener-Lur'e system[54]. The linear continuous-time dynamics are assumed to be first-order lag with dead time (i.e., delay); these dynamics have been extensively considered in the literature, especially for Ziegler-Nichols PID tuning[55,56,57,58,59,60,61,62,63,64,65,66,67,68,69]. In this paper, the plant gain is assumed to have known sign but unknown magnitude, and the dead time is assumed to be unknown. The sensor and actuator nonlinearities are assumed to be monotonic, with known trend, but are otherwise unknown, and the feedback nonlinearity is assumed to be monotonic, but is otherwise unknown. Since the controller is digital, the closed-loop system is a sampled-data system, and thus the effect of the sampling rate must be considered. Unlike fixed-gain PID controllers for processes with dead time, the adaptive digital PID controller does not use a Smith predictor[70,71,72].

The approach of the paper is nonstandard, focusing on a numerical investigation of the adaptive digital PID controller. Within this numerical investigation, the paper has three main contributions. The first contribution is the *Simulation-Based Conjecture* (SBC), which states assumptions under which the command-following error is conjectured to be bounded or convergent. The assumptions of SBC include knowledge about the plant parameters as well as properties and knowledge about the sensor, actuator, and feedback nonlinearities. No attempt is made to prove SBC; instead, numerical examples are presented to support its plausibility and motivate future research to prove it.

The second contribution is a demonstration of the effect of the initialization of the recursive-least-squares (RLS) controller update on the performance of the adaptive digital PID controller. Unlike fixed-gain PID control, where tuning refers to the assignment of feedback parameters, the adaptive digital PID controller is tuned by initializing the RLS matrix P_k, which the adaptive digital PID controller uses to adjust the PID gains. The examples thus provide guidance for determining the effect of this initialization on the transient closed-loop performance. This guidance is not provided by the statement of SBC, nor would it be provided by a proof of SBC, were such a proof available.

The third contribution is an investigation of the performance of the adaptive digital PID controller in situations that go beyond the claims of the conjecture. In real-world applications, a PID controller may be subjected to a vast range of conditions that may be unknown and unmodelable. It is therefore essential to assess the ability of the adaptive digital PID controller to operate reliably under conditions that violate the assumptions of SBC.

The contents of the paper are as follows. Section 2 states the sampled-data PID control problem in terms of the basic servo loop with first-order-lag-plus-dead-time dynamics and sensor, actuator, and feedback nonlinearities. The structure of the digital PID controller is presented, including the anti-windup integrator. Section 3 considers stabilizability of the exactly discretized linear dynamics under fixed-gain control. The goal of this section is to show that, under integral control, increased dead time significantly reduces the range of stabilizing gains that the adaptive controller must attain. For the same plant with PID control, Section 4 uses the final value theorem to show that the integrator guarantees asymptotic command following and disturbance rejection for step commands and constant disturbances.

Section 5 presents the adaptive digital PID controller, which is based on RLS. The controller update involves a recursive expression for the 3×3 matrix P_k as well as the controller gain vector θ_k. Section 6 demonstrates how the continuous-time

dynamics are numerically discretized in order to ensure accuracy of the intersample behavior. Section 7 presents the nominal parameters that are used for all of the examples in this paper.

The remainder of the paper consists of numerical examples illustrating the performance of the adaptive digital PID controller under the assumptions of SBC as well as under conditions that violate the assumptions of SBC. Section 8 presents linear examples (i.e., without sensor, actuator, and feedback nonlinearities) that support SBC, while Section 9 presents linear examples that demonstrate the effect of violating assumptions of SBC. Sections 10 and 11 present examples that illustrate the effect of sensor, actuator, and feedback nonlinearities, including examples that support SBC as well as examples that violate the assumptions of SBC. In all examples, unless stated otherwise, the sensor noise η is zero. Section 12 goes beyond the focus of the paper by providing a brief investigation of the adaptive digital PID controller for second-order systems. Finally, Section 13 provides an extension of the adaptive digitial PID controller that is applicable to a wider class of plants.

2 | ADAPTIVE DIGITAL PID CONTROL PROBLEM

The basic servo loop for a sampled-data Hammerstein-Wiener-Lur'e system with first-order-lag-plus-dead-time dynamics is shown in Figure 1, where r is the command and d is the disturbance. The linear continuous-time dynamics are given by the transfer function

$$G(s) = \frac{Ke^{-\tau_d s}}{\tau_c s + 1}, \tag{1}$$

where $K > 0$ is the DC gain, $\tau_d \geq 0$ is the dead time, and $\tau_c > 0$ is the time constant (also called the lag). The plant is controlled by the adaptive digital PID controller $G_{c,k}$, whose input is the normalized error $\bar{e}_k$ and whose output is the discrete-time requested control u_k. The gains of $G_{c,k}$, and thus the control u_k, are updated at each time step k, with update period $T_s > 0$, by the adaptive control law given in Section 5. The digital-to-analog (D/A) interface for this plant is a zero-order-hold (ZOH) device, whose output is the piecewise-constant continuous-time requested control $u(t)$. In particular, for all $k \geq 0$ and all $t \in [kT_s, (k+1)T_s)$, $u(t)$ is given by

$$u(t) = u_k. \tag{2}$$

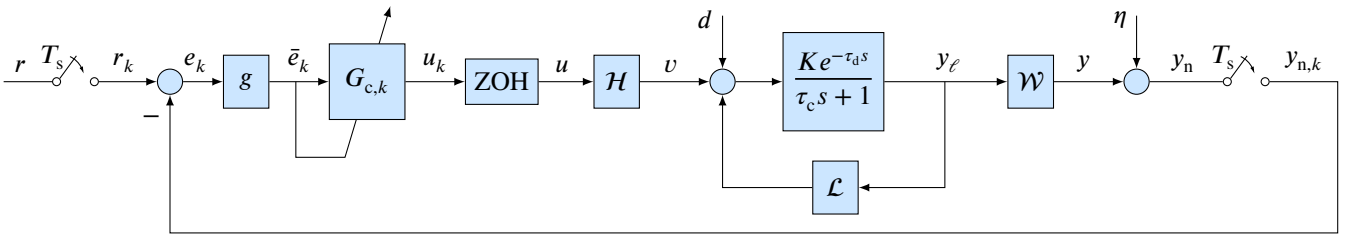

FIGURE 1 Basic servo loop for the sampled-data Hammerstein-Wiener-Lur'e system with first-order-lag-plus-dead-time dynamics, where y_n is the noisy measurement. The error $e_k = r_k - y_{n,k}$ is passed through the error-normalization function g to generate the normalized error $\bar{e}_k$. The normalized error $\bar{e}_k$ is the input to the PID controller $G_{c,k}$, whose gains are adaptively updated at each time step.

The actual control is the continuous-time signal $v = \mathcal{H}(u)$, where the Hammerstein input nonlinearity $\mathcal{H} : \mathbb{R} \to \mathbb{R}$ represents the actuator nonlinearity. The output of G is y_ℓ, where the subscript "ℓ" denotes "linear." The sensor output is $y = \mathcal{W}(y_\ell)$, where the Wiener output nonlinearity $\mathcal{W} : \mathbb{R} \to \mathbb{R}$ represents the sensor nonlinearity. The output y_ℓ is fed back to G through the Lur'e feedback nonlinearity $\mathcal{L} : \mathbb{R} \to \mathbb{R}$. In special cases, one or more of the nonlinearities $\mathcal{H}$, $\mathcal{W}$, and $\mathcal{L}$ may be absent. In particular, if $\mathcal{H}$, $\mathcal{W}$, and $\mathcal{L}$ are absent, then they are replaced by the gains 1, 1, and 0, respectively.

In the presence of sensor noise η, the measurement is the noisy sensor output $y_n = y + \eta$. The analog-to-digital (A/D) device samples y_n with sample time T_s to produce the discrete-time measurement $y_{n,k} \triangleq y_n(kT_s)$. In the absence of sensor noise η, $y_{n,k}$ is replaced by $y_k \triangleq y(kT_s)$. The error is given by $e_k = r_k - y_{n,k}$, where r_k is the sampled version of the command r. Note that e_k is a noisy sampled version of the true error $r - y_\ell$.

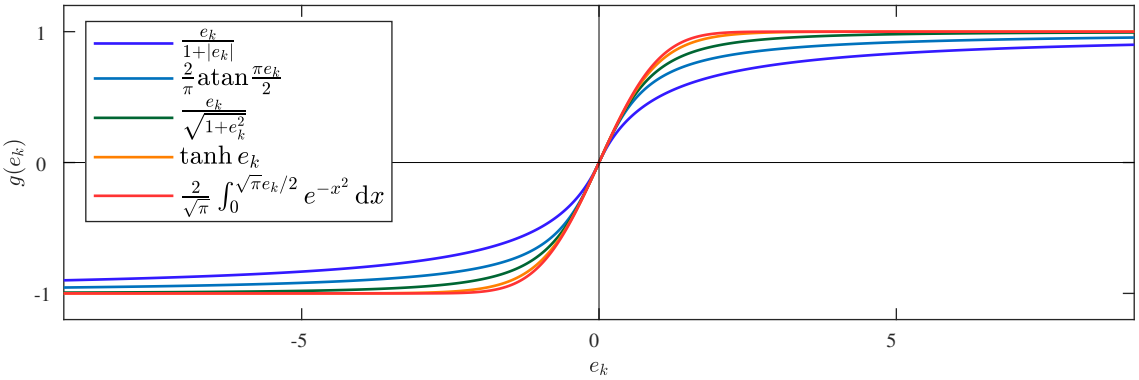

FIGURE 2 Error-normalization functions defined by (4) and (5) with $\mu = 1$ and $\nu = 1$.

The error e_k passes through the error-normalization function $g : \mathbb{R} \to \mathbb{R}$ to generate the normalized error $\bar{e}_k$. The error-normalization function g is a sigmoid function that satisfies

$$g'(0) = \nu, \qquad \lim_{e_k \to \infty} g(e_k) = -\lim_{e_k \to -\infty} g(e_k) = \mu, \tag{3}$$

where $\nu > 0$ and $\mu > 0$. Candidate sigmoid functions that satisfy (3) include the odd, increasing, C^∞ functions

$$g(e_k) = \frac{\mu\nu e_k}{\mu + \nu|e_k|}, \qquad g(e_k) = \frac{2\mu}{\pi}\operatorname{atan}\frac{\pi\nu e_k}{2\mu}, \qquad g(e_k) = \frac{\mu\nu e_k}{\sqrt{\mu^2 + \nu^2 e_k^2}}, \tag{4}$$

$$g(e_k) = \mu\tanh\frac{\nu e_k}{\mu}, \qquad g(e_k) = \frac{2\mu}{\sqrt{\pi}}\int_0^{\sqrt{\pi}\nu e_k/(2\mu)} e^{-x^2}\,\mathrm{d}x. \tag{5}$$

By constraining the magnitude of the input to $G_{\mathrm{c},k}$, these functions ensure robustness to the transients arising from the choice of P_0 required by the adaptive digital PID controller. Note that the units of μ/ν must be equal to the units of e_k. Choosing μ to be dimensionless, it follows that νe_k and $\bar{e}_k = g(e_k)$ are also dimensionless and thus the units of ν are the same as the units of $1/e_k$. All five functions are plotted in Figure 2 for $\mu = 1$ and $\nu = 1$.

The discrete-time requested control u_k, which is determined by the adaptive digital PID controller, has the form

$$u_k = \kappa_{\mathrm{p},k}\bar{e}_{k-1} + \kappa_{\mathrm{i},k}\xi_{k-1} + \kappa_{\mathrm{d},k}(\bar{e}_{k-1} - \bar{e}_{k-2}), \tag{6}$$

where $\kappa_{\mathrm{p},k}$, $\kappa_{\mathrm{i},k}$, and $\kappa_{\mathrm{d},k}$ are time-varying PID gains and

$$\xi_k \triangleq \sum_{j=0}^{k} \bar{e}_j. \tag{7}$$

Note that, in (6), the data used by the controller to determine u_k are sampled at steps $k-1$ and $k-2$. This restriction avoids direct feedthrough, which requires instantaneous computation, and corresponds to a strictly proper controller. Therefore, (6) is suitable for real-time digital implementation. This digital PID controller structure facilitates the adaptive control algorithm described in Section 5. Alternative digital PID controller structures are considered in [73,74,12].

It turns out that control-magnitude saturation determined by the actuator nonlinearity $\mathcal{H}$ may cause ξ_k to diverge; this is the integrator-windup phenomenon. In order to suppress integrator windup, we replace (7) with

$$\xi_k \triangleq \sum_{j=0}^{k} \bar{e}_j - \begin{cases} \left(\operatorname{sign}\sum_{j=0}^{k}\bar{e}_j\right)(\underline{u} - u_k), & u_k < \underline{u}, \\ 0, & \underline{u} \le u_k \le \overline{u}, \\ \left(\operatorname{sign}\sum_{j=0}^{k}\bar{e}_j\right)(u_k - \overline{u}), & u_k > \overline{u}, \end{cases} \tag{8}$$

where $\underline{u} < \overline{u}$ are the lower and upper anti-windup thresholds; the choice of these thresholds is discussed in Section 5. A related anti-windup technique is given in [75, p. 310–311].

3 | STABILIZABILITY OF THE EXACTLY DISCRETIZED DYNAMICS UNDER FIXED-GAIN INTEGRAL CONTROL

This section analyzes stabilizability of the sampled-data first-order-lag-plus-dead-time plant in the absence of sensor, actuator, and feedback nonlinearities, with the error-normalization function absent, under the assumption that the integrator gain is constant, and with the proportional and derivatives gains absent. Hence, only integral action is considered.

To exactly discretize (1), we first remove the dead time from G to obtain $\hat{G}(s) \triangleq \frac{K}{\tau_c s+1}$. The zero-order-hold discretization of $\hat{G}$ is given by

$$\hat{G}_{\mathrm{d}}(\mathbf{z}) \triangleq \frac{K(1-\alpha)}{\mathbf{z}-\alpha}, \tag{9}$$

where $\alpha \triangleq e^{-\frac{T_s}{\tau_c}} \in (0,1)$. Assuming that $\tau_{\mathrm{d}} = n_d T_{\mathrm{s}}$, where n_{d} is a nonnegative integer, it follows that the discrete-time counterpart of the dead time $e^{-\tau_{\mathrm{d}} s} = e^{-n_{\mathrm{d}} T_{\mathrm{s}} s}$ is $\mathbf{z}^{-n_{\mathrm{d}}}$. Using (9), the exact discretization of (1) with sample time T_{s} is thus given by

$$G_{\mathrm{d}}(\mathbf{z}) \triangleq \frac{K(1-\alpha)}{\mathbf{z}^{n_{\mathrm{d}}}(\mathbf{z}-\alpha)}. \tag{10}$$

Next, let $\kappa_{\mathrm{i}} \in \mathbb{R}$, and consider the discrete-time integral controller

$$G_{\mathrm{c}}(\mathbf{z}) = \frac{\kappa_{\mathrm{i}}}{\mathbf{z}-1}, \tag{11}$$

which yields the loop transfer function

$$L(\mathbf{z}) \triangleq G_{\mathrm{d}}(\mathbf{z}) G_{\mathrm{c}}(\mathbf{z}) = \frac{K(1-\alpha)\kappa_{\mathrm{i}}}{\mathbf{z}^{n_{\mathrm{d}}}(\mathbf{z}-\alpha)(\mathbf{z}-1)}. \tag{12}$$

The characteristic polynomial of the closed-loop system is thus given by

$$p(\mathbf{z}) \triangleq \mathbf{z}^{n_{\mathrm{d}}}(\mathbf{z}-1)(\mathbf{z}-\alpha) + \beta, \tag{13}$$

where

$$\beta \triangleq K(1-\alpha)\kappa_{\mathrm{i}}. \tag{14}$$

Proposition 1. Consider the closed-loop characteristic polynomial p defined by (13), where $\alpha \in (0,1)$, $\beta \in \mathbb{R}$, and n_{d} is a nonnegative integer. For all nonnegative integers n_{d}, define

$$\mathcal{S}(n_{\mathrm{d}}) \triangleq \{(\alpha,\beta) \in (0,1)\times\mathbb{R} : \ p \text{ is asymptotically stable}\}.$$

Then, the following statements hold:

i) If p is asymptotically stable, then $0 < \beta < 1$.

ii) Let $n_{\mathrm{d}} = 0$. Then, p is asymptotically stable if and only if $0 < \beta < 1$ and

$$\beta < 1 - \alpha. \tag{15}$$

iii) Let $n_{\mathrm{d}} = 1$. Then, p is asymptotically stable if and only if $0 < \beta < 1$ and

$$\beta^2 + (\alpha+1)\beta < 1 - \alpha. \tag{16}$$

iv) Let $n_{\mathrm{d}} = 2$. Then, p is asymptotically stable if and only if $0 < \beta < 1$ and

$$-\beta^3 + (\alpha+1)\beta^2 + (\alpha^2+2)\beta < 1 - \alpha. \tag{17}$$

v) $\mathcal{S}(2) \subsetneq \mathcal{S}(1) \subsetneq \mathcal{S}(0)$.

vi) There exists $\overline{\beta} > 0$ such that, for all $\beta \in (0, \overline{\beta})$, p is asymptotically stable.

Proof. *i*)–*iv*) follow by applying the Jury test[76, p. 35] to (13). To show *v*), note that

$$\beta < (\alpha+1)\beta < \beta^2 + (\alpha+1)\beta,$$

which implies $\mathcal{S}(1) \subsetneq \mathcal{S}(0)$. Next, assume that $\beta \in \mathcal{S}(2)$, and it follows that

$$\beta < 2\beta - \beta^3 < -\beta^3 + (\alpha+1)\beta^2 + (\alpha^2+2)\beta < 1 - \alpha,$$

which implies

$$\beta^3 < \beta^2 < \beta(1-\alpha).$$

Thus,

$$\begin{aligned}\beta^2 + (\alpha+1)\beta &< \beta^2 + (\alpha+1)\beta + (1-\alpha)\beta - \beta^3 \\ &= \beta^2 + 2\beta - \beta^3 < \beta^2 + (\alpha^2+2)\beta - \beta^3 \\ &< (\alpha+1)\beta^2 + (\alpha^2+2)\beta - \beta^3 \\ &< 1-\alpha.\end{aligned}$$

Hence, $\beta \in \mathcal{S}(1)$. Since, in addition, $\mathcal{S}(2) \neq \mathcal{S}(1)$, it follows that $\mathcal{S}(2) \subsetneq \mathcal{S}(1)$. To prove *vi*), note that the angle of departure for the root $\mathbf{z} = 1$ of (13) as a function of $\beta > 0$ is 180 deg. It thus follows that there exists $\overline{\beta} > 0$ such that, for all $\beta \in (0, \overline{\beta})$, the roots of (13) lie in the open unit disk and thus the corresponding closed-loop system is asymptotically stable. □

It follows from *vi*) of Proposition 1 that for all nonnegative integers n_d and all $\alpha \in (0,1)$, the discretized plant (10) is stabilizable by an integral controller of the form (11). The stability regions for $n_\mathrm{d} \in \{0, 1, \ldots, 15\}$ are illustrated in Figure 3, which shows that these regions are nested. An open conjecture is that these regions are nested for all nonnegative n_d.

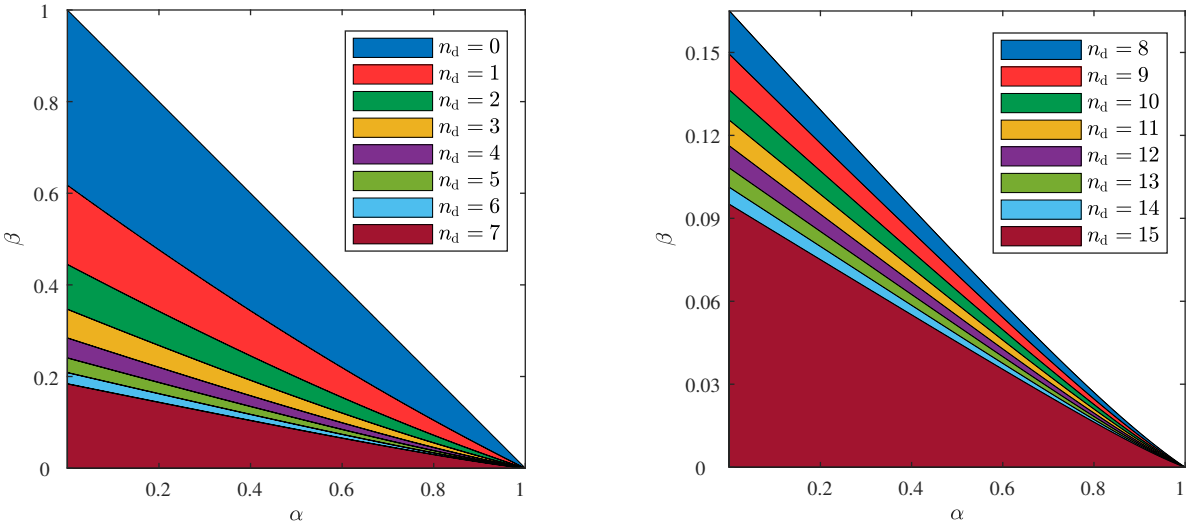

FIGURE 3 Stability regions in terms of (α, β) for $n_\mathrm{d} \in \{0, 1, \ldots, 15\}$. The regions are nested.

4 | ASYMPTOTIC ANALYSIS OF THE EXACTLY DISCRETIZED DYNAMICS UNDER FIXED-GAIN PID CONTROL

This section analyzes the asymptotic response of the sampled-data first-order-lag-plus-dead-time plant in the absence of sensor, actuator, and feedback nonlinearities, with the error-normalization function absent, and under the assumption that the gains of the PID controller (6), (7) are fixed (i.e., $\kappa_{\mathrm{p},k} \equiv \kappa_\mathrm{p} \in \mathbb{R}$, $\kappa_{\mathrm{i},k} \equiv \kappa_\mathrm{i} \in \mathbb{R}$, $\kappa_{\mathrm{d},k} \equiv \kappa_\mathrm{d} \in \mathbb{R}$).

The PID controller (6), (7) has the discrete-time linear time-invariant transfer function

$$G_\mathrm{c}(\mathbf{z}) \triangleq \frac{\kappa_\mathrm{p}}{\mathbf{z}} + \frac{\kappa_\mathrm{i}}{\mathbf{z}-1} + \frac{\kappa_\mathrm{d}(\mathbf{z}-1)}{\mathbf{z}^2} = \frac{a_2\mathbf{z}^2 + a_1\mathbf{z} + a_0}{\mathbf{z}^2(\mathbf{z}-1)}, \tag{18}$$

where

$$a_2 \triangleq \kappa_\mathrm{p} + \kappa_\mathrm{i} + \kappa_\mathrm{d}, \quad a_1 \triangleq -\kappa_\mathrm{p} - 2\kappa_\mathrm{d}, \quad a_0 \triangleq \kappa_\mathrm{d}. \tag{19}$$

Note that the order of G_c is three or less depending on its zeros. In particular, if $\kappa_i = 0$, then $a_2 + a_1 + a_0 = 0$, and thus the numerator of G_c has a root at $\mathbf{z} = 1$, which cancels the pole at $\mathbf{z} = 1$. In this case, (18) becomes

$$G_c(\mathbf{z}) = \frac{(\kappa_p + \kappa_d)\mathbf{z} - \kappa_d}{\mathbf{z}^2}. \tag{20}$$

However, if $\kappa_i \neq 0$, then $a_2 + a_1 + a_0 = \kappa_i \neq 0$, and thus $\mathbf{z} = 1$ is not a zero of G_c. The DC gain of G_c is thus given by

$$|G_c(1)| = \begin{cases} \kappa_p, & \kappa_i = 0, \\ \infty, & \kappa_i \neq 0. \end{cases} \tag{21}$$

Combining the plant (10) with the controller (18) implies that the closed-loop transfer function $\tilde{G}_{er}$ from the command r to the error e is given by

$$\begin{aligned} \tilde{G}_{er}(\mathbf{z}) &\triangleq \frac{1}{1 + G_d(\mathbf{z})G_c(\mathbf{z})} \\ &= \frac{\mathbf{z}^{n_d+2}(\mathbf{z} - \alpha)(\mathbf{z} - 1)}{\mathbf{z}^{n_d+2}(\mathbf{z} - \alpha)(\mathbf{z} - 1) + K(1 - \alpha)(a_2\mathbf{z}^2 + a_1\mathbf{z} + a_0)}. \end{aligned} \tag{22}$$

Assuming that the closed-loop transfer function $\tilde{G}_{er}$ is asymptotically stable, the asymptotic response of $\tilde{G}_{er}$ to a unit step command with $d = 0$ and $\eta = 0$ is given by the discrete-time final-value theorem [77, p. 139]

$$\begin{aligned} \lim_{k\to\infty} e_k &= \lim_{\mathbf{z}\to 1} (\mathbf{z} - 1)\tilde{G}_{er}(\mathbf{z})\frac{\mathbf{z}}{\mathbf{z} - 1} \\ &= \lim_{\mathbf{z}\to 1} \frac{\mathbf{z}^{n_d+3}(\mathbf{z} - \alpha)(\mathbf{z} - 1)}{\mathbf{z}^{n_d+2}(\mathbf{z} - \alpha)(\mathbf{z} - 1) + K(1 - \alpha)(a_2\mathbf{z}^2 + a_1\mathbf{z} + a_0)} \\ &= \begin{cases} \dfrac{1}{1 + K\kappa_p}, & \kappa_i = 0, \\ 0, & \kappa_i \neq 0. \end{cases} \end{aligned} \tag{23}$$

Likewise, the closed-loop transfer function $\tilde{G}_{ed}$ from the disturbance d to the error e is given by

$$\begin{aligned} \tilde{G}_{ed}(\mathbf{z}) &\triangleq \frac{G_d(\mathbf{z})}{1 + G_d(\mathbf{z})G_c(\mathbf{z})} \\ &= \frac{K(1 - \alpha)\mathbf{z}^2(\mathbf{z} - 1)}{\mathbf{z}^{n_d+2}(\mathbf{z} - \alpha)(\mathbf{z} - 1) + K(1 - \alpha)(a_2\mathbf{z}^2 + a_1\mathbf{z} + a_0)}. \end{aligned} \tag{24}$$

Assuming that the closed-loop transfer function $\tilde{G}_{ed}$ is asymptotically stable, the asymptotic response of $\tilde{G}_{ed}$ to a unit step disturbance with $r = 0$ and $\eta = 0$ is given by

$$\begin{aligned} \lim_{k\to\infty} e_k &= \lim_{\mathbf{z}\to 1} (\mathbf{z} - 1)\tilde{G}_{ed}(\mathbf{z})\frac{\mathbf{z}}{\mathbf{z} - 1} \\ &= \lim_{\mathbf{z}\to 1} \frac{K(1 - \alpha)\mathbf{z}^3(\mathbf{z} - 1)}{\mathbf{z}^{n_d+2}(\mathbf{z} - \alpha)(\mathbf{z} - 1) + K(1 - \alpha)(a_2\mathbf{z}^2 + a_1\mathbf{z} + a_0)} \\ &= \begin{cases} \dfrac{K}{1 + K\kappa_p}, & \kappa_i = 0, \\ 0, & \kappa_i \neq 0. \end{cases} \end{aligned} \tag{25}$$

Therefore, if the closed-loop transfer functions $\tilde{G}_{er}$ and $\tilde{G}_{ed}$ are asymptotically stable and $\kappa_i \neq 0$, then, for all step commands and step disturbances, the asymptotic command-following error is zero for arbitrary values of κ_p, κ_d, n_d, K, and α.

5 | ADAPTIVE DIGITAL PID CONTROLLER AND THE SIMULATION-BASED CONJECTURE

The control (6) can be expressed as

$$u_k = \phi_k\theta_k, \tag{26}$$

where

$$\phi_k \triangleq \begin{bmatrix} \bar{e}_{k-1} & \xi_{k-1} & \bar{e}_{k-1} - \bar{e}_{k-2} \end{bmatrix} \in \mathbb{R}^{1\times 3}, \quad \theta_k \triangleq \begin{bmatrix} \kappa_{\mathrm{p},k} \\ \kappa_{\mathrm{i},k} \\ \kappa_{\mathrm{d},k} \end{bmatrix} \in \mathbb{R}^3. \tag{27}$$

Note that the regressor ϕ_k is constructed from the past values of e_k and ξ_k; and the controller coefficient vector θ_k contains the time-dependent proportional, integral, and derivative gains $\kappa_{\mathrm{p},k}$, $\kappa_{\mathrm{i},k}$, and $\kappa_{\mathrm{d},k}$.

To determine the adaptive law for updating θ_k, let $\theta \in \mathbb{R}^3$, and consider the *retrospective performance variable* defined by

$$\hat{z}_k(\theta) \triangleq \bar{e}_k - \sigma(u_{k-1} - \phi_{k-1}\theta), \tag{28}$$

where σ is either 1 or -1. Furthermore, define the *retrospective cost function* $J_k : \mathbb{R}^3 \to [0, \infty)$ by

$$J_k(\theta) \triangleq \sum_{i=0}^{k} \hat{z}_i^2(\theta) + (\theta - \theta_0)^{\mathrm{T}} P_0^{-1} (\theta - \theta_0), \tag{29}$$

where $\theta_0 \in \mathbb{R}^3$ is the initial vector of PID gains and $P_0 \in \mathbb{R}^{3\times 3}$ is a positive-definite matrix that provides regularization. Applying recursive least squares minimization [78], [79, p. 20] to (29) implies that, for all $k \geq 0$,

$$\theta_{k+1} = \theta_k + (\sigma\bar{e}_k - u_{k-1} + \phi_{k-1}\theta_k) P_{k+1} \phi_{k-1}^{\mathrm{T}}, \tag{30}$$

where

$$P_{k+1} = P_k - \frac{1}{1 + \phi_{k-1} P_k \phi_{k-1}^{\mathrm{T}}} P_k \phi_{k-1}^{\mathrm{T}} \phi_{k-1} P_k, \tag{31}$$

and where $\bar{e}_{-3} = \bar{e}_{-2} = \bar{e}_{-1} \triangleq 0$, $\xi_{-1} \triangleq 0$, and $u_{-1} \triangleq 0$ are the initial conditions. The adaptive digital PID controller is thus given by (8), (26), (27), (30), and (31). Note that this choice of initial conditions implies that $\phi_{-1} = 0$. It thus follows that $P_1 = P_0$ and $\theta_1 = \theta_0$. Consequently, if $\theta_0 = 0$, then the first possibly nonzero control input is u_2. A timing diagram showing the implementation of the adaptive digital PID controller is given in Figure 4. Note that the adaptive digital PID control can be specialized to adaptive digital PI, PD, ID, P, I, and D control by omitting the corresponding components of ϕ_k and θ_k.

The following result describes properties of (26)–(31). A proof is given in [78, Theorem 1].

Proposition 2. Consider (26)–(31), where $\theta_0 \in \mathbb{R}^3$ and $P_0 \in \mathbb{R}^{3\times 3}$ is positive definite. Then, for all $k \geq 0$, θ_{k+1} is the unique global minimizer of J_k.

Next, we present the Simulation-Based Conjecture (SBC), which specifies assumptions under which the signals in the basic servo loop are bounded or convergent. The following definitions are used in SBC. Let $f : \mathbb{R} \to \mathbb{R}$. Then, f is nondecreasing

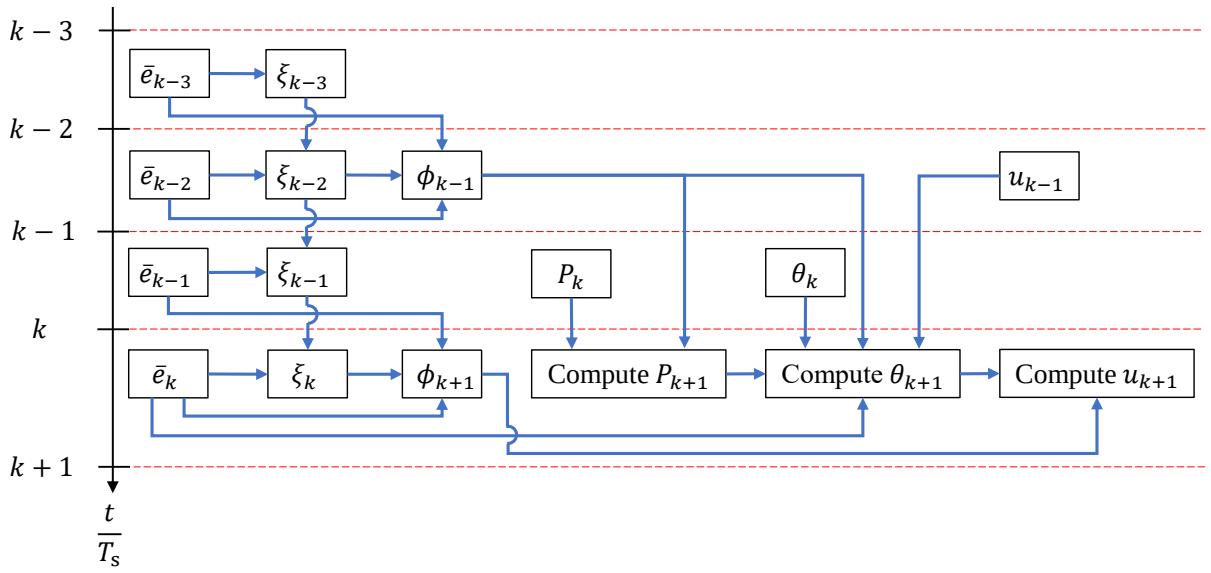

FIGURE 4 Timing diagram for the adaptive digital PID controller. The controller coefficient vector θ_{k+1} and the control $u_{k+1} = \phi_{k+1}\theta_{k+1}$ are computed between steps k and $k + 1$ for implementation at step $k + 1$.

(resp., nonincreasing) if, for all $x, y \in \mathbb{R}$ such that $x \leq y$, it follows that $f(x) \leq f(y)$ (resp., $f(x) \geq f(y)$). Furthermore, f is increasing (resp., decreasing) if, for all $x, y \in \mathbb{R}$ such that $x < y$, it follows that $f(x) < f(y)$ (resp., $f(x) > f(y)$). If $\mathcal{H}$ is nondecreasing, then $\operatorname{trend} \mathcal{H} = 1$; if $\mathcal{H}$ is nonincreasing, then $\operatorname{trend} \mathcal{H} = -1$. The same terminology applies to $\mathcal{W}$.

For SBC, the lower and upper anti-windup thresholds needed for (8) determine the range of feasible commands r, where the command r is *feasible* if there exists a constant control input u that can produce the output $y = r$. Feasibility is addressed by (A12). For SBC, the existence of a limit implies that the limit is finite.

Simulation-Based Conjecture (SBC). Consider the basic servo loop shown in Figure 1, where the adaptive digital PID controller $G_{c,k}$ is given by (8), (26), (27), (31), and (30). Furthermore, consider the following assumptions:

(A1) K is constant and nonzero, and $\operatorname{sign} K$ is known, but K is otherwise unknown.

(A2) τ_c is constant and positive, but τ_c is otherwise unknown.

(A3) τ_d is constant and nonnegative, but τ_d is otherwise unknown.

(A4) r is constant but is otherwise unknown.

(A5) d is constant but is otherwise unknown.

(A6) $\mathcal{H}$ is either nondecreasing or nonincreasing and $\operatorname{trend} \mathcal{H}$ is known, but $\mathcal{H}$ is otherwise unknown.

(A7) $\mathcal{W}$ is either nondecreasing or nonincreasing and $\operatorname{trend} \mathcal{W}$ is known, but $\mathcal{W}$ is otherwise unknown.

(A8) $\mathcal{L}$ is either nondecreasing or nonincreasing, but $\mathcal{L}$ is otherwise unknown.

(A9) $\sigma \triangleq (\operatorname{trend} \mathcal{H})(\operatorname{trend} \mathcal{W}) \operatorname{sign} K$.

(A10) η is bounded but is otherwise unknown.

(A11) $\eta = 0$, that is, $y_n = y$.

(A12) $\mathcal{F}(r, d) \triangleq \{(u, y_\ell) \in [\underline{u}, \overline{u}] \times \mathbb{R} : K(\mathcal{L}(y_\ell) + \mathcal{H}(u) + d) = y_\ell \text{ and } \mathcal{W}(y_\ell) = r\}$ is nonempty.

(A13) $\mathcal{W}$ is either increasing or decreasing.

(A14) $\mathcal{W}(r) = r$.

Then, for all $\nu > 0$ and all positive-definite P_0, the following statements hold:

i) Assume that (A1)–(A10) are satisfied. Then, for all initial conditions of the plant and integrator state, u_k, ξ_k, y_k, $\kappa_{p,k}$, $\kappa_{i,k}$, and $\kappa_{d,k}$ are bounded.

ii) Assume that (A1)–(A12) are satisfied. Then, for all initial conditions of the plant and integrator state, $\lim_{k\to\infty} u_k$, $\lim_{k\to\infty} \xi_k$, $\lim_{k\to\infty} y_k$, $\lim_{k\to\infty} \kappa_{p,k}$, $\lim_{k\to\infty} \kappa_{i,k}$, and $\lim_{k\to\infty} \kappa_{d,k}$ exist, and $\lim_{t\to\infty} y(t) = r$.

iii) Assume that (A1)–(A14) are satisfied. Then, for all initial conditions of the plant and integrator state, $\lim_{t\to\infty} y_\ell(t) = r$.

Although the setpoint command r is usually known in practice, (A4) allows for the possibility that only the error e_k is known. This situation occurs in applications where the error is measured directly as the offset from the command, but the commanded setpoint r is not separately measured. A measurement of r is useful in the case where command feedforward is used; however, only feedback control using e_k is considered in this paper.

For a given command r and a disturbance d, set $\mathcal{F}(r, d)$ defined in (A12) is the *feasibility set*. This set consists of the constant values of the input u and output y for which the output of the sensor nonlinearity $\mathcal{W}$ is equal to the command r in the presence of the disturbance d. If $\mathcal{F}(r, d)$ is not empty, then there exist a constant input u and a constant output y_ℓ under which the output y of $\mathcal{W}$ is equal to the command r in the presence of the disturbance d. In this case, the command r is *feasible*; otherwise, r is *infeasible*. Note that the feasibility of r depends on d as well as the gain K and the nonlinearities $\mathcal{H}$, $\mathcal{W}$, and $\mathcal{L}$. Finally, note that, in the case where $\mathcal{H}$ and $\mathcal{W}$ are absent, $\mathcal{F}(r, d)$ is given by

$$\mathcal{F}(r, d) \triangleq \left\{ u \in [\underline{u}, \overline{u}] \,:\, K\left(\mathcal{L}(r) + u + d\right) = r \right\}, \tag{32}$$

which is nonempty since $u = r/K - \mathcal{L}(r) - d \in \mathcal{F}(r, d)$.

Note that, because d, K, $\mathcal{H}$, $\mathcal{W}$, and $\mathcal{L}$ are assumed to be unknown, it is not possible to verify (A12) in order to determine whether or not a given setpoint command r is feasible. Furthermore, for a given setpoint command r that is known to be feasible, it is not possible to determine *a priori* the control input u needed to ensure that $\lim_{t\to\infty} y(t) = r$. However, it follows from SBC that the adaptive digital PID controller yields the required asymptotic control input. Note that (A13) and (A14) are sufficient conditions under which the output y_ℓ of G converges to r.

In order to maximize the range of feasible commands r, it is desirable to choose $\overline{u} - \underline{u}$ to be as large as possible. On the other hand, choosing $\overline{u} - \underline{u}$ to be as small as possible tends to reduce the effect of windup as reflected by the magnitude of ξ_k. This tradeoff must thus be considered in selecting $\overline{u}$ and $\underline{u}$. If $\lim_{u\to-\infty} \mathcal{H}(u) = -\infty$, then we set $\underline{u} = -\infty$, which implies that the first case in (8) is absent. Likewise, if $\lim_{u\to\infty} \mathcal{H}(u) = \infty$, then we set $\overline{u} = \infty$, which implies that the third case in (8) is absent. However, since all real actuators are subject to magnitude saturation, these cases do not occur in practice. For example, the standard saturation function is

$$\mathcal{H}(u) = \begin{cases} u, & |u| \le 1, \\ \text{sign } u, & |u| > 1. \end{cases} \tag{33}$$

In this case, it is desirable to choose $\underline{u} = -1$ and $\overline{u} = 1$ in order to minimize the impact of integrator windup. As will be shown, choosing $\underline{u} << -1$ and $\overline{u} >> 1$ may exacerbate windup; however, these choices do not contradict SBC. Choosing suitable values of $\underline{u}$ and $\overline{u}$ may require some knowledge of $\mathcal{H}$; however, this knowledge is not assumed in SBC.

Note that (A6)–(A8) do not require $\mathcal{H}$, $\mathcal{W}$, and $\mathcal{L}$ to be continuous; however, since these functions are either nonincreasing or nondecreasing, they can have only jump discontinuities. For example, $\mathcal{W}$ may represent sensor quantization. To avoid cases that are not amenable to simulation, these functions are chosen to have at most a finite number of jumps in every finite interval. Finally, $\mathcal{H}$, $\mathcal{W}$, and $\mathcal{L}$ may be piecewise C^1 with slope discontinuities.

6 | NUMERICAL SIMULATION OF THE INTERSAMPLE BEHAVIOR

This section describes the numerical integration method used to simulate the intersample behavior of the continuous-time dynamics of G combined with the adaptive digital PID controller. The adaptive digital controller $G_{c,k}$ shown in Figure 1 operates on the measured noisy error e_k available at the time step k to provide the requested control u_{k+1} at the next time step $k + 1$. However, the continuous-time dynamics evolve between sample times. In order to assess the effect of the adaptive digital PID controller on the intersample behavior, the state trajectory is numerically integrated between sample instants using the Matlab ODE45 function. In particular, for all examples, ODE45 is called 1000 times during each sample interval of length T_s. ODE45 uses the default tolerance 10^{-8} to determine the required variable step lengths during each integration interval of length $T_s/1000$. The choice of integration interval of length $T_s/1000$ is used to relate the variance of the discrete-time process and sensor noise to the intensities of the corresponding continuous-time noise signals.

In the case where the dead time τ_d is an integer multiple n_d of the sample time T_s, the effect of the dead time τ_d at the sample times is exactly represented by z^{-n_d}. Since the continuous-time dynamics without dead time can be exactly integrated with a zero-order-hold input, it follows that, in this case, the plant with dead time can be exactly propagated at the sample times. This ability can be used to assess the accuracy of the fixed-step numerical integration. In particular, for each example where τ_d is an integer multiple n_d of T_s, the sampled values are propagated using exact discretization of the continuous-time dynamics. These values are superimposed on the fixed-step numerical integration of the continuous-time dynamics from the initial condition. This technique is illustrated in Figure 5 for the plant (1), with $K = 1$, $\tau_c = 1$ s, and $\tau_d = 5$ s; and where $d = 0$, $\eta = 0$, and $u = 1$. Letting $T_s = 1$ s/sample implies that $n_d = \tau_d/T_s = 5$ samples, and thus the state at the sample times can be obtained using the exactly discretized dynamics as well as fixed-step numerical integration. Figure 5 shows the step response of the plant. This procedure is used to validate the accuracy of the numerical integration for all examples for which exact discretization is possible.

7 | NOMINAL PARAMETERS FOR ALL EXAMPLES IN THIS PAPER

For all of the examples in this paper, θ_k is initialized as $\theta_0 = 0$ in order to reflect the absence of additional prior modeling information. However, the digital PID gains can be initialized arbitrarily in practice based on prior knowledge. In addition, for all of the examples, g is chosen to be the first function in (4), and, unless stated otherwise, $\mu = 1$, $\nu = 0.02$, and $P_0 = p_0 I_3$, where $p_0 = 1$ and I_3 is the 3×3 identity matrix.

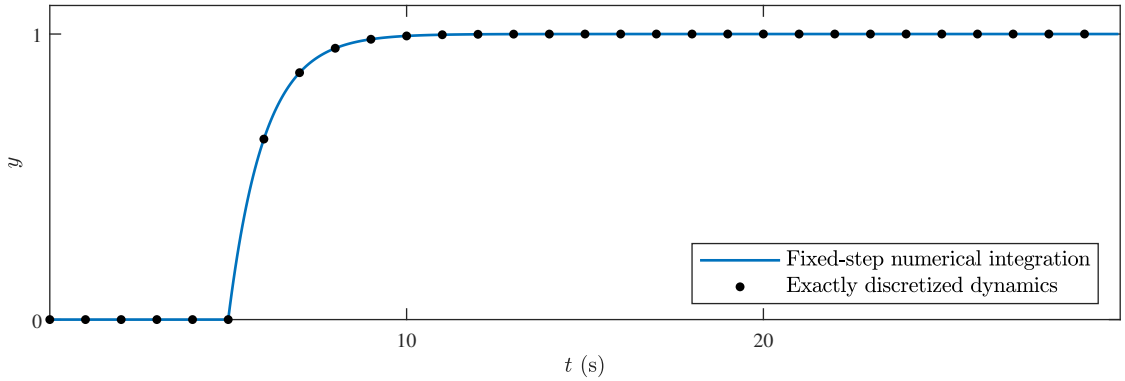

FIGURE 5 Fixed-step numerical integration based on ODE45 (blue line) is used to integrate (1) with $K = 1$, $\tau_c = 1$ s, and $\tau_d = 5$ s, where $d = 0$, $\eta = 0$, and $u = 1$. The black dots represent the response of the exactly discretized plant (1) with $T_s = 1$ s/sample. This procedure is used to validate the accuracy of the numerical integration for all examples for which exact discretization is possible (i.e., τ_d is an integer multiple of T_s).

For all of the examples, unless stated otherwise, the nominal plant parameters are $K = 1$, $\tau_c = 1$ s, $\tau_d = 1$ s, and $T_s = 0.1$ s/sample. With these nominal values, it follows that $n_d = 10$ samples. Unless stated otherwise, for all examples in this paper, the command r and disturbance d are abruptly changing and are given by

$$r(t) = \begin{cases} 8, & 0 \le t < 0.2t_f, \\ -9, & 0.2t_f \le t < 0.6t_f, \\ 4, & 0.6t_f \le t \le t_f, \end{cases} \qquad d(t) = \begin{cases} -5, & 0 \le t < 0.4t_f, \\ 8, & 0.4t_f \le t \le t_f, \end{cases} \tag{34}$$

where the duration t_f of the simulation for each example is given by the final time on the horizontal axis of the associated time-history figures. Since r and d are not constant, these choices of the command and disturbance are not consistent with SBC. However, after each change in r and d, which are piecewise constant, the asymptotic error can be assessed, where "asymptotic" refers to the response just before the next change in r or d. Unless stated otherwise, for all examples in this paper, the sensor noise η is zero. Finally, for all examples in this paper, unless stated otherwise, the anti-windup thresholds are chosen to be $\overline{u} = -\underline{u} = 50$. Except in cases where r is infeasible and windup can occur, these values are inconsequential.

8 | LINEAR EXAMPLES SUPPORTING SBC

The examples in this section consider the performance of the adaptive digital PID controller for the basic servo loop shown in Figure 1, where $v = \mathcal{H}(u) = u$, $y = \mathcal{W}(y_\ell) = y_\ell$, and $\mathcal{L}(y_\ell) = 0$. In order to investigate the effect of plant parameters and controller weightings on closed-loop performance, the nominal plant parameters and controller weightings are modified in each example by perturbing them both above and below their nominal values. In particular the examples in this section consider the effect of variations in K, τ_c, τ_d, and T_s, where both fast and slow sampling are considered, and where "fast" refers to a sample interval that is shorter than the dead time and "slow" refers to a sample interval that is longer than the dead time. The values considered are shown in Table 1.

TABLE 1 Summary of adaptive digital PID control for linear examples supporting SBC.

Example	Investigated Effect	Remarks
1	RLS initialization $P_0 = p_0 I_3$	$p_0 = 0.1, 1, 10$
2	Slope $\nu = g'(0)$	$\nu = 0.01, 0.02, 0.04$
3	Gain K	$K = 0.5, 1, 2$
4	Time constant τ_c	$\tau_c = 0.2, 1, 5$ s
5	Dead time τ_d	$\tau_d = 0.49, 3, 5.01$ s
6	Fast sampling with $T_s < \tau_d$	$T_s = 0.047, 0.1, 0.23$ s/sample
7	Slow sampling with $T_s > \tau_d$	$T_s = 1.9, 5, 11.7$ s/sample
8	Sensor noise η	Uniform white noise with $\mu_\eta = 1, 2, 3$

Example 1. *RLS initialization* $P_0 = p_0 I_3$. Figure 6 shows asymptotic command following and disturbance rejection for $p_0 = 0.1, 1, 10$. Note that larger values of p_0 yield more aggressive response leading to faster rise time and larger overshoot. ◇

Example 2. *Slope* $\nu = g'(0)$. Figure 7 shows asymptotic command following and disturbance rejection for $\nu = 0.01, 0.02, 0.04$. Note that larger values of ν yield more aggressive response leading to faster rise time and larger overshoot. ◇

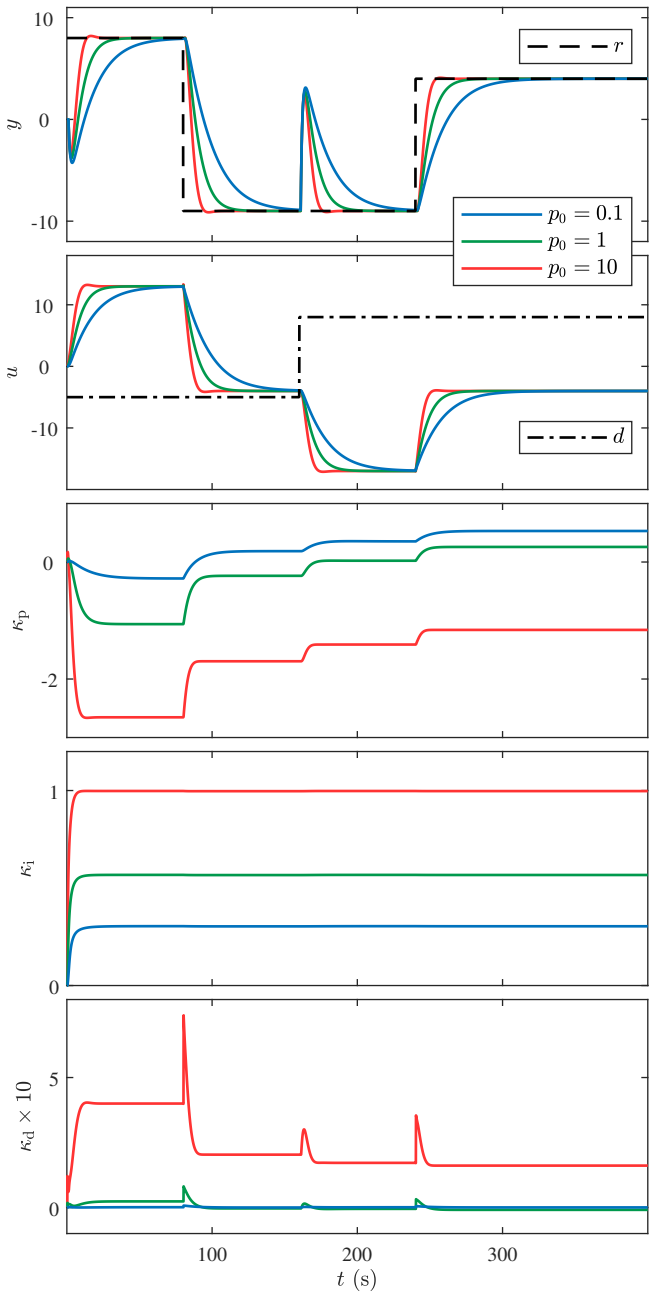

FIGURE 6 Example 1. Command following and disturbance rejection are achieved with $p_0 = 0.1, 1, 10$.

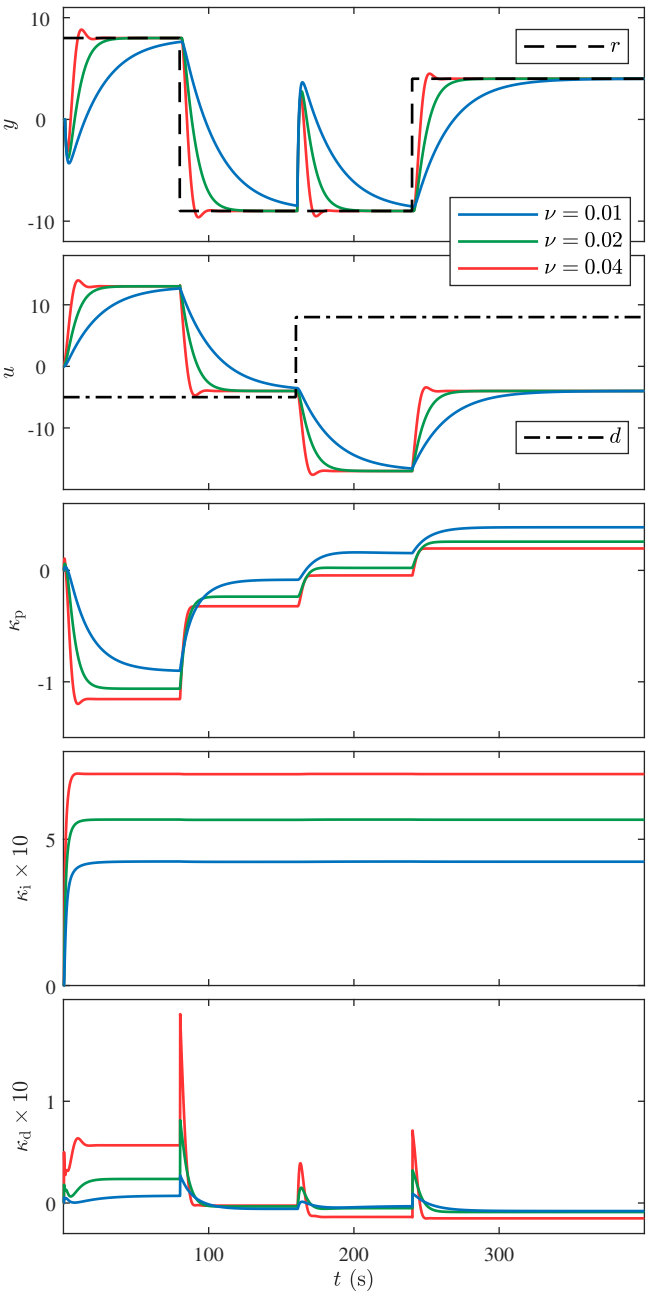

FIGURE 7 Example 2. Command following and disturbance rejection are achieved with $\nu = 0.01, 0.02, 0.04$.

Example 3. *Gain K*. Figure 8 shows asymptotic command following and disturbance rejection for $K = 0.5, 1, 2$. It can be seen that the overshoot increases as K increases. For a unit step command and zero disturbance, Figure 9 shows the percent overshoot and settling time as a function of K for several values of p_0. Reducing p_0 reduces the overshoot and tends to increase the settling time for small values of K, but can decrease the settling time for large values of K. ◇

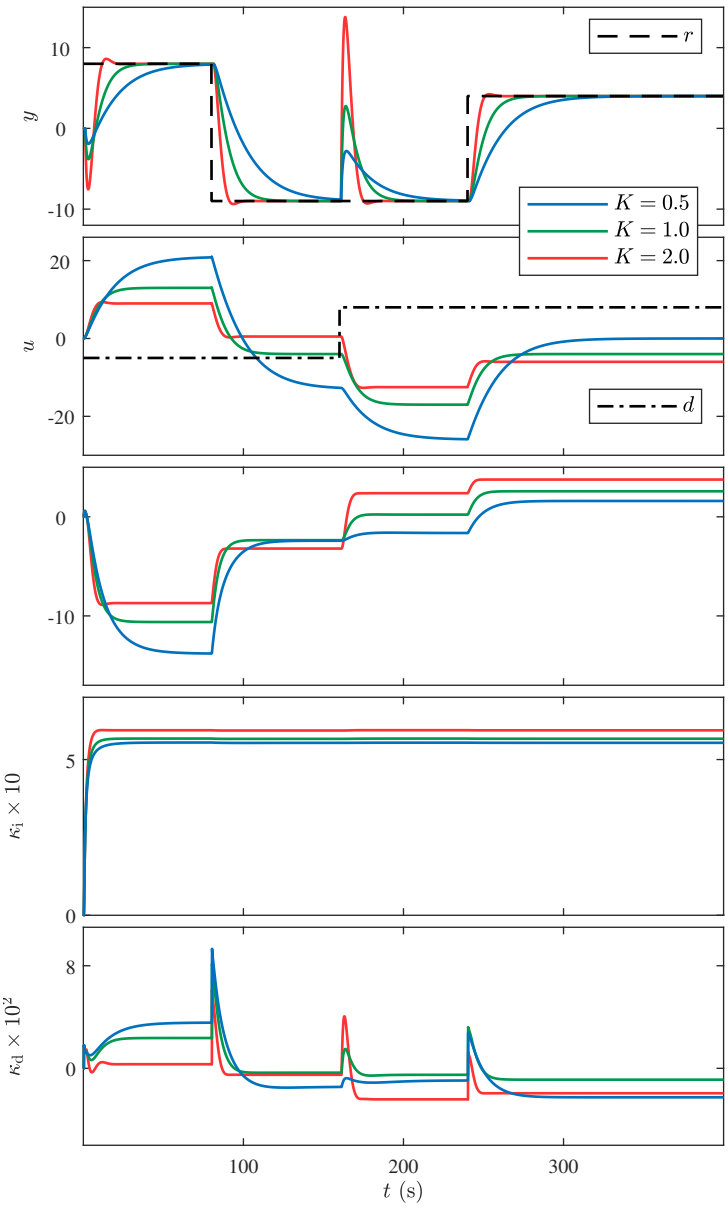

FIGURE 8 Example 3: Command following and disturbance rejection for various values of K. The overshoot is larger for larger K.

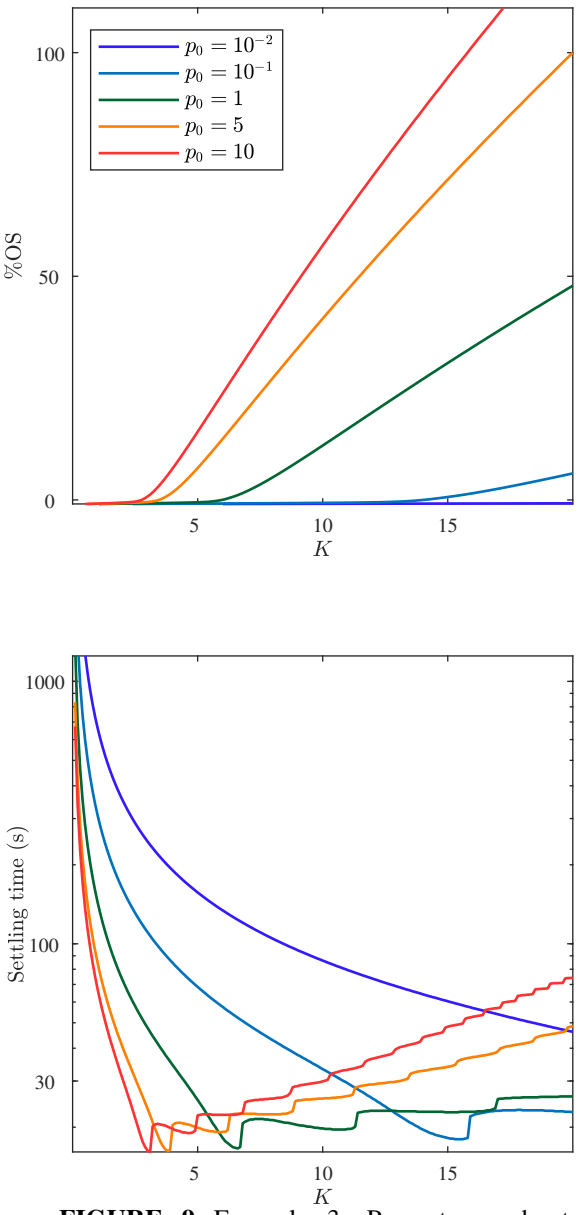

FIGURE 9 Example 3: Percent overshoot (%OS) and settling time as a function of K for several values of p_0 with $r = 1$ and $d = 0$.

Example 4. *Time constant* τ_c. Figure 10 shows asymptotic command following and disturbance rejection for $\tau_c = 0.2, 1, 5$ s. It can be seen that the overshoot increases as τ_c increases, which corresponds to slower plant dynamics. For a unit step command and zero disturbance, Figure 11 shows the percent overshoot and settling time as a function of τ_c for various values of p_0. Reducing p_0 reduces the overshoot and tends to increase the settling time for small values of τ_c, but can decrease the settling time for large values of τ_c. ◇

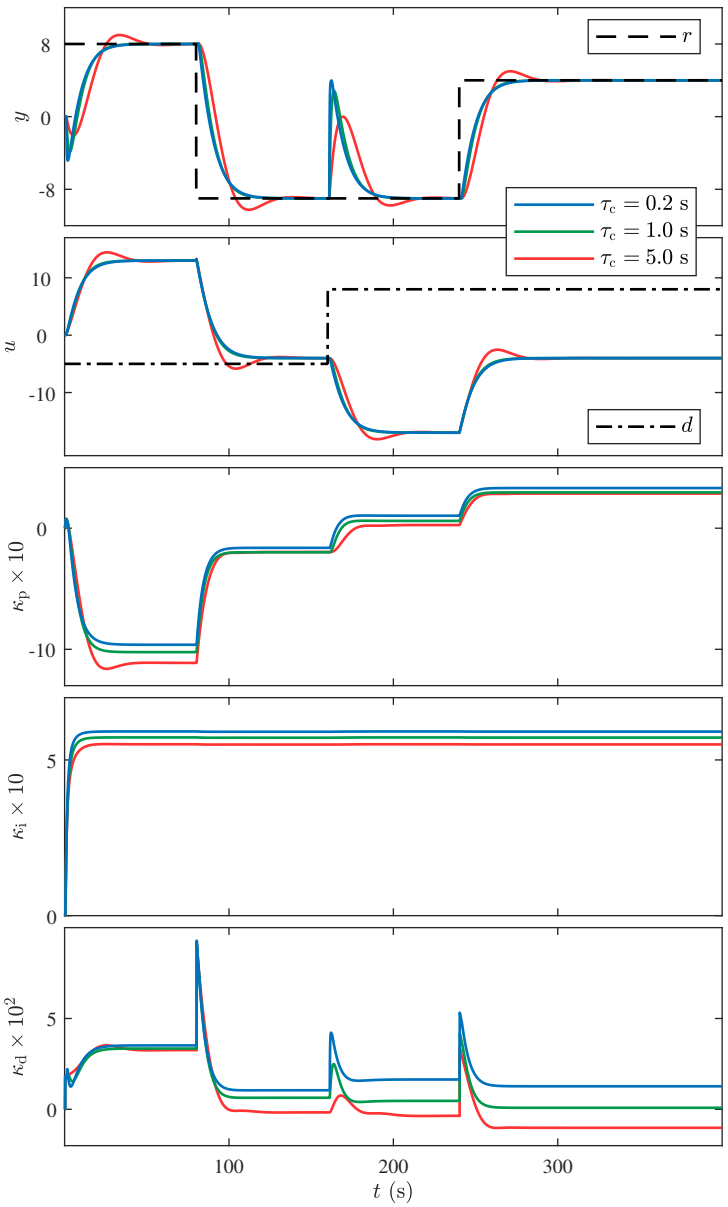

FIGURE 10 Example 4: Command following and disturbance rejection for various values of τ_c. The overshoot is larger for larger τ_c.

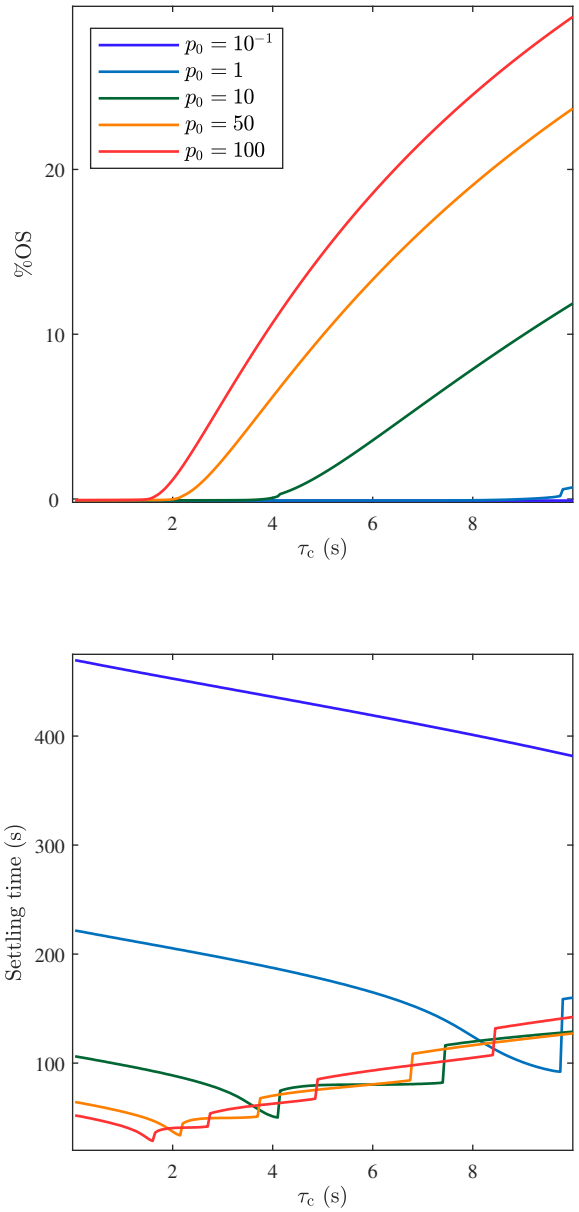

FIGURE 11 Example 4: Percent overshoot (%OS) and settling time as a function of τ_c for various values of p_0 with $r = 1$ and $d = 0$.

Example 5. *Dead time* τ_d. Figure 12 shows asymptotic command following and disturbance rejection for $\tau_d = 0.49, 3, 5.01$ s. Note that τ_d/T_s need not be an integer. It can be seen that the overshoot increases as τ_d increases. For a unit step command and zero disturbance, Figure 13 shows the percent overshoot and settling time as a function of τ_d for several values of p_0. Reducing p_0 reduces the overshoot and tends to increase the settling time for small values of τ_d, but can decrease the settling time for large values of τ_d. ◇

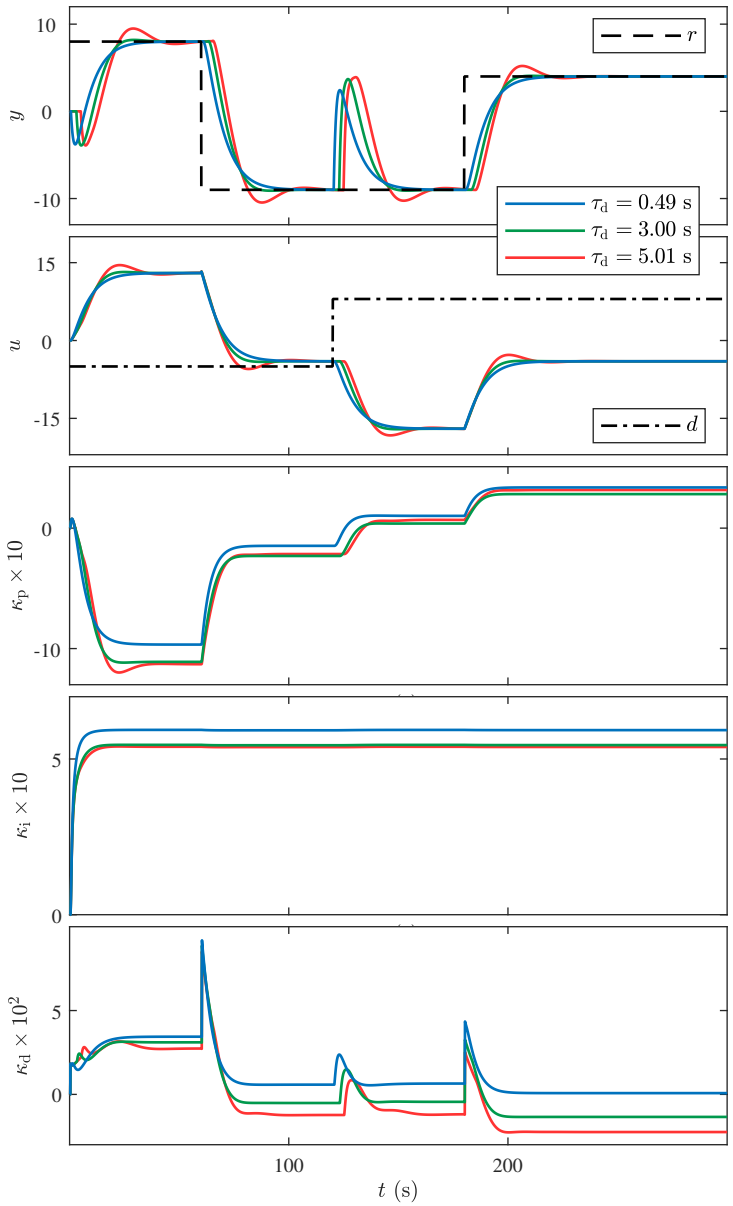

FIGURE 12 Example 5: Command following and disturbance rejection for various values of τ_d. The overshoot is larger for larger τ_d.

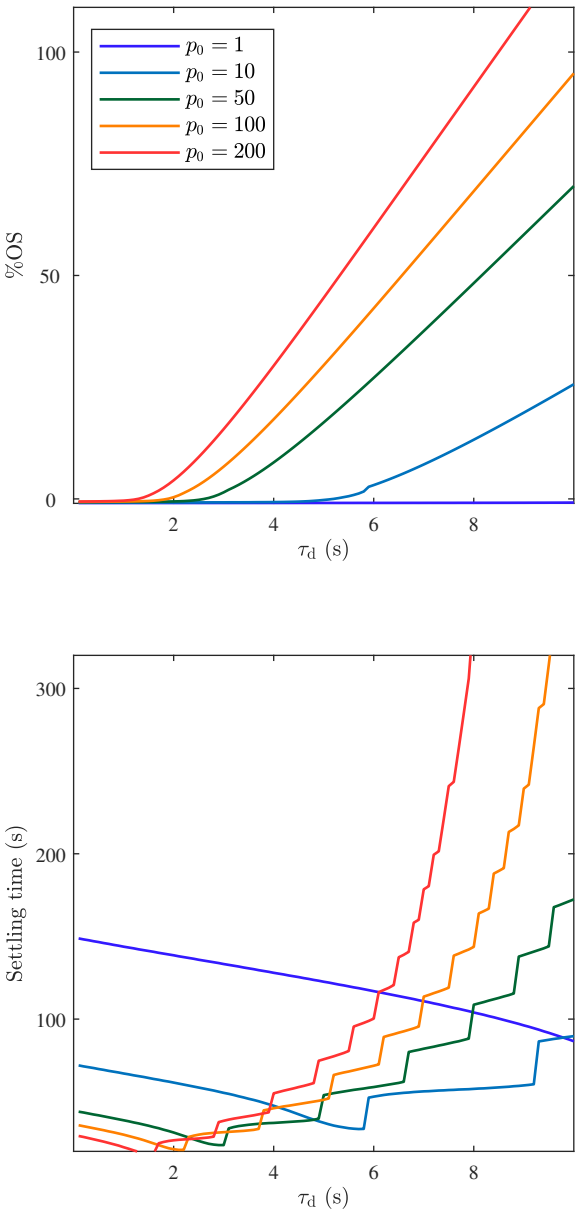

FIGURE 13 Example 5: Percent overshoot (%OS) and settling time as a function of τ_d for various values of p_0 with $r = 1$ and $d = 0$.

Example 6. *Fast sampling with $T_s < \tau_d$.* Figure 14 shows asymptotic command following and disturbance rejection for $T_s = 0.047, 0.1, 0.23$ s/sample. Fast sampling, that is, $T_s < \tau_d$, increases overshoot and decreases settling time. For a unit step command and zero disturbance, Figure 15 shows the percent overshoot and settling time as a function of T_s for several values of p_0. Reducing p_0 reduces the overshoot and increases the settling time. ◇

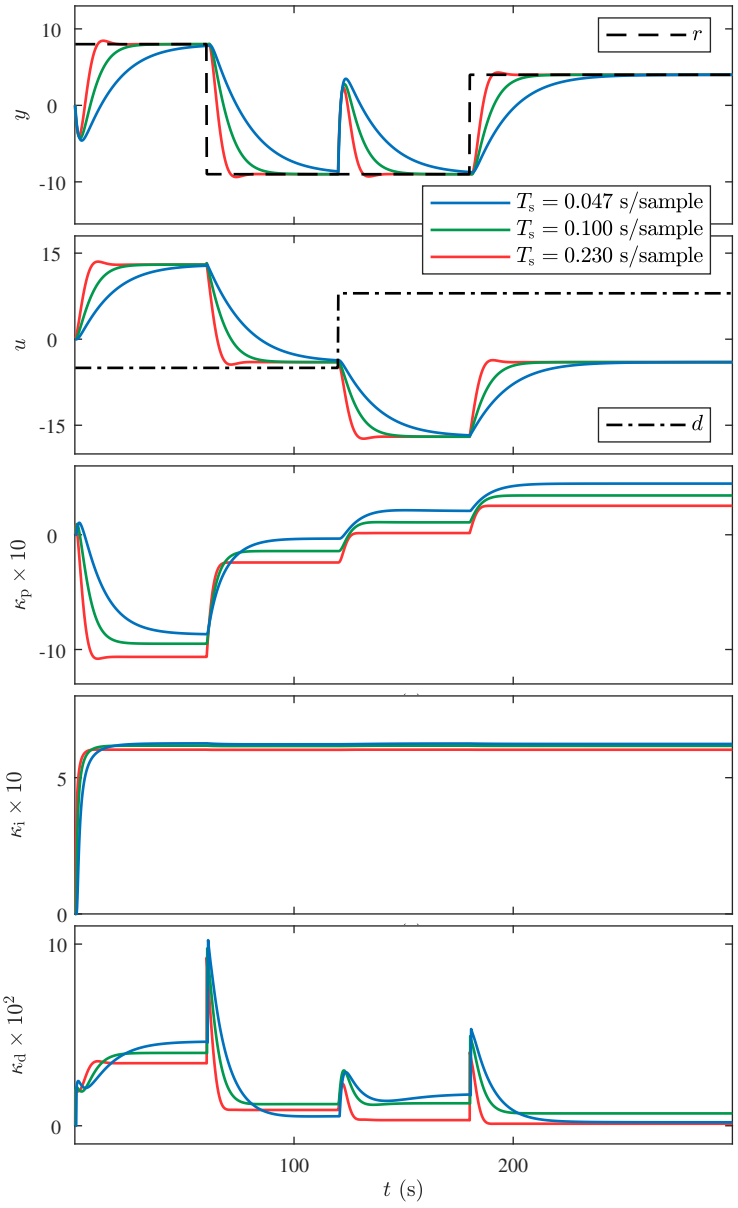

FIGURE 14 Example 6: Command following and disturbance rejection with fast sampling, that is, $T_s < \tau_d$. The overshoot is larger for larger sample times.

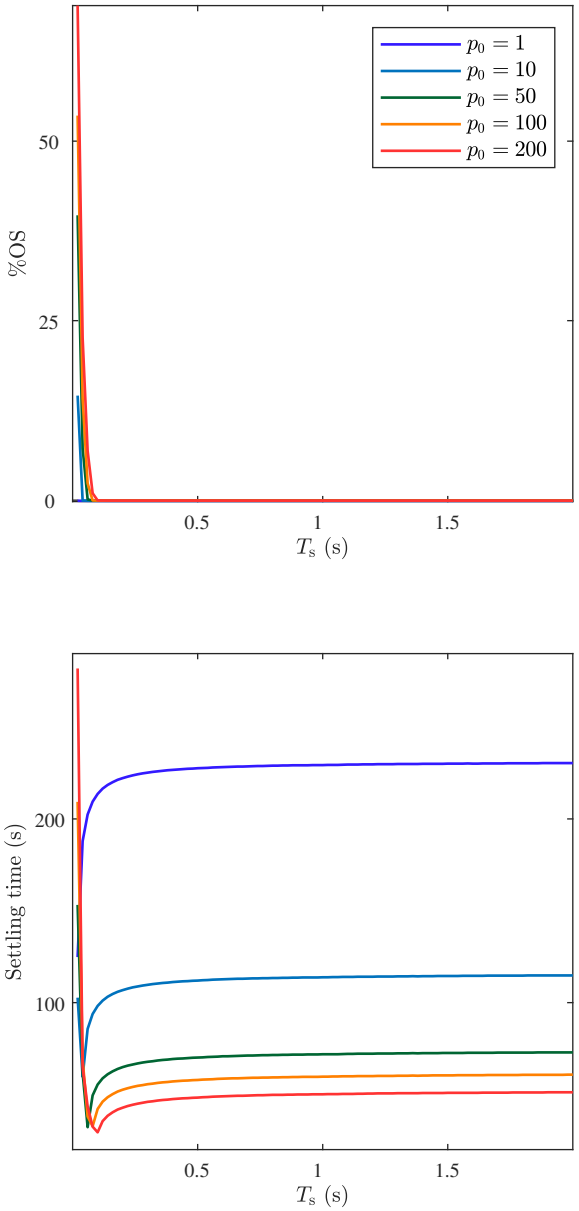

FIGURE 15 Example 6: Percent overshoot (%OS) and settling time as a function of T_s for various values of p_0 with $r = 1$ and $d = 0$.

Example 7. *Slow sampling with $T_s > \tau_d$.* Figure 16 shows asymptotic command following and disturbance rejection for $T_s = 1.9, 5, 11.7$ s/sample. Slow sampling, that is, $T_s > \tau_d$, tend to reduce or eliminate overshoot and increases settling time. ◇

Example 8. *Sensor noise η.* Assume that η is white noise that is uniformly distributed in $[0, 2\mu_\eta]$, where $\mu_\eta = 1, 2, 3$ is the mean. Figure 17 shows that the noisy measurement y_n and the response y approximately follow the command r. However, the response y has an offset with r, which is due to the nonzero-mean uniformly distributed white sensor noise. ◇

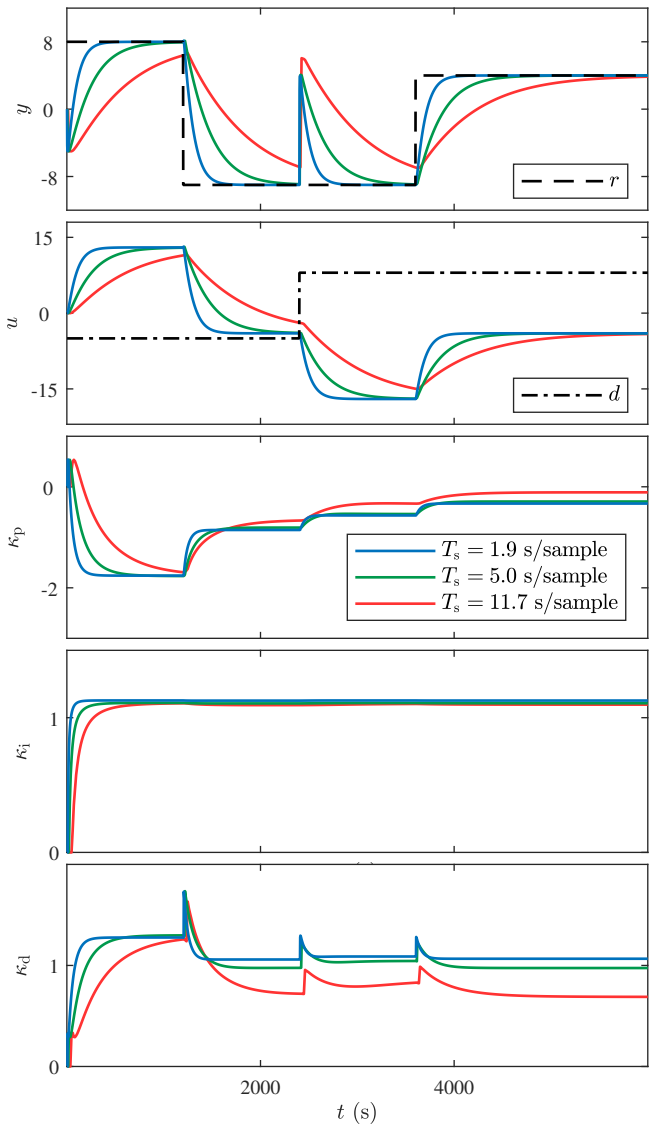

FIGURE 16 Example 7: Command following and disturbance rejection with slow sampling, that is, $T_s > \tau_d$. Slow sampling tend to reduce or eliminate overshoot and increases settling time.

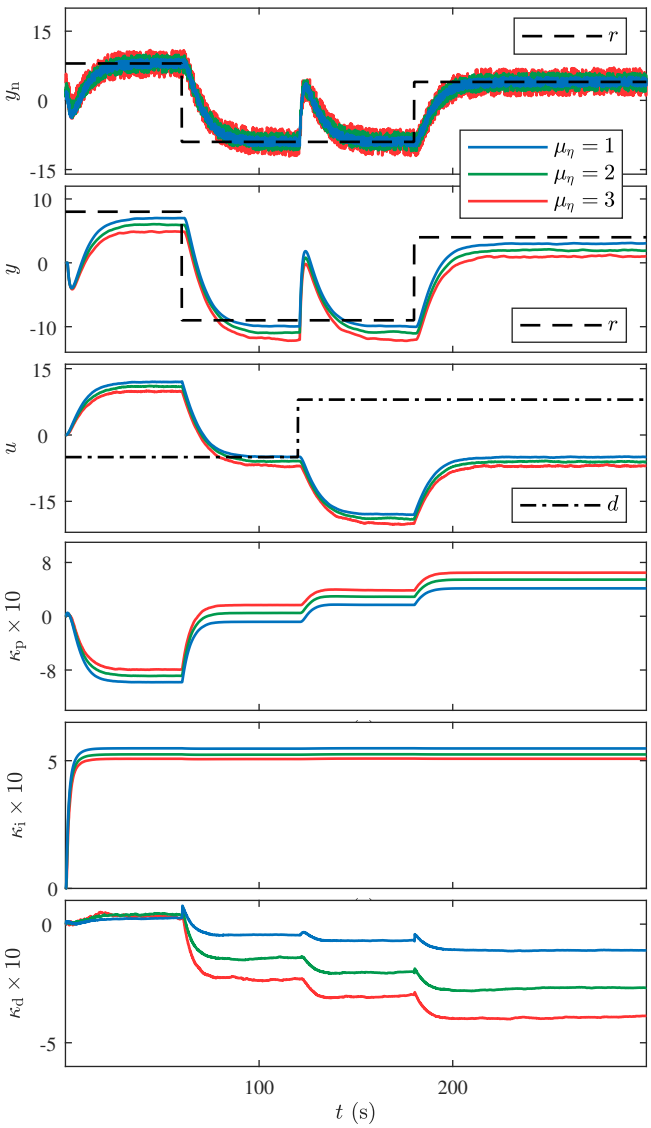

FIGURE 17 Example 8: Command following and disturbance rejection with nonzero-mean uniformly distributed white sensor noise. The noisy measurement y_n follows the command r; however, y has an offset with r.

9 | LINEAR EXAMPLES VIOLATING THE ASSUMPTIONS OF SBC

The examples in this section consider the performance of the adaptive digital PID controller for the basic servo loop shown in Figure 1 in the case where one or more of the assumptions (A1)–(A9) are violated. For all of the examples in this section, the sampled-data system is linear; that is, $v = \mathcal{H}(u) = u$, $y = \mathcal{W}(y_\ell) = y_\ell$, and $\mathcal{L}(y_\ell) = 0$. In order to investigate the effect of violating the assumptions of SBC, we consider examples with conditions that may be encountered in practice and that violate these assumptions. In particular, the examples in this section consider incorrect sign K, nonstep commands r, nonstep disturbances d, sensor noise η, actuator dynamics, slowly varying K, τ_c, τ_d, abruptly varying K, τ_c, τ_d, and three kinds of sampling jitter. The values considered are summarized in Table 2.

TABLE 2 Summary of adaptive digital PID control for linear examples violating the assumptions of SBC. The notation in the third column is defined within the respective example.

Example	Investigated Effect	Remarks
9	Incorrect sign K	$K = \pm 1$, $\sigma = \pm 1$
10	Sigmoidal command r	$p_0 = 10^{-8}, 10^{-7}, 10^{-6}$
11	Harmonic and broadband disturbance d	$d(t) = 15 + 2\sin 0.5t + \overline{d}(t)$
12	Sensor noise η	Gaussian white noise with $\sigma_\eta = 0.5, 1, 2$
13	Actuator dynamics	$f_a = 0.05, 0.1, 0.2$ Hz
14	Slowly varying K	$K_{max} = 3, 5$
15	Slowly varying τ_c	$\tau_{c,max} = 5, 10$
16	Slowly varying τ_d	$\tau_{d,max} = 3, 6$
17	Abruptly varying K	$K = 1$ changes to $\bar{K} = 4, 7$
18	Abruptly varying τ_c	$\tau_c = 1$ changes to $\bar{\tau}_c = 0.1, 10$
19	Abruptly varying τ_d	$\tau_d = 1$ changes to $\bar{\tau}_d = 4, 8$
20	Absolute clock jitter with asynchronous A/D and D/A devices	$T_{s,k} = 1 + s_k - s_{k-1}$, $T_{h,k} = 1 + h_k - h_{k-1}$
21	Relative clock jitter with synchronous A/D and D/A devices	$T_{s,k} = T_{h,k} = 1 + s_k$
22	Relative clock jitter with asynchronous A/D and D/A devices	$T_{s,k} = 1 + s_k$, $T_{h,k} = 1 + h_k$

Example 9. *Incorrect* sign K. Since $\mathcal{H}(u) = u$ and $\mathcal{W}(y_\ell) = y_\ell$, (A9) implies that σ must be chosen such that $\sigma = \operatorname{sign} K$. Figure 18 shows asymptotic command following and disturbance rejection for the cases where $(K, \sigma) = (1, 1), (-1, -1)$, that is, σ is chosen such that $\sigma = \operatorname{sign} K$. Figure 18 also shows the cases where $(K, \sigma) = (-1, 1), (1, -1)$, that is, the choice of σ does not satisfy $\sigma = \operatorname{sign} K$. In this case, the control u and the response y do not converge. ◇

Example 10. *Sigmoidal command* r. Consider the case, where the command r is not piecewise-constant; specifically, consider the sigmoidal command

$$r(t) = \begin{cases} \dfrac{17}{1 + e^{0.01(t-120)}} - 9, & 0 \le t < 200\,\text{s}, \\ \dfrac{13}{1 + e^{0.01(260-t)}} - 9, & t \ge 200\,\text{s}. \end{cases} \tag{35}$$

Figure 19 shows asymptotic command following and disturbance rejection for $p_0 = 10^{-8}, 10^{-7}, 10^{-6}$. Note that the overshoot increases as p_0 increases. ◇

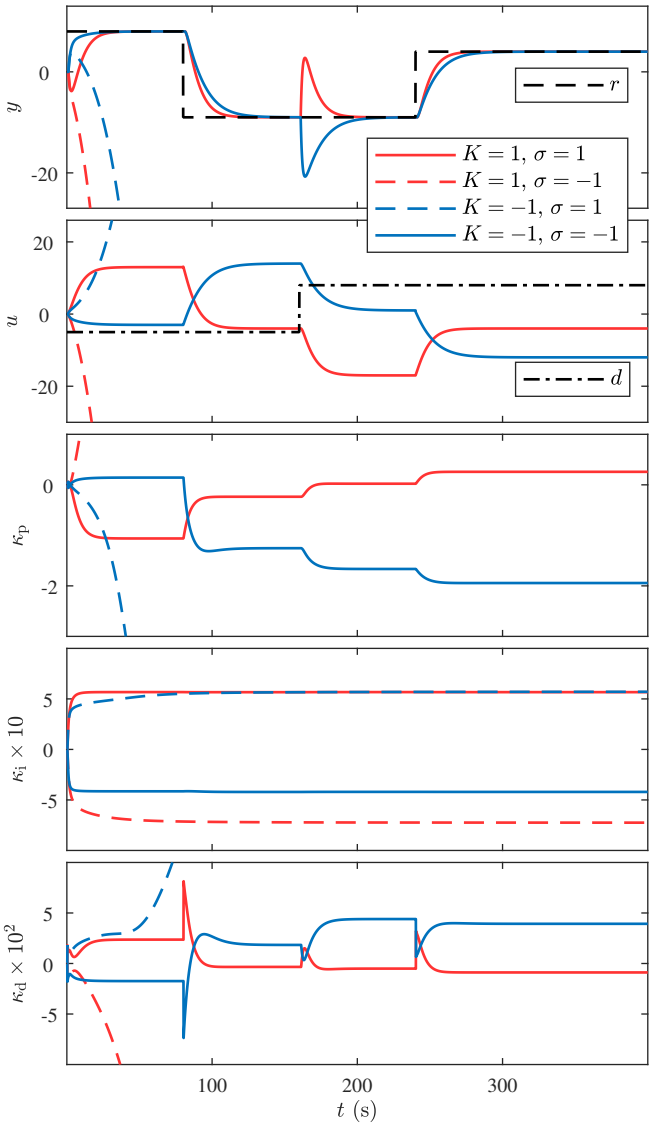

FIGURE 18 Example 9: Command following and disturbance rejection for various choices of K and σ. Asymptotic command following and disturbance rejection is only achieved in the case $\sigma = \operatorname{sign} K$.

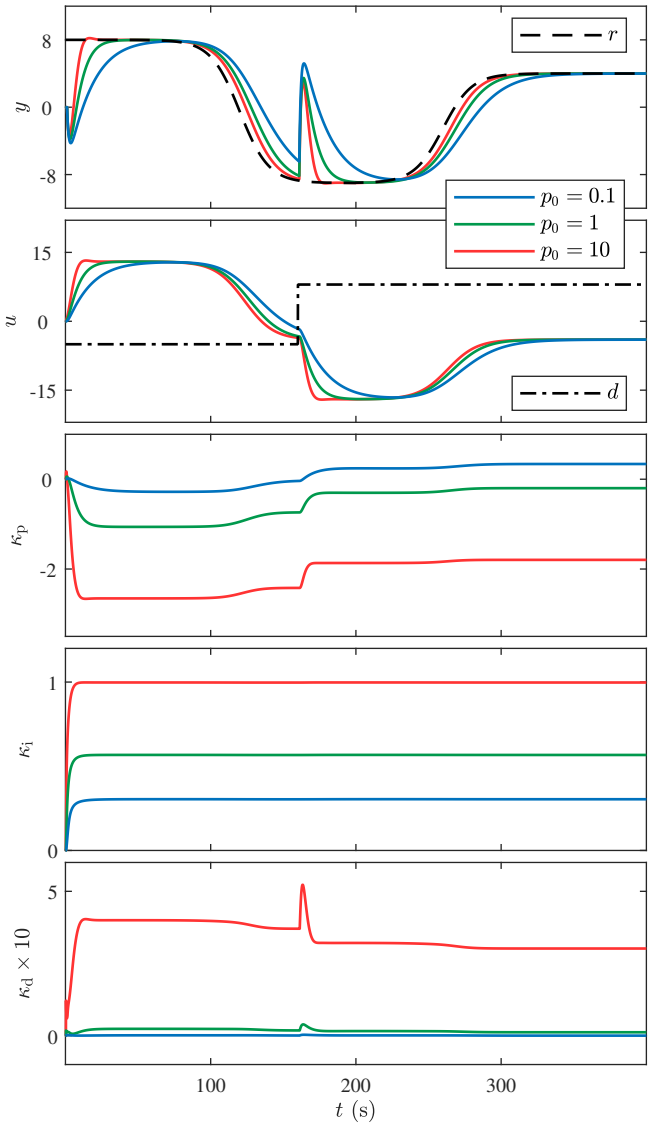

FIGURE 19 Example 10: Command following and disturbance rejection with a sigmoidal command, where the measurement y tends to follow the nonconstant command r closely.

Example 11. *Harmonic and broadband disturbance d.* Consider the case where the disturbance d is not constant; specifically, consider

$$d(t) = 15 + 2\sin 0.5t + \overline{d}(t), \tag{36}$$

where $\overline{d}$ is zero-mean, Gaussian continuous-time white noise with approximate intensity[80,81,82] $1000\sigma_d^2/T_s = 1000/T_s$, where $\sigma_d = 1$ is the standard deviation of the discrete-time Gaussian random variable at each time step, and the intensity is the variance (i.e., the square of the standard deviation) divided by the numerical integration step size $T_s/1000$. Figure 20 shows that the controller cannot eliminate the effect of disturbance on the response y, however, the response y approximately follows the command r with oscillations. ◇

Example 12. *Sensor noise η.* Assume that η is Gaussian white noise with mean 2 and intensity $1000\sigma_\eta^2/T_s$, where $\sigma_\eta = 0.5, 1, 2$. Figure 21 shows that the noisy measurement y_n and the response y approximately follow the command r. However, the response y has an offset with r, which is due to the nonzero-mean Gaussian white sensor noise. ◇

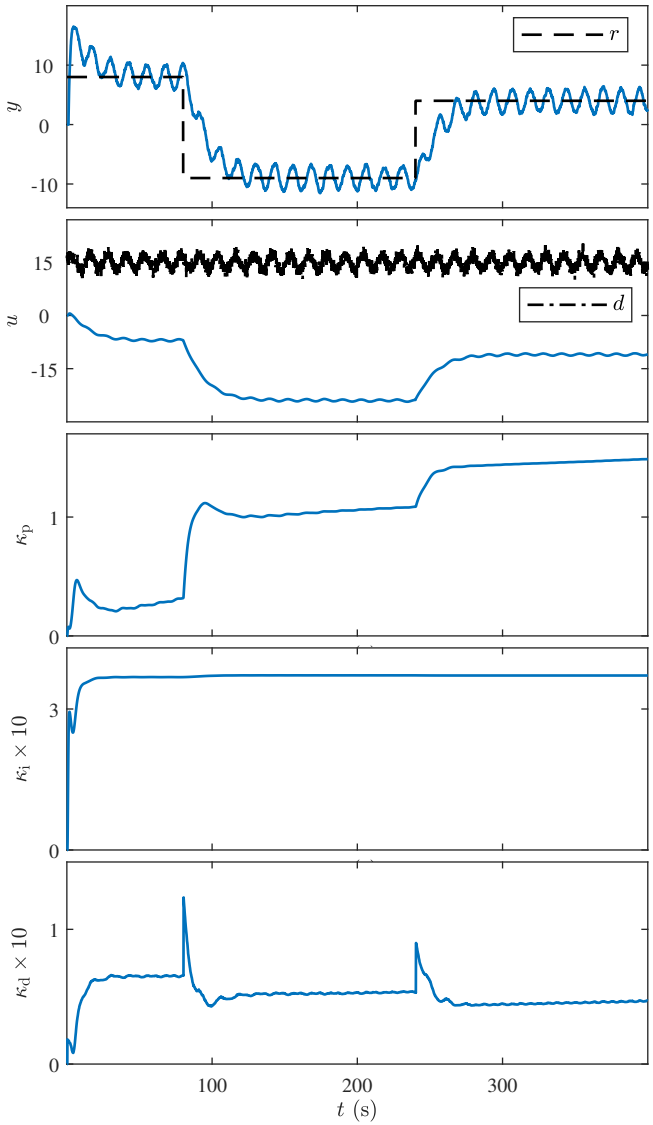

FIGURE 20 Example 11: Command following and disturbance rejection with nonzero-mean Gaussian-plus-harmonic disturbance. The controller is unable to follow the command asymptotically. The response y oscillates about the command r.

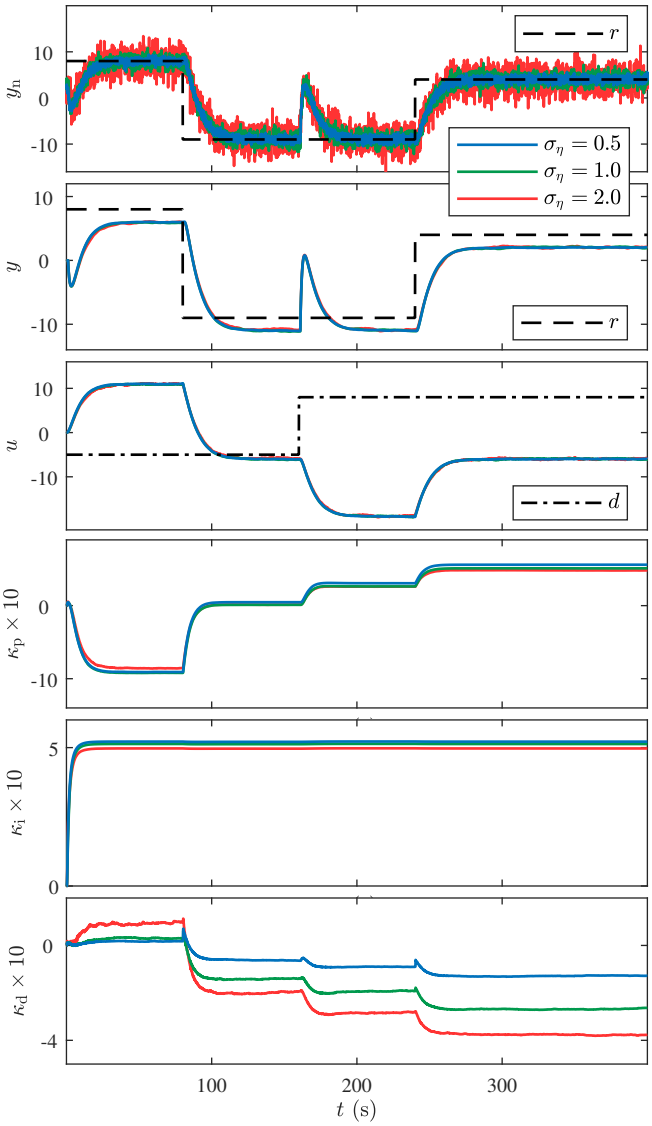

FIGURE 21 Example 12: Command following and disturbance rejection with nonzero-mean Gaussian white sensor noise. The noisy measurement y_n follows the command r; however, y has an offset with r due to the nonzero-mean Gaussian white sensor noise.

Example 13. *Actuator dynamics.* Assume that the actuator has dynamics given by

$$G_{\mathrm{a}}(s) = \frac{\omega_{\mathrm{a}}^2}{s^2 + \sqrt{2}\omega_{\mathrm{a}} s + \omega_{\mathrm{a}}^2}, \tag{37}$$

where $\omega_{\mathrm{a}} \triangleq 2\pi f_{\mathrm{a}}$, and f_{a} is the actuator cutoff frequency. Figure 22 shows asymptotic command following and disturbance rejection for $f_{\mathrm{a}} = 0.05, 0.1, 0.2$. The overshoot decreases as f_{a} is increased. Note that, since $\tau_{\mathrm{c}} = 1$, the actuator dynamics are slower than the plant dynamics. ◇

Example 14. *Slowly varying K.* Assume that K increases linearly from 1 to $K_{\max}$ from $t = 0$ s to $t = 150$ s and then decreases linearly from $K_{\max}$ to 1 from $t = 150$ s to $t = 300$ s. Figure 23 shows asymptotic command following and disturbance rejection for $K_{\max} = 3, 5$. Numerical simulations suggest that if the rate of change of K is sufficiently small, then asymptotic command following and disturbance rejection can be achieved. ◇

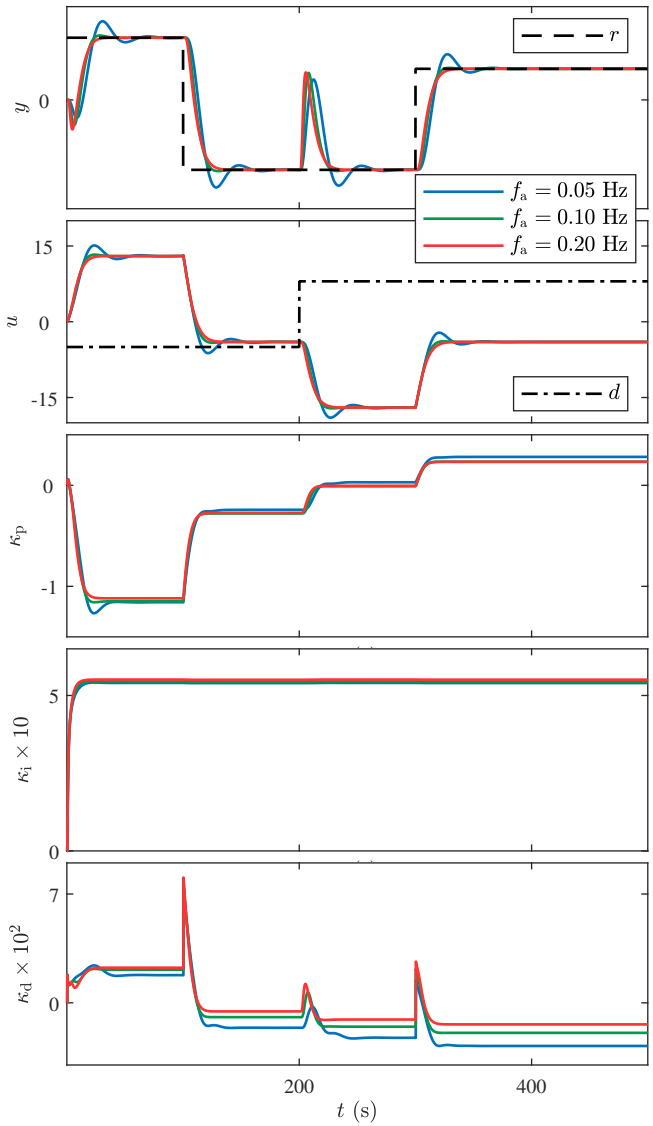

FIGURE 22 Example 13: Command following and disturbance rejection with an actuator whose second-order dynamics are slower than the plant dynamics.

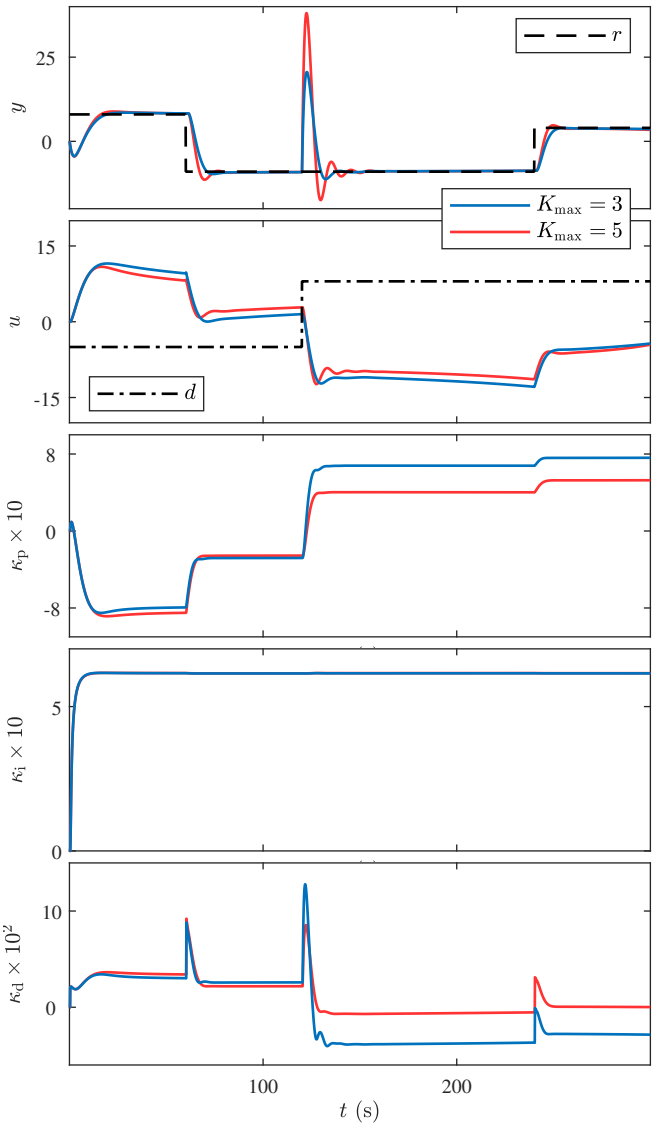

FIGURE 23 Example 14: Command following and disturbance rejection can be achieved with slowly varying gain K.

Example 15. *Slowly varying* τ_c. Assume that τ_c increases linearly from 1 s to $\tau_{c,\max}$ from $t = 0$ s to $t = 150$ s and then decreases linearly from $\tau_{c,\max}$ to 1 s from $t = 150$ s to $t = 300$ s. Figure 24 shows asymptotic command following and disturbance rejection for $\tau_{c,max} = 3, 5$. Numerical simulations suggest that if the rate of change of τ_c is sufficiently small, then asymptotic command following and disturbance rejection can be achieved. ◇

Example 16. *Slowly varying* τ_d. Assume that τ_d increases linearly from 1 s to $\tau_{d,\max}$ from $t = 0$ s to $t = 150$ s and then decreases linearly from $\tau_{d,\max}$ to 1 s from $t = 150$ s to $t = 300$ s. Figure 25 shows asymptotic command following and disturbance rejection for $\tau_{d,max} = 3, 6$. Numerical simulations suggest that if the rate of change of τ_d is sufficiently small, then asymptotic command following and disturbance rejection can be achieved. ◇

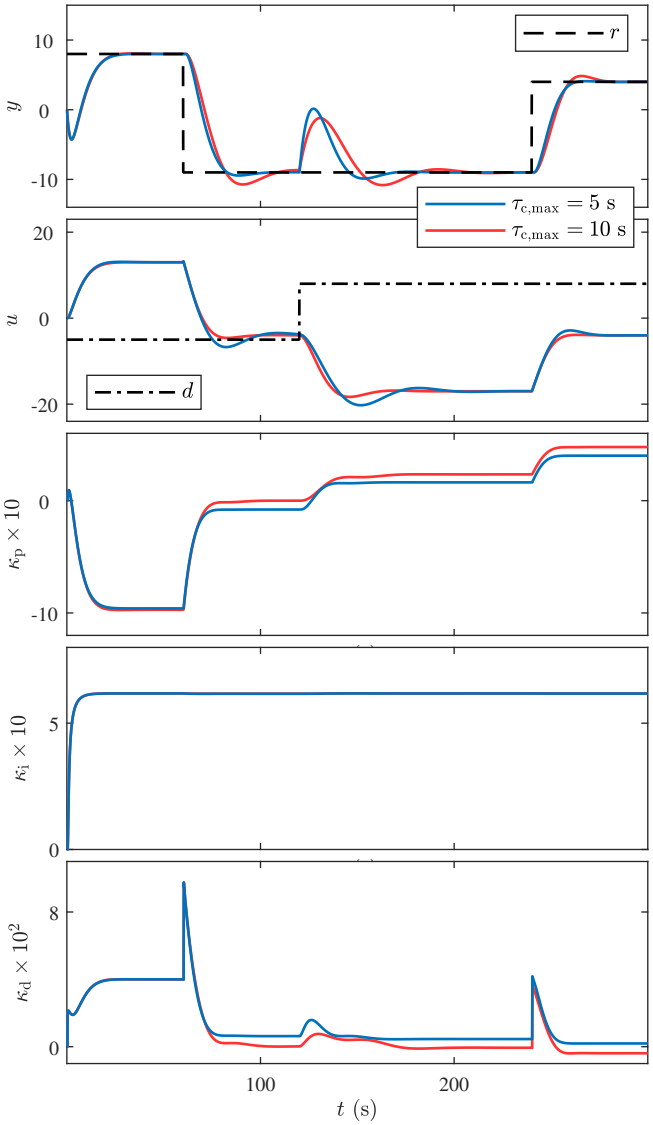

FIGURE 24 Example 15: Command following and disturbance rejection can be achieved with slowly varying time constant τ_c.

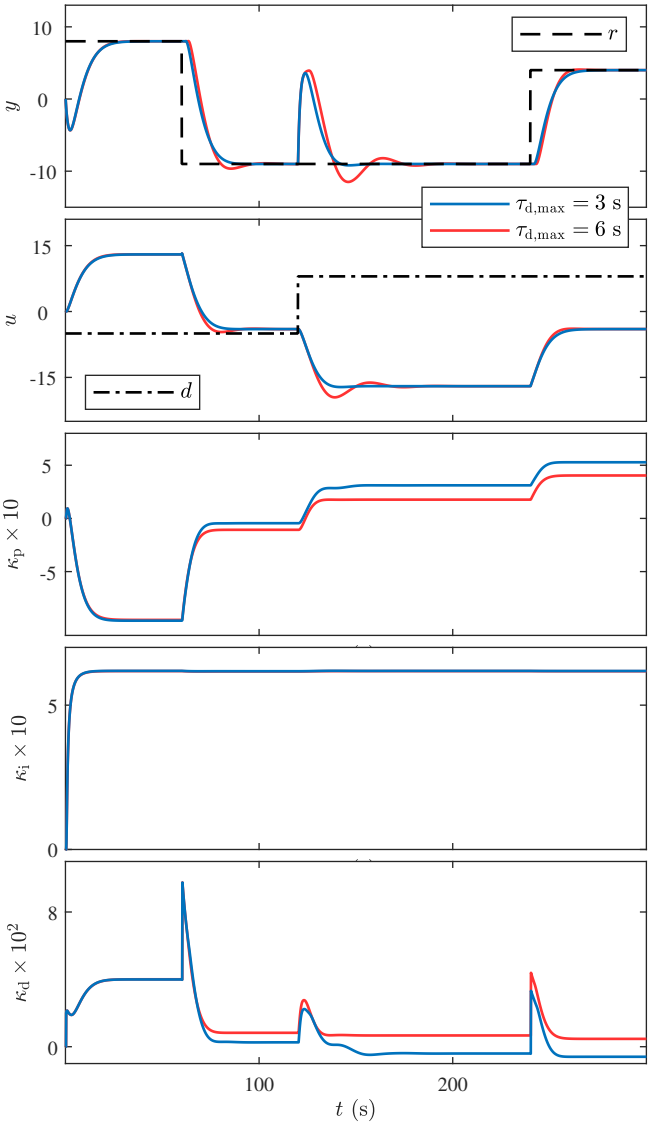

FIGURE 25 Example 16: Command following and disturbance rejection can be achieved with slowly varying dead time τ_d.

Example 17. *Abruptly varying K.* Assume that K increases abruptly from 1 to $\bar{K}$ at $t = 90$ s. Figure 26 shows asymptotic command following and disturbance rejection for $\bar{K} = 4, 7$. In the case where $\bar{K} = 7$, the closed-loop system becomes unstable immediately after the abrupt change but stability is recovered. Figure 27 shows the error-normalization g and the points computed during the simulation. ◇

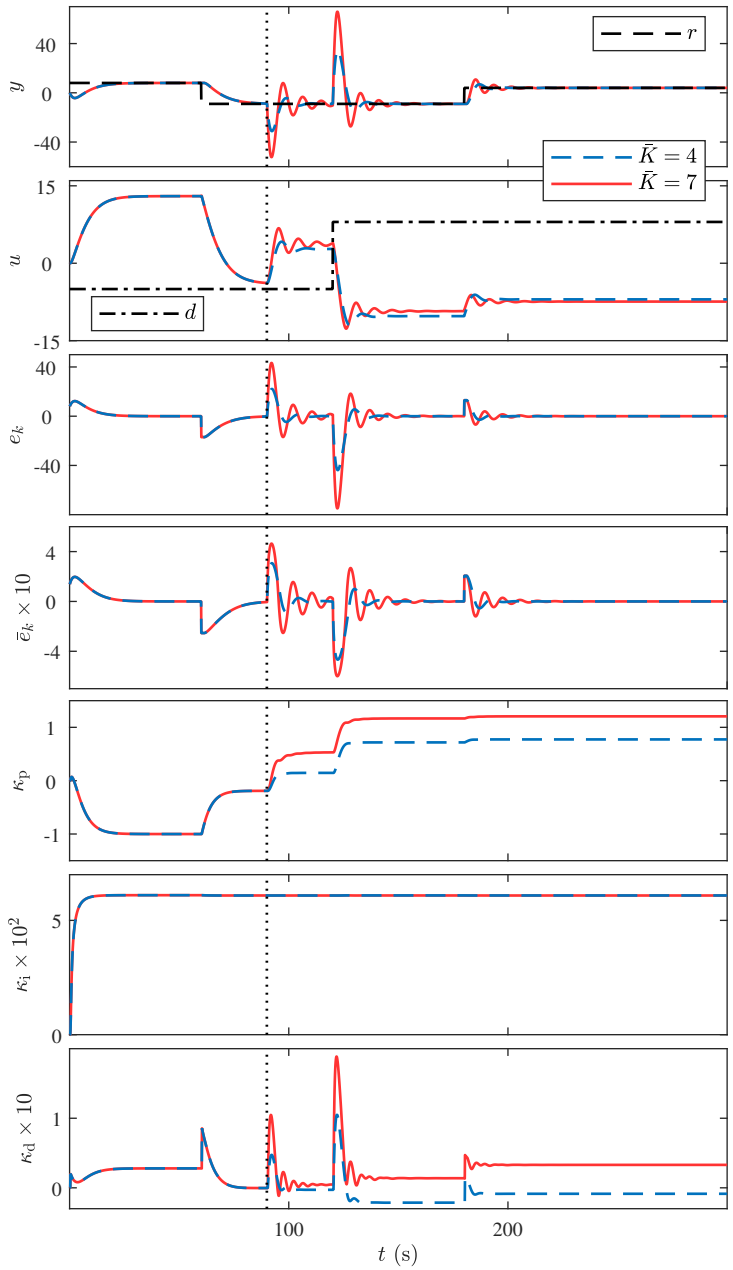

FIGURE 26 Example 17: Command following and disturbance rejection with abruptly varying gain K. The controller adapts to the abrupt changes in the gain K and achieves asymptotic command following and disturbance rejection. For $\bar{K} = 7$ the closed-loop is unstable for some time after the abrupt change in K and the adaptive controller recovers closed-loop stability.

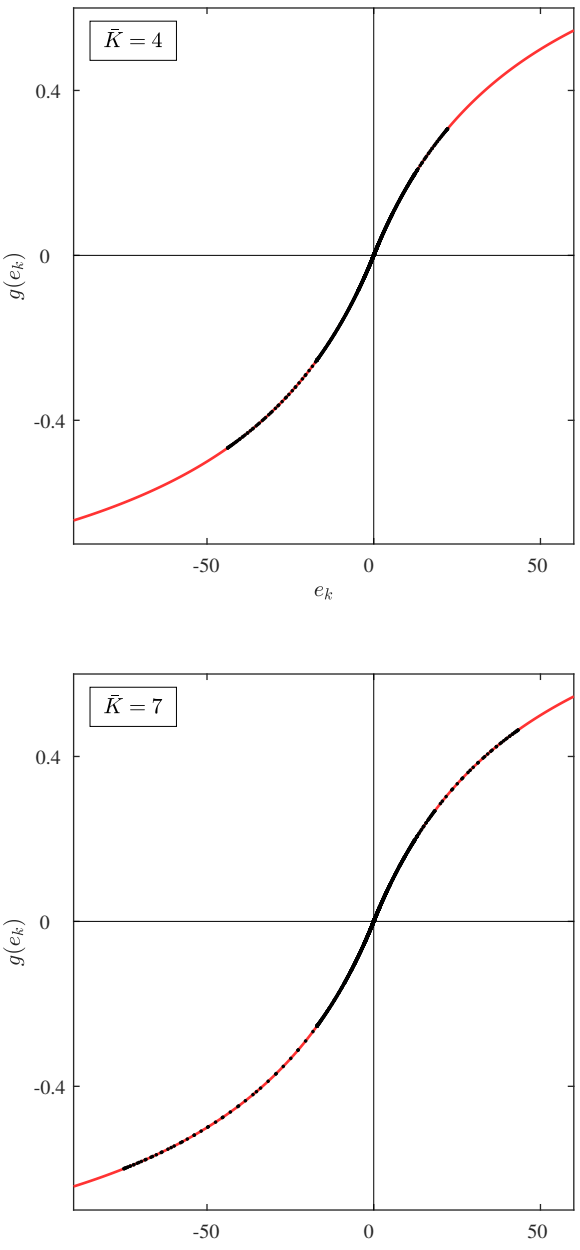

FIGURE 27 Example 17: Error-normalization g as a function of e_k. Each black dot denotes a point $(e_k, g(e_k))$ computed during the simulation.

Example 18. *Abruptly varying* τ_c. Assume that τ_c increases abruptly from 1 s to $\bar{\tau}_c$ at $t = 180$ s. Figure 29 shows asymptotic command following and disturbance rejection for $\bar{\tau}_c = 0.1, 10$. In this case, the closed-loop system remains stable after the abrupt change in τ_c. ◇

Example 19. *Abruptly varying* τ_d. Assume that τ_d increases abruptly from 1 s to $\bar{\tau}_d$ at $t = 270$ s. Figure 28 shows asymptotic command following and disturbance rejection for $\bar{\tau}_d = 4, 8$. In the case where $\bar{\tau}_d = 8$, the closed-loop system becomes unstable immediately after the abrupt change but the adaptive digital PID control restabilizes the closed-loop system. ◇

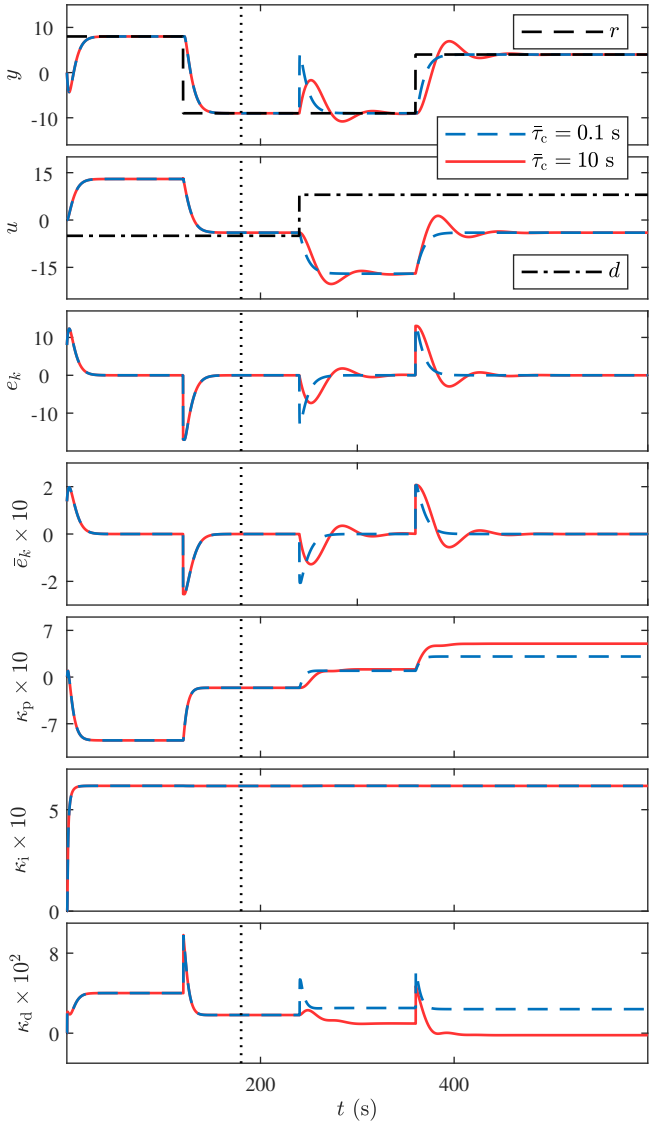

FIGURE 28 Example 18: Command following and disturbance rejection with abruptly changing time constant τ_c. The controller adapts to the abrupt changes in the time constant τ_c and achieves asymptotic command following and disturbance rejection.

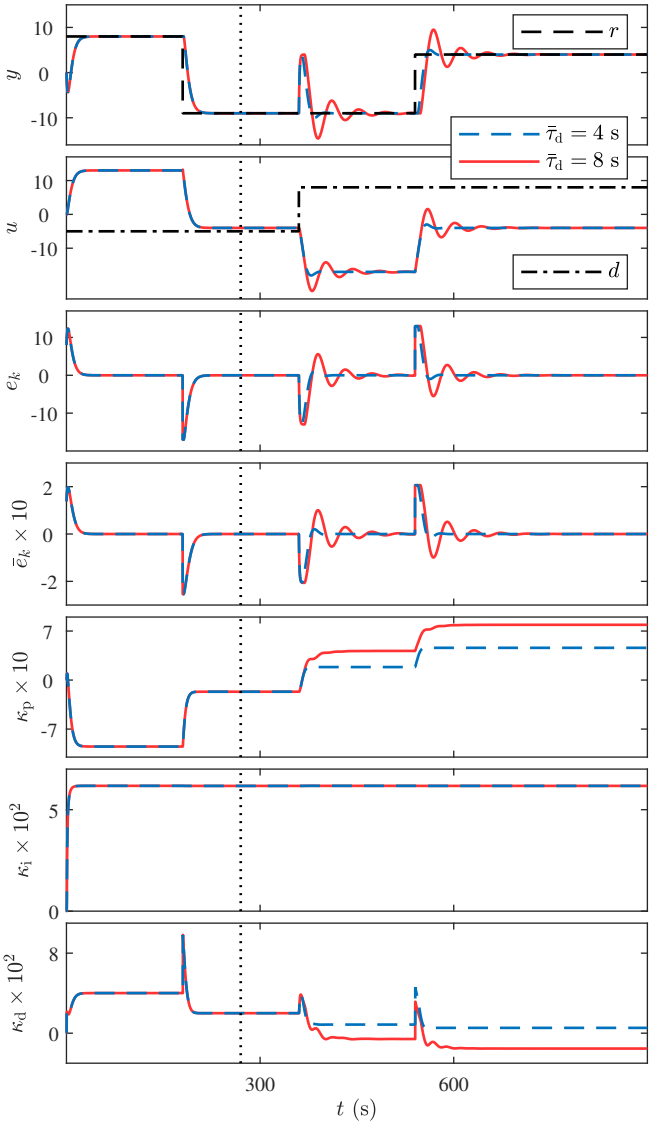

FIGURE 29 Example 19: Command following and disturbance rejection with abruptly changing dead time τ_d. The controller adapts to the abrupt changes in the dead time τ_d and achieves asymptotic command following and disturbance rejection. For $\bar{\tau}_d = 8$ the closed-loop is unstable for some time after the abrupt change in τ_d and the adaptive controller recovers closed-loop stability.

Example 20. *Absolute clock jitter with asynchronous A/D and D/A devices.* Assume that the A/D and D/A devices operate asynchronously, and thus the sample interval $T_{s,k}$ and the hold interval $T_{h,k}$ vary at each time step k due to timing jitter as shown in Figure 30. Let $T_{s,k}$ and $T_{h,k}$ be given by

$$T_{s,k} = 1 + s_k - s_{k-1}, \quad T_{h,k} = 1 + h_k - h_{k-1}, \tag{38}$$

where s_k and h_k are uniformly distributed random variables in $[0, j]$, where $j \in \{0.2, 0.4, 0.8\}$. Figure 31 shows that, as in the case of slowly varying dead time shown in Example 16, the jitter has no discernible effect on the closed-loop performance. ◇

FIGURE 30 Example 20: Timing diagram for absolute clock jitter with asynchronous A/D and D/A devices. The black vertical bars indicate the nominal absolute clock intervals.

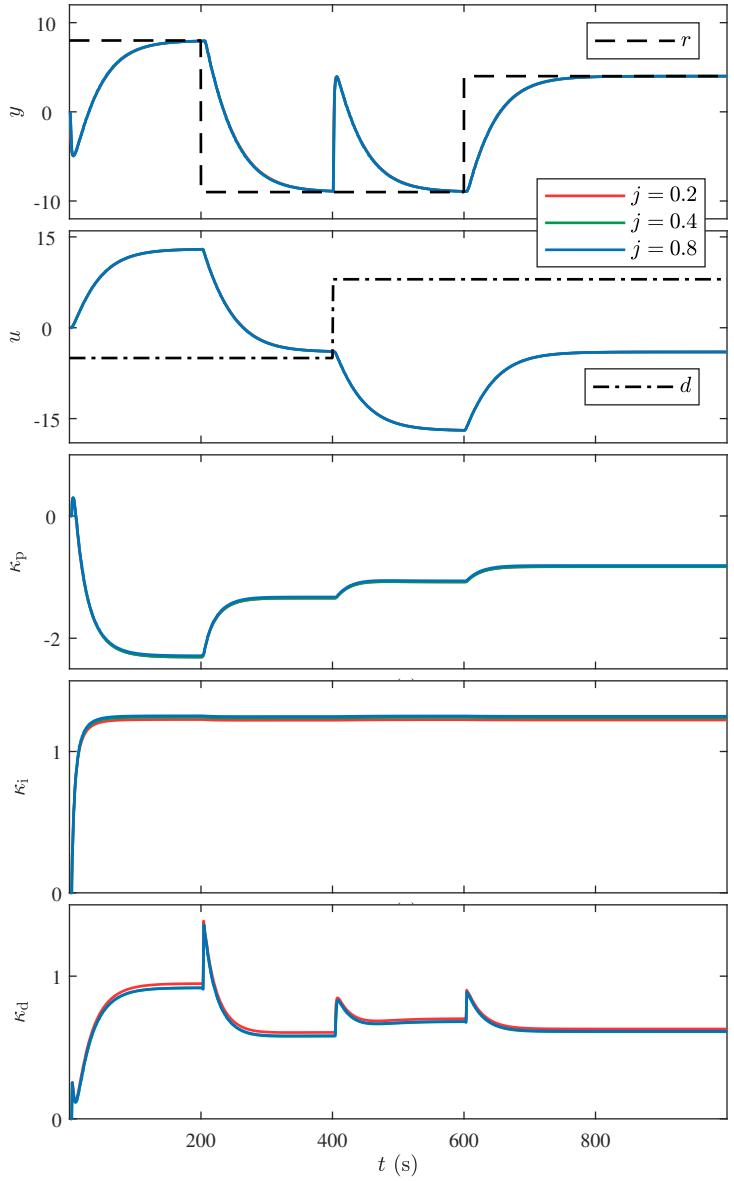

FIGURE 31 Example 20: Command following and disturbance rejection with absolute clock jitter with asynchromous A/D and D/A devices. No discernible effect on the closed-loop performance is observed.

Example 21. *Relative clock jitter with synchronous A/D and D/A.* Assume that the A/D and D/A devices operate synchronously, that is $T_{s,k} = T_{h,k}$, but the sample interval $T_{s,k}$ varies at each time step k due to timing jitter as shown in Figure 32. Let j be a positive integer, and let $T_{s,k}$ be given by

$$T_{s,k} = 1 + s_k, \tag{39}$$

where s_k is a uniformly distributed random variable in $[0, j]$. Let $j \in \{0.2, 0.4, 0.8\}$. Figure 33 shows that, as in the case of slowly varying dead time shown in Example 16, the jitter has no discernible effect on the closed-loop performance. ◇

FIGURE 32 Example 21: Timing diagram for relative clock jitter with synchronous A/D and D/A devices. The interval between the blue and green vertical bars and the black vertical bars indicates the nominal relative clock intervals.

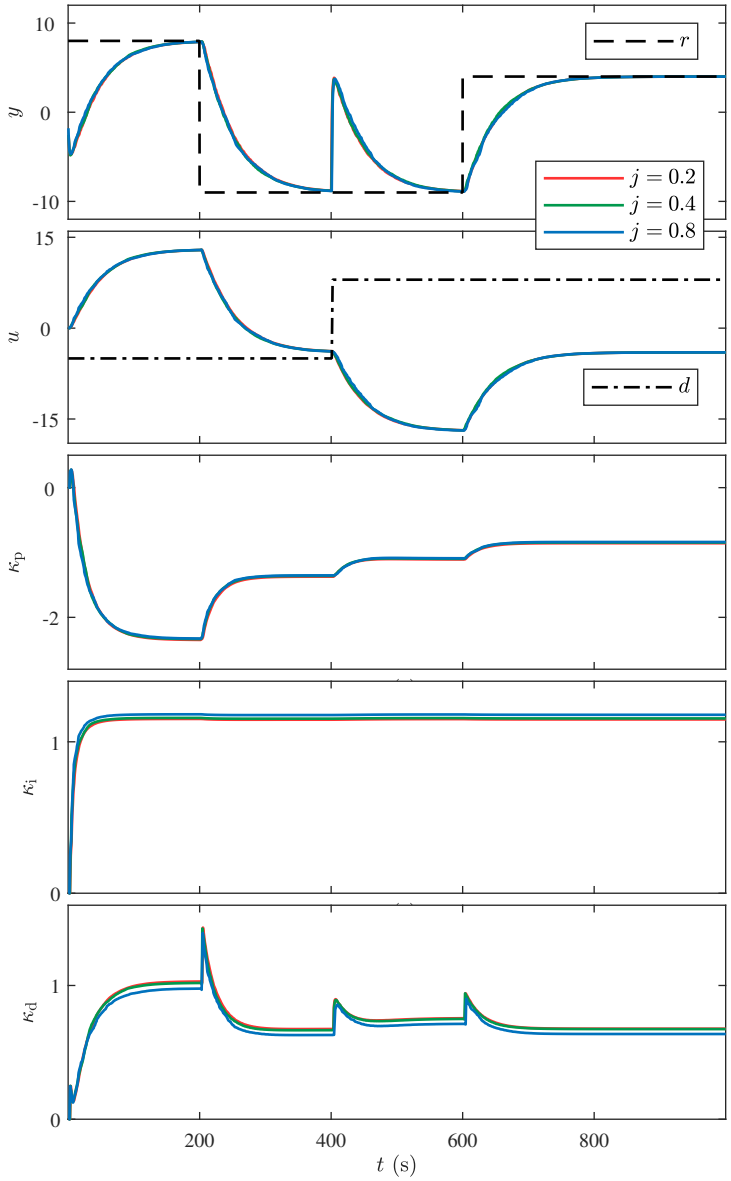

FIGURE 33 Example 21: Command following and disturbance rejection with relative clock jitter with synchromous A/D and D/A devices. No discernible effect on the closed-loop performance is observed.

Example 22. *Relative clock jitter with asynchronous A/D and D/A devices.* Assume that the A/D and D/A devices operate asynchronously, and thus the sample interval $T_{s,k}$ and the hold interval $T_{h,k}$ vary at each time step k due to timing jitter as shown in Figure 34. Let $T_{s,k}$ and $T_{h,k}$ be given by

$$T_{s,k} = 1 + s_k, \quad T_{h,k} = 1 + h_k, \tag{40}$$

where s_k and h_k are uniformly distributed random variables in $[0, j]$, where $j \in \{0.2, 0.4, 0.8\}$. Figure 35 shows that, as in the case of slowly varying dead time shown in Example 16, the jitter has no discernible effect on the closed-loop performance. ◇

FIGURE 34 Example 22: Timing diagram for relative clock jitter with asynchronous A/D and D/A devices. The interval between the blue and green vertical bars and the black vertical bars indicates the nominal relative clock intervals.

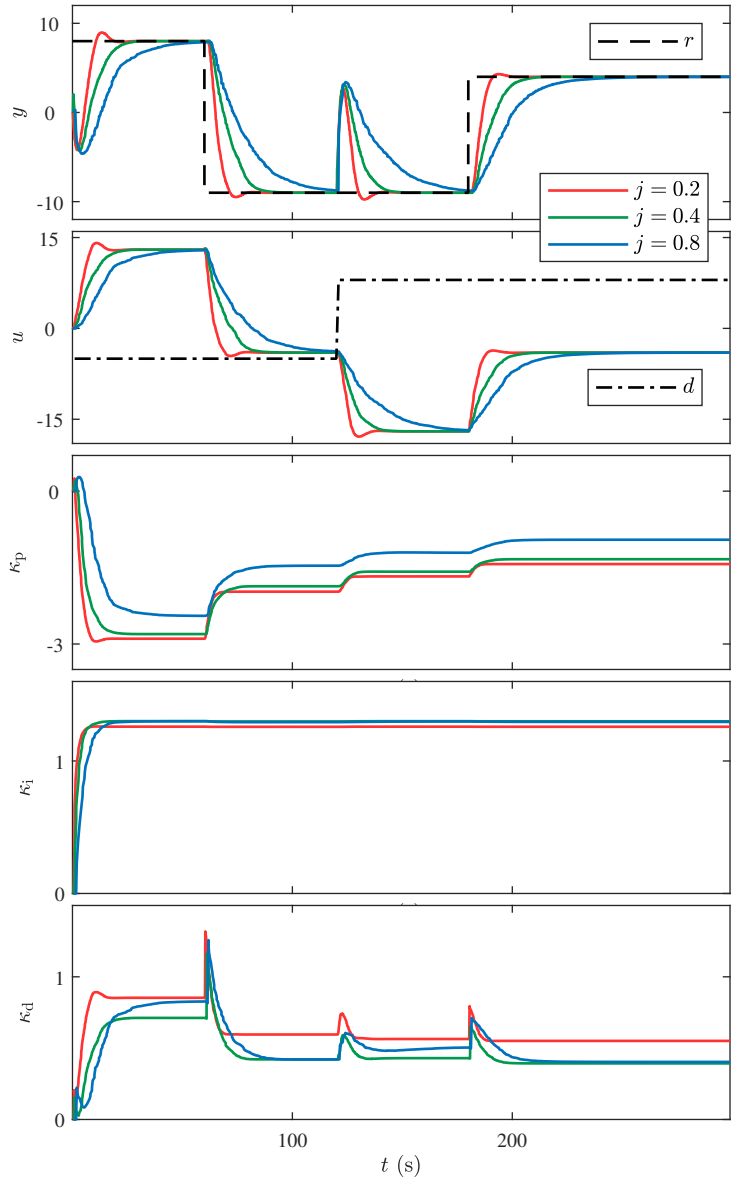

FIGURE 35 Example 22: Command following and disturbance rejection with relative clock jitter with asynchromous A/D and D/A devices. No discernible effect on the closed-loop performance is observed.

10 | NONLINEAR EXAMPLES SUPPORTING SBC

The examples in this section consider the performance of the adaptive digital PID controller for the basic servo loop shown in Figure 1 in the case where either $\mathcal{H}$, $\mathcal{W}$, or $\mathcal{L}$ is a nonlinear map. All of these examples satisfy the assumptions of SBC. In order to investigate the effect of $\mathcal{H}$, $\mathcal{W}$, and $\mathcal{L}$ on the closed-loop performance, various choices of these functions are considered. In particular, the examples in this section consider the effect of control-magnitude saturation and deadzone as well as sensor-magnitude saturation and deadzone. The properties considered are summarized in Table 3. Note that Example 23 supports (A1)–(A9) but does not satisfy the additional assumption (A12).

TABLE 3 Summary of adaptive digital PID control for nonlinear examples supporting SBC.

Example	Investigated Effect	Remarks
23	Infeasible r	(A12) is not satisfied
24	Increasing $\mathcal{W}$ with $r = \mathcal{W}(r)$	(A12) is satisfied
25	Control-magnitude saturation $\mathcal{H}$	Asymmetric
26	Control-magnitude deadzone $\mathcal{H}$	Asymmetric
27	Sensor-magnitude saturation $\mathcal{W}$	Asymmetric
28	Sensor-magnitude deadzone $\mathcal{W}$	Asymmetric
29	Continuous $\mathcal{H}$ and $\mathcal{W}$	Nondecreasing $\mathcal{H}$ and $\mathcal{W}$
30	Continuous $\mathcal{H}$ and $\mathcal{W}$	Nonincreasing $\mathcal{H}$, nondecreasing $\mathcal{W}$
31	Discontinuous $\mathcal{H}$	Nondecreasing $\mathcal{H}$
32	Discontinuous $\mathcal{W}$	Nondecreasing $\mathcal{W}$
33	Continuous $\mathcal{L}$	Nondecreasing $\mathcal{L}$, consider $\mathcal{L}$ and $-\mathcal{L}$
34	Discontinuous $\mathcal{L}$	Nondecreasing $\mathcal{L}$, consider $\mathcal{L}$ and $-\mathcal{L}$

Example 23. *Infeasible r.* Assume that $\mathcal{H}$ and $\mathcal{L}$ are absent, and let $\mathcal{W}$ be given by the magnitude-saturation nonlinearity

$$\mathcal{W}(y_\ell) = \begin{cases} -3, & y_\ell \le -3, \\ y_\ell, & -3 < y_\ell < 3, \\ 3, & y_\ell \ge 3. \end{cases} \tag{41}$$

Figure 36 shows asymptotic command following and disturbance rejection, where either $\overline{u} = -\underline{u} = 1$ (blue trace) or $\overline{u} = -\underline{u} = 5$ (red trace). Figure 37 shows $\mathcal{W}$ and the points computed during the simulation. Since for all $t > 0$, $|r(t)| \ge 4$, (41) implies that (A12) is not satisfied, that is, r is infeasible. Note that, although command following is not achieved in this case, u_k, ξ_k, y_k, $\kappa_{\mathrm{p},k}$, $\kappa_{\mathrm{i},k}$, and $\kappa_{\mathrm{d},k}$ remain bounded. The boundedness of these signals is due to the anti-windup technique (8). ◇

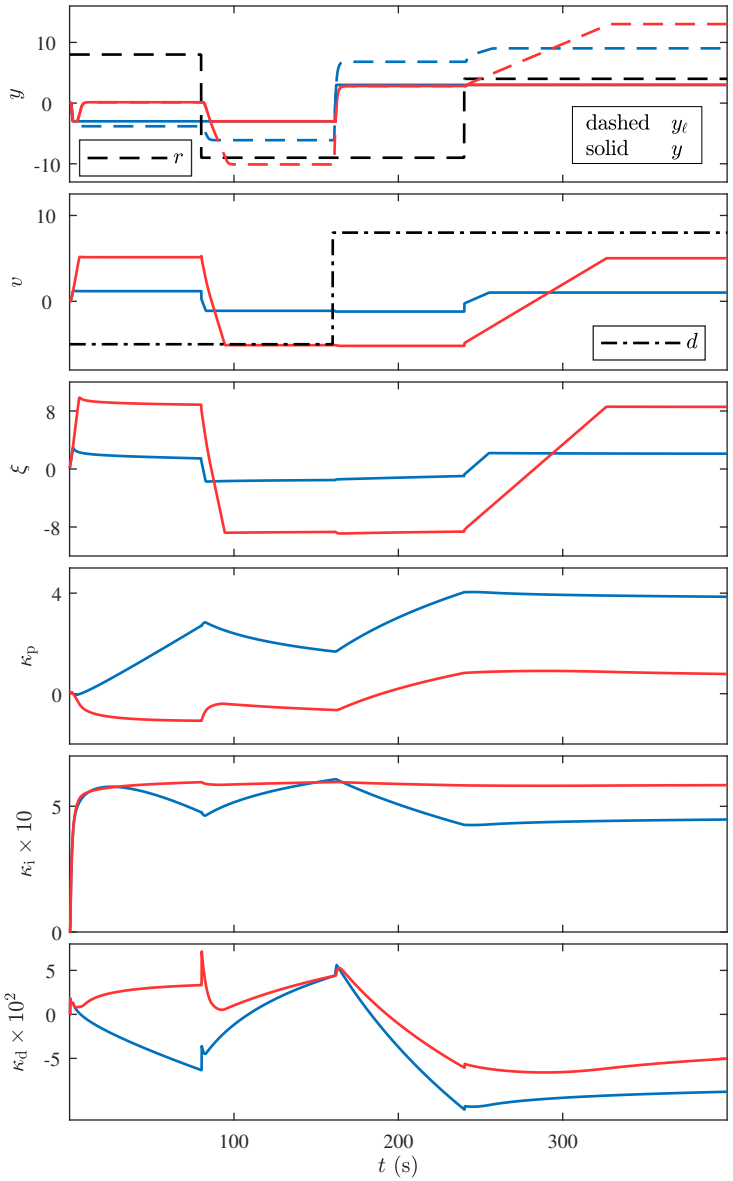

FIGURE 36 Example 23: Command following and disturbance rejection with infeasible command r. Command following is not achieved but all signals remain bounded.

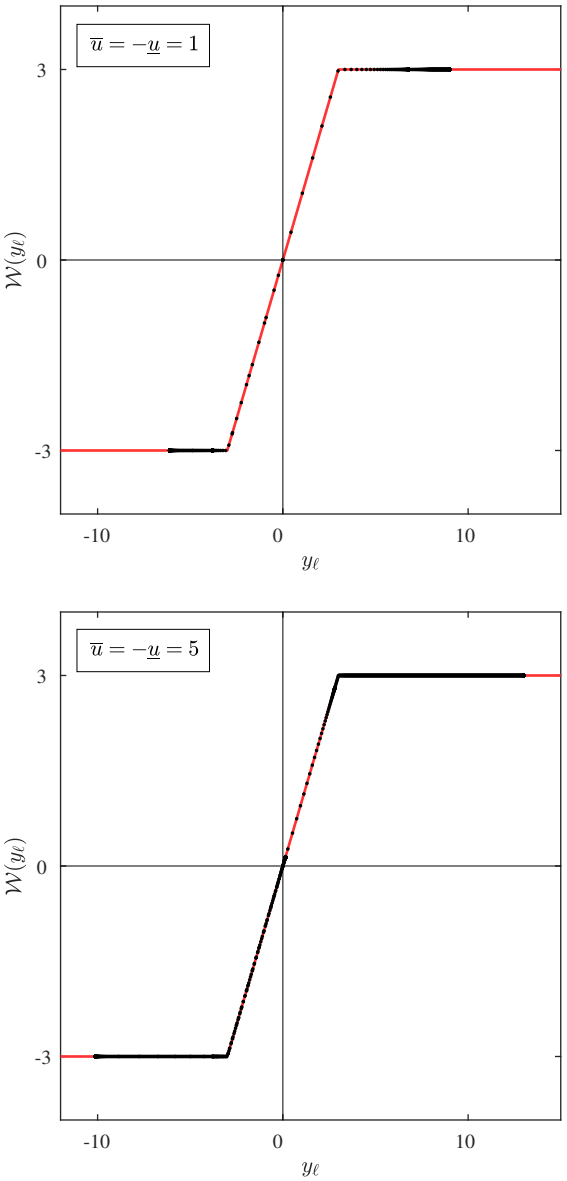

FIGURE 37 Example 23: $\mathcal{W}$ as a function of y_ℓ. Each black dot denotes a point $(y_\ell(t), \mathcal{W}(y_\ell(t)))$ computed during the simulation.

Example 24. *Increasing $\mathcal{W}$ with $r = \mathcal{W}(r)$.* Let $\mathcal{W}$ be given by

$$\mathcal{W}(y_\ell) = \frac{1}{79}\left((y_\ell - 1)^3 + 289\right). \tag{42}$$

Note that $\mathcal{W}$ is increasing and for all $t > 0$, $\mathcal{W}(r(t)) = r(t)$, that is, $\mathcal{W}(8) = 8$, $\mathcal{W}(-9) = -9$, and $\mathcal{W}(4) = 4$. Figure 38 shows asymptotic command following and disturbance rejection. Figure 39 shows $\mathcal{W}$ and the points computed during the simulation. In this case, note that (A13) and (A14) are satisfied, and command following is achieved by both y_ℓ and y, as stated by SBC. ◇

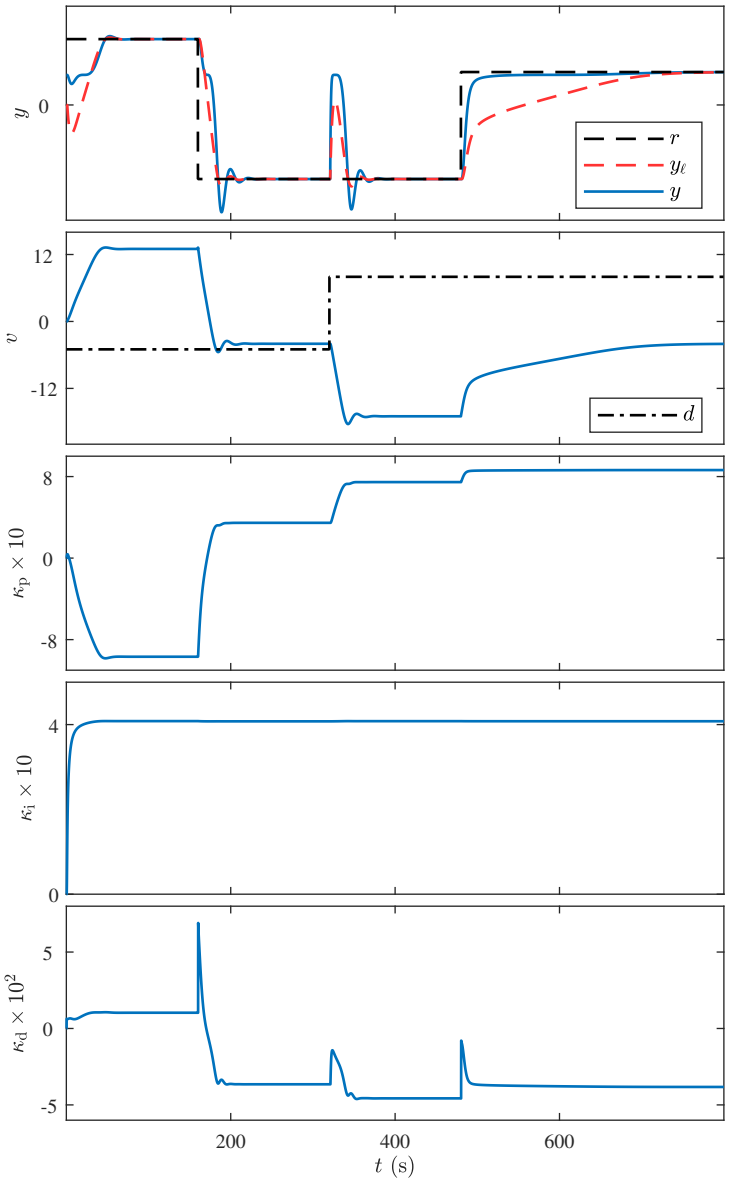

FIGURE 38 Example 24: Command following and disturbance rejection with increasing $\mathcal{W}$ and $r = \mathcal{W}(r)$. Both y_ℓ and y follow the command r asymptotically.

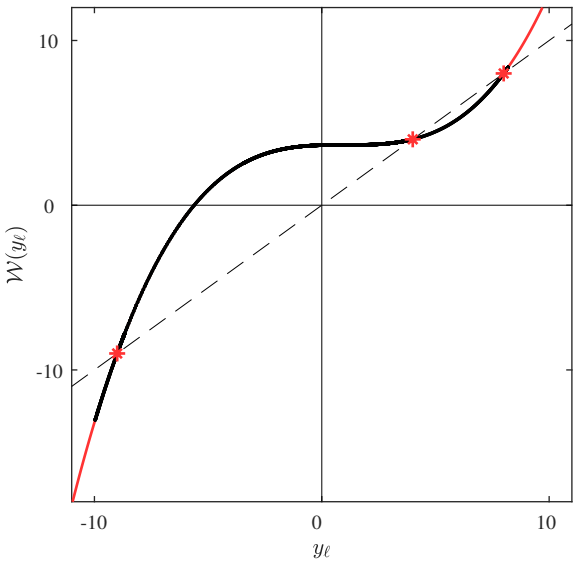

FIGURE 39 Example 24: $\mathcal{W}$ as a function of y_ℓ. Each black dot denotes a point $(y_\ell(t), \mathcal{W}(y_\ell(t)))$ computed during the simulation. The red stars indicate the points $(y_\ell, \mathcal{W}(y_\ell)) = (r, r)$. The dashed line is the locus of $(\bar{y}, \mathcal{W}(\bar{y}))$ that satisfy $\bar{y} = \mathcal{W}(\bar{y})$.

Example 25. *Control-magnitude saturation $\mathcal{H}$.* Assume that $\mathcal{W}$ and $\mathcal{L}$ are absent, and let $\mathcal{H}$ be given by the asymmetric magnitude-saturation nonlinearity

$$\mathcal{H}(u) = \begin{cases} -18, & u \le -18, \\ u, & -18 < u < 15, \\ 15, & u \ge 15. \end{cases} \tag{43}$$

Let $\tau_c = 10$ s and $\overline{u} = -\underline{u} = 20$. Figure 40 shows that asymptotic command following and disturbance rejection are achieved in the presence of control-magnitude saturation. ◇

Example 26. *Control-magnitude deadzone $\mathcal{H}$.* Assume that $\mathcal{W}$ and $\mathcal{L}$ are absent, and let $\mathcal{H}$ be given by

$$\mathcal{H}(u) = \begin{cases} u + 8, & u < -8, \\ 0, & -8 \le u \le 12, \\ u - 12, & u > 12. \end{cases} \tag{44}$$

Let $\overline{u} = -\underline{u} = 30$. Figure 41 shows that asymptotic command following and disturbance rejection are achieved in the presence of control-magnitude deadzone. ◇

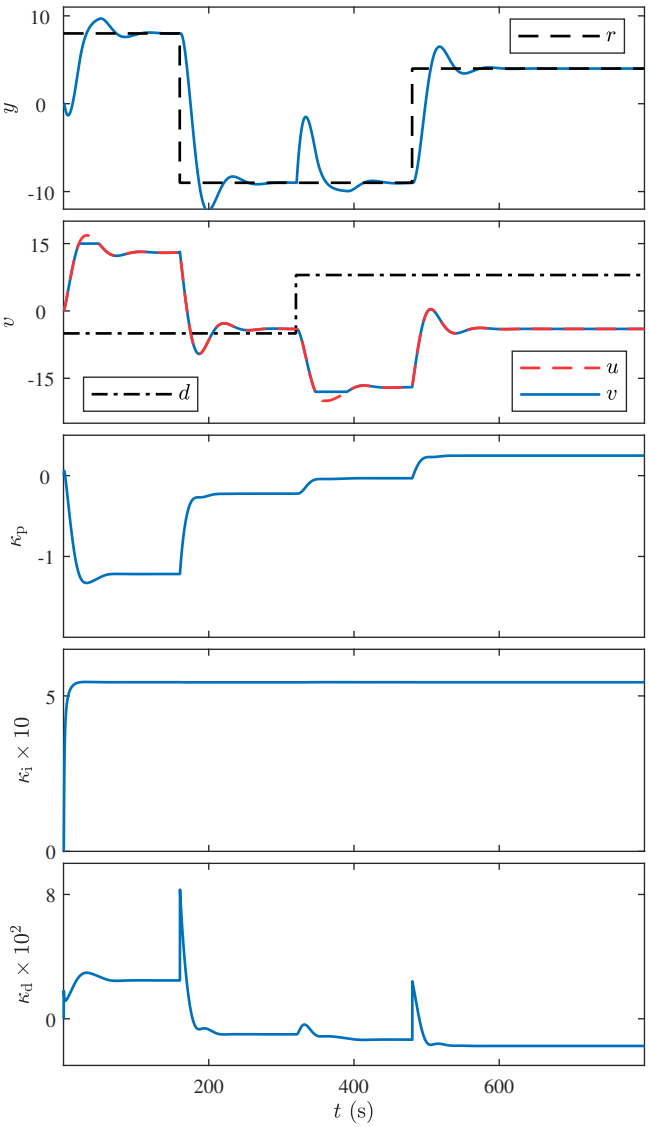

FIGURE 40 Example 25: Command following and disturbance rejection with control-magnitude saturation.

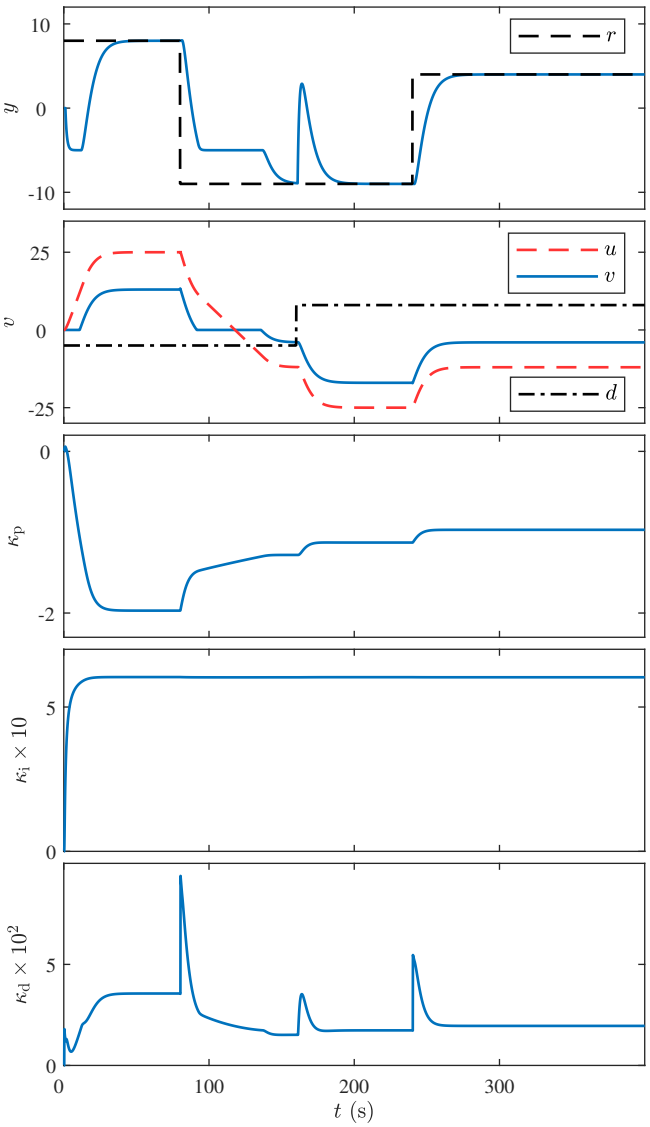

FIGURE 41 Example 26: Command following and disturbance rejection with control-magnitude deadzone.

Example 27. *Sensor-magnitude saturation* $\mathcal{W}$. Assume that $\mathcal{H}$ and $\mathcal{L}$ are absent, and let $\mathcal{W}$ be given by

$$\mathcal{W}(y_\ell) = \begin{cases} -10, & y_\ell \le -10, \\ y_\ell, & -10 < y_\ell < 9, \\ 9, & y_\ell \ge 9, \end{cases} \tag{45}$$

Let $K = 3$ and $\overline{u} = -\underline{u} = 30$. Figure 42 shows that asymptotic command following and disturbance rejection are achieved in the presence of sensor-magnitude saturation. ◇

Example 28. *Sensor-magnitude deadzone* $\mathcal{W}$. Assume that $\mathcal{H}$ and $\mathcal{L}$ are absent, and let $\mathcal{W}$ be given by

$$\mathcal{W}(y_\ell) = \begin{cases} y_\ell + 8, & y_\ell < -8, \\ 0, & -8 \le y_\ell \le 12, \\ y_\ell - 12, & y_\ell > 12. \end{cases} \tag{46}$$

Let $\overline{u} = -\underline{u} = 30$. Figure 43 shows that asymptotic command following and disturbance rejection are achieved in the presence of sensor-magnitude deadzone. ◇

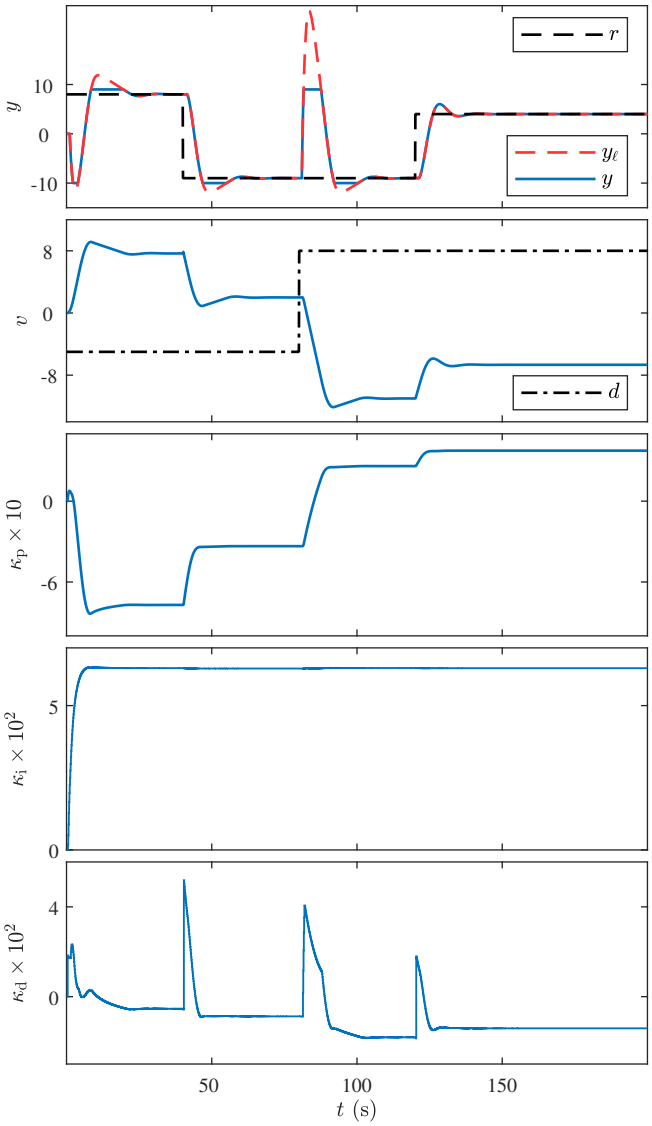

FIGURE 42 Example 27: Command following and disturbance rejection with sensor-magnitude saturation.

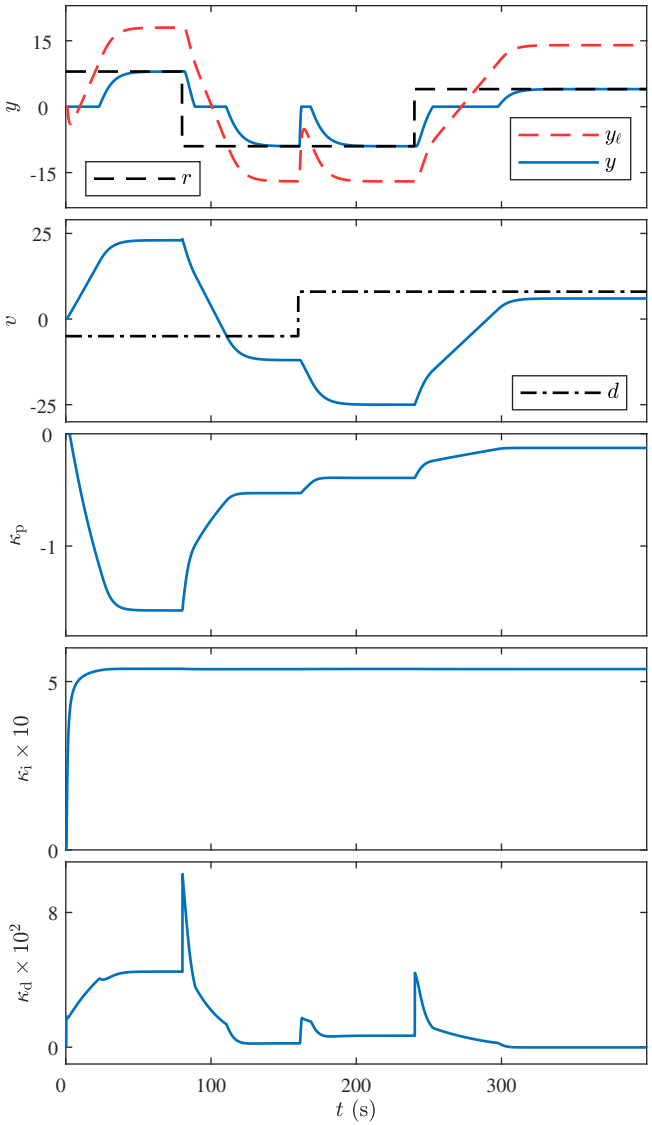

FIGURE 43 Example 28: Command following and disturbance rejection with sensor-magnitude deadzone.

Example 29. *Continuous $\mathcal{H}$ and $\mathcal{W}$.* Consider the case where $\mathcal{H}$ and $\mathcal{W}$ are present and given by

$$\mathcal{W}(y_\ell) = \frac{40(1 - e^{-y_\ell})}{1 + e^{-y_\ell}} - 26, \quad \mathcal{H}(u) = u + 5\tanh u + 5. \tag{47}$$

Figure 44 shows asymptotic command following and disturbance rejection. Figure 45 shows $\mathcal{H}$ and $\mathcal{W}$ as well as the points computed during the simulation. Since $\mathcal{H}$ and $\mathcal{W}$ are increasing, and $K = 1$, (A9) implies that σ must be chosen to be 1. ◇

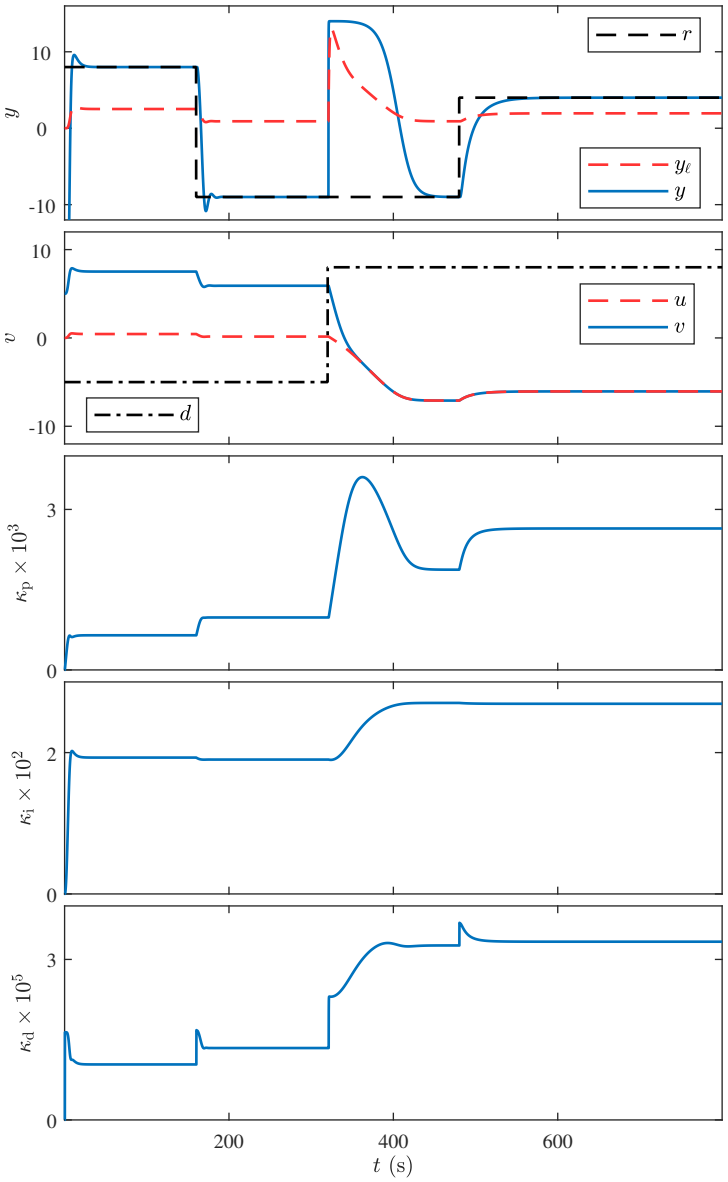

FIGURE 44 Example 29: Command following and disturbance rejection with nondecreasing $\mathcal{H}$ and $\mathcal{W}$.

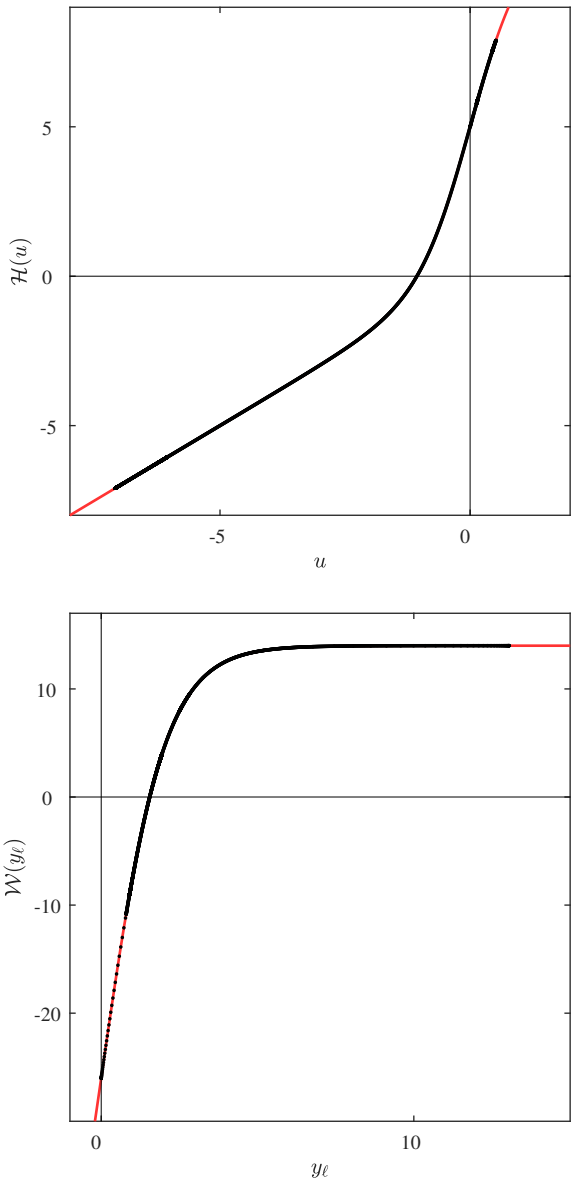

FIGURE 45 Example 29: $\mathcal{H}$ as a function of u and $\mathcal{W}$ as a function of y_ℓ. Each black dot denotes a point $(u(t), \mathcal{H}(u(t)))$ and $(y_\ell(t), \mathcal{W}(y_\ell(t)))$ computed during the simulation.

Example 30. *Continuous $\mathcal{H}$ and $\mathcal{W}$ with negative trends.* Reconsider Example 29 with $\mathcal{H}$ multiplied by -1. Figure 46 shows asymptotic command following and disturbance rejection. Figure 47 shows $\mathcal{H}$ and $\mathcal{W}$ as well as the points computed during the simulation. Since $\mathcal{H}$ is decreasing, $\mathcal{W}$ is increasing, and $K = 1$, (A9) implies that σ must be chosen to be -1. ◇

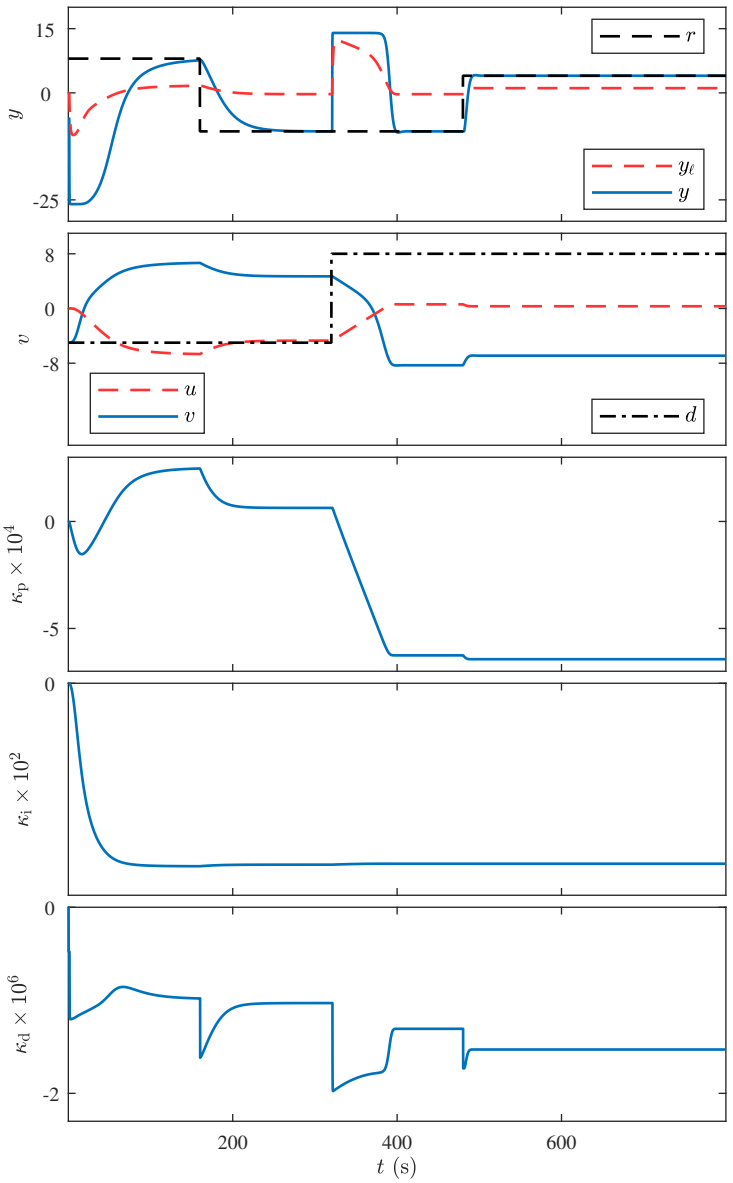

FIGURE 46 Example 30: Command following and disturbance rejection with nonincreasing $\mathcal{H}$ and nondecreasing $\mathcal{W}$.

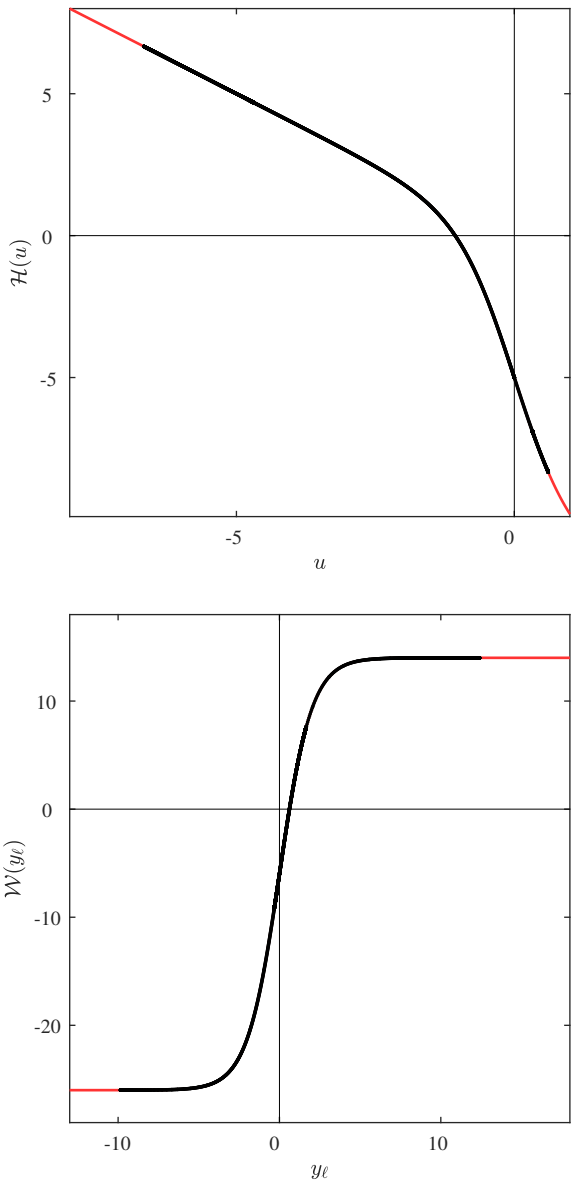

FIGURE 47 Example 30: $\mathcal{H}$ as a function of u and $\mathcal{W}$ as a function of y_ℓ. Each black dot denotes a point $(u(t), \mathcal{H}(u(t)))$ and $(y_\ell(t), \mathcal{W}(y_\ell(t)))$ computed during the simulation.

Example 31. *Discontinuous* $\mathcal{H}$. Assume that $\mathcal{W}$ and $\mathcal{L}$ are absent and let $\mathcal{H}$ be the discontinuous actuator nonlinearity

$$\mathcal{H}(u) = u + 4\left\lceil \frac{u-3}{4} \right\rceil - 3. \tag{48}$$

Figure 48 shows asymptotic command following and disturbance rejection. Figure 49 shows $\mathcal{H}$ and the points computed during the simulation. Note that SBC does not impose any assumption on the continuity of $\mathcal{H}$. ◇

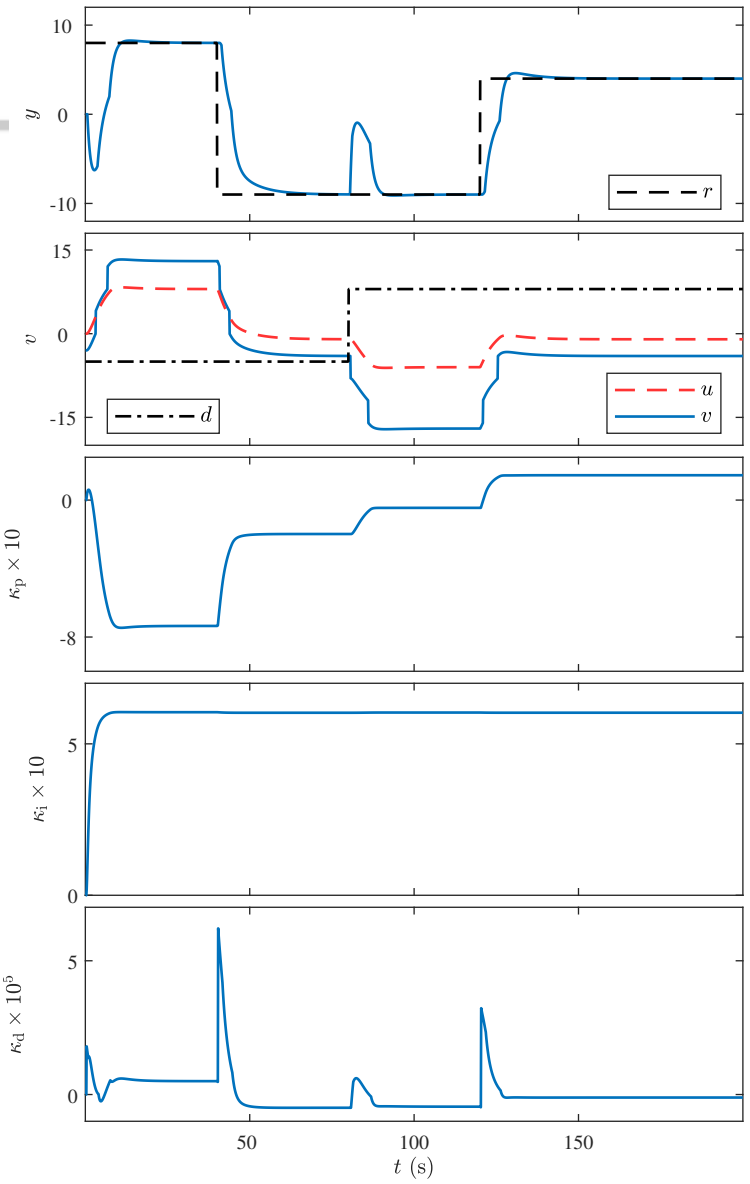

FIGURE 48 Example 31: Command following and disturbance rejection with with discontinuous $\mathcal{H}$. Note that SBC does not impose a continuity assumption on $\mathcal{H}$.

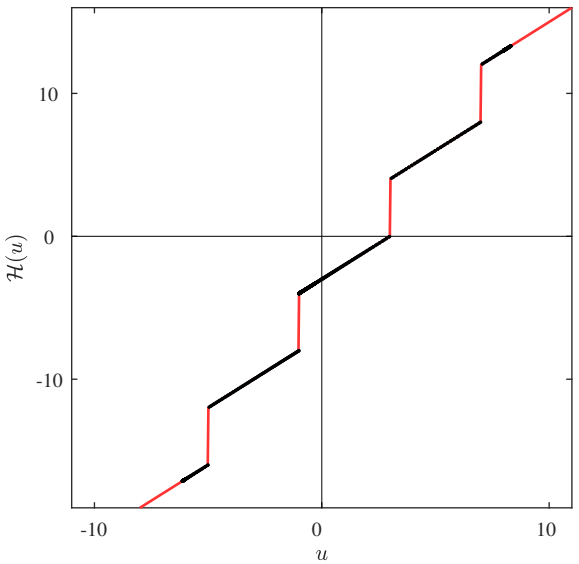

FIGURE 49 Example 31: $\mathcal{H}$ as a function of u. Each black dot denotes a point $(u(t), \mathcal{H}(u(t)))$ computed during the simulation.

Example 32. *Discontinuous* $\mathcal{W}$. Assume that $\mathcal{H}$ and $\mathcal{L}$ are absent and let $\mathcal{W}$ be the discontinuous output nonlinearity

$$\mathcal{W}(y_\ell) = y_\ell + 4\left\lfloor \frac{y_\ell + 3}{4} \right\rfloor + 3. \tag{49}$$

Figure 50 shows asymptotic command following and disturbance rejection. Figure 51 shows $\mathcal{W}$ and the points computed during the simulation. Note that SBC does not impose any assumption on the continuity of $\mathcal{W}$. ◇

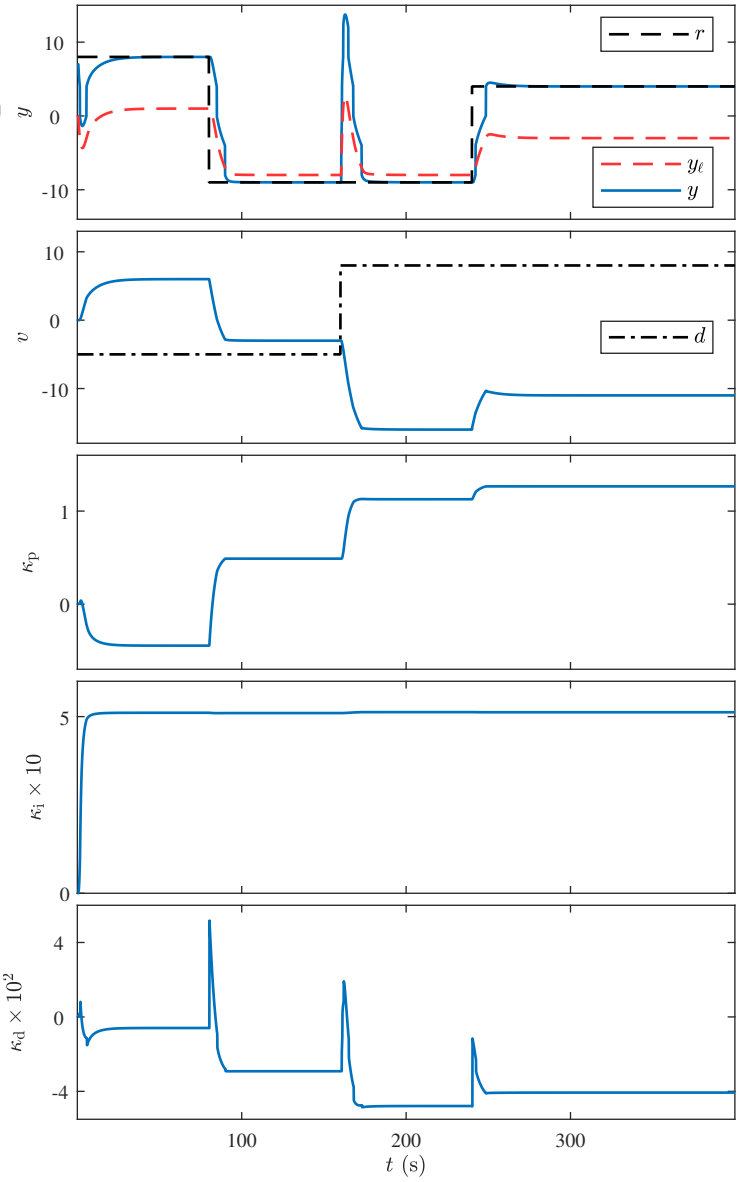

FIGURE 50 Example 32: Command following and disturbance rejection with discontinuous $\mathcal{W}$. Note that SBC does not impose a continuity assumption on $\mathcal{W}$.

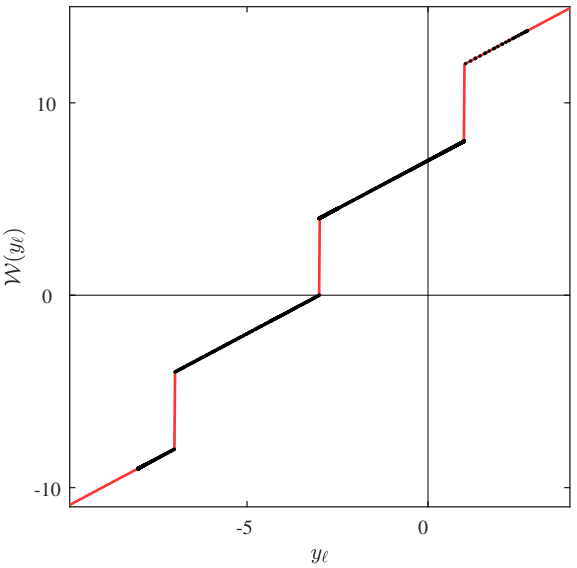

FIGURE 51 Example 32: $\mathcal{W}$ as a function of y_ℓ. Each black dot denotes a point $(y_\ell(t), \mathcal{W}(y_\ell(t)))$ computed during the simulation.

Example 33. *Continuous* $\mathcal{L}$. Assume that $\mathcal{H}$ and $\mathcal{W}$ are absent, and let $\mathcal{L}$ be the continuous, increasing feedback nonlinearity

$$\mathcal{L}(y_\ell) = 1 + \begin{cases} \sqrt{y_\ell}, & y_\ell \geq 0, \\ -\sqrt{-y_\ell}, & y_\ell < 0. \end{cases} \tag{50}$$

Since SBC does not assume that trend $\mathcal{L}$ is known, the system is simulated with both $\mathcal{L}$ and $\mathcal{L}$ replaced with $-\mathcal{L}$. In both cases, Figure 52 shows asymptotic command following and disturbance rejection. ◇

Example 34. *Discontinuous* $\mathcal{L}$. Assume that $\mathcal{H}$ and $\mathcal{W}$ are absent and let $\mathcal{L}$ be the discontinuous, nondecreasing feedback nonlinearity

$$\mathcal{L}(y_\ell) = 1 + \left\lceil \frac{y_\ell}{2} \right\rceil. \tag{51}$$

Since SBC does not assume that trend $\mathcal{L}$ is known, the system is simulated with both $\mathcal{L}$ and $\mathcal{L}$ replaced with $-\mathcal{L}$. In both cases, Figure 53 shows asymptotic command following and disturbance rejection. Note that SBC does not impose any assumption on the continuity of $\mathcal{L}$. ◇

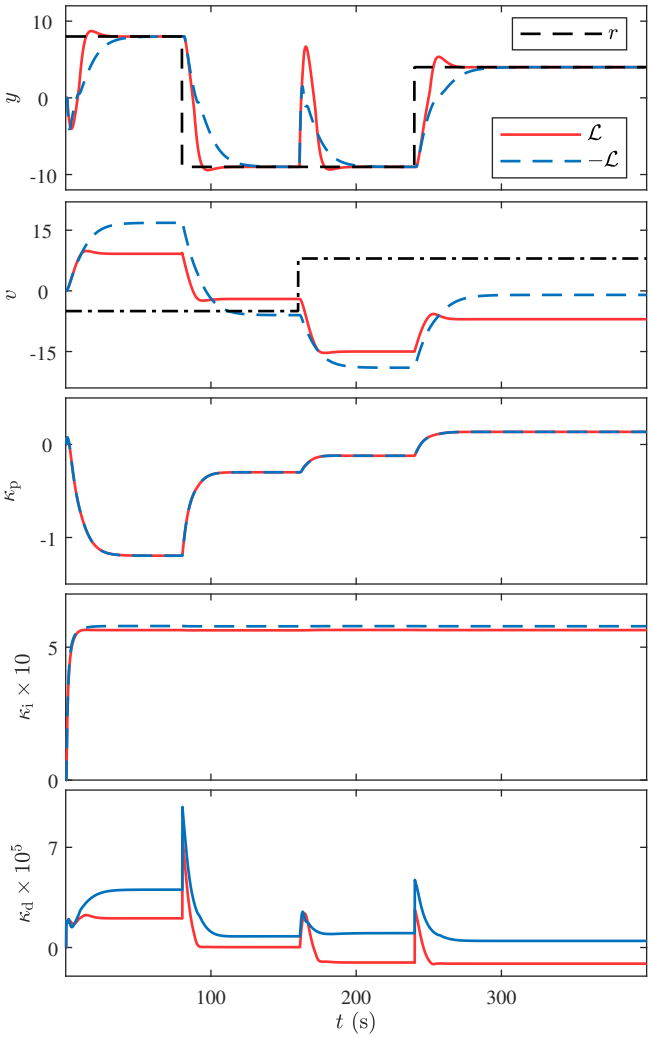

FIGURE 52 Example 33: Command following and disturbance rejection with continuous $\mathcal{L}$ and $-\mathcal{L}$. Note that SBC does not impose any assumption on trend $\mathcal{L}$.

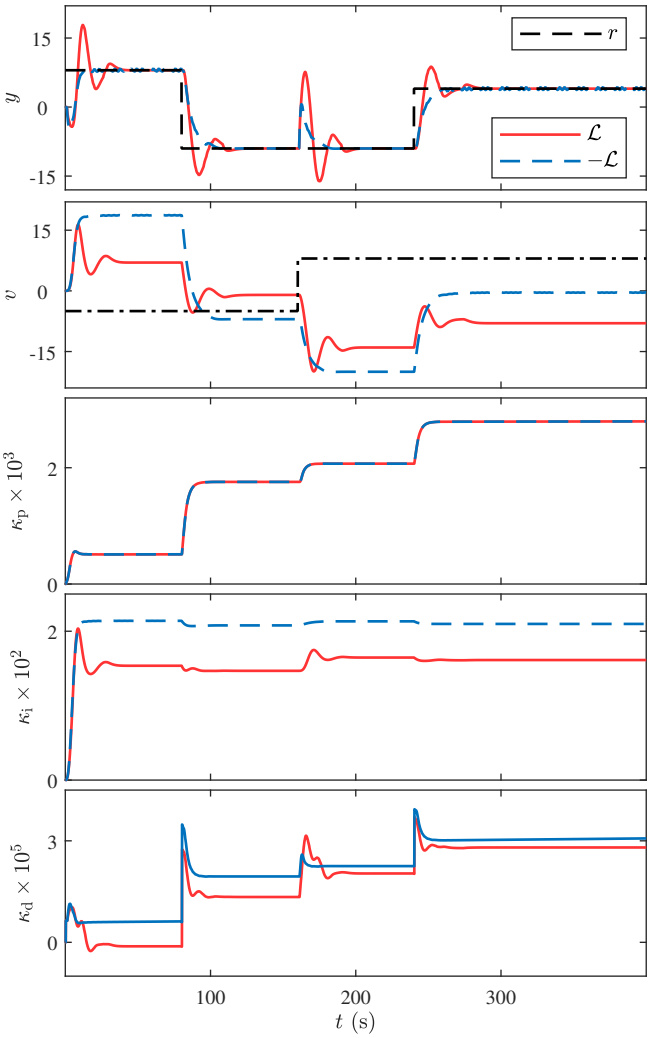

FIGURE 53 Example 34: Command following and disturbance rejection with discontinuous $\mathcal{L}$ and $-\mathcal{L}$. Note that SBC does not impose any assumptions on trend $\mathcal{L}$ or continuity of $\mathcal{L}$.

11 | NONLINEAR EXAMPLES VIOLATING THE ASSUMPTIONS OF SBC

The examples in this section consider the performance of the adaptive digital PID controller for the basic servo loop shown in Figure 1 in the case where one or more of (A1)–(A9) are violated. For all of these examples, either $\mathcal{H}$ or $\mathcal{W}$ is a nonlinear function. In order to investigate the effect of violating the assumptions of SBC with nonlinear $\mathcal{W}, \mathcal{H}$, we consider examples with conditions that may be encountered in practical applications and that violate SBC. In particular the examples in this section consider the effect of control and measurement-rate saturation, infeasible r due to control and magnitude saturation, infeasible r due to discontinuous $\mathcal{H}$ and $\mathcal{W}$, and nonmonotonic $\mathcal{H}$, $\mathcal{W}$, and $\mathcal{L}$. The properties and values considered are summarized in Table 4.

TABLE 4 Summary of adaptive digital PID control for nonlinear examples violating the assumptions of SBC.

Example	Investigated Effect	Remarks
35	Control-rate saturation	$(\underline{\delta}_u, \overline{\delta}_u) = (-2, 1), (-3, 2), (-4, 3)$
36	Measurement-rate saturation	$(\underline{\delta}_y, \overline{\delta}_y) = (-2, 1), (-3, 2), (-4, 3)$
37	Infeasible r due to control-magnitude saturation $\mathcal{H}$	Asymmetric
38	Infeasible r due to sensor-magnitude saturation $\mathcal{W}$	Increasing sensor saturation
39	Infeasible r due to discontinuous $\mathcal{H}$	Quantization
40	Infeasible r due to discontinuous $\mathcal{W}$	Quantization
41	Nonmonotonic $\mathcal{H}$, $\mathcal{W}$, and $\mathcal{L}$	(A6)–(A8) are not satisfied
42	Nonmonotonic $\mathcal{H}$, $\mathcal{W}$, and $\mathcal{L}$	(A6)–(A8) are not satisfied

Example 35. *Control-rate saturation.* Let $\overline{\delta}_u > 0$ and $\underline{\delta}_u < 0$ be the positive and negative control-rate-saturation levels, respectively. In terms of samples, the maximum allowable increase and decrease in the control input over each sampling period are thus $\overline{\delta}_u T_\mathrm{s}$ and $\underline{\delta}_u T_\mathrm{s}$, respectively. Let $(\underline{\delta}_u, \overline{\delta}_u) = (-1, 0.5), (-2, 1), (-3, 2)$. Figure 54 shows asymptotic command following and disturbance rejection. These simulations suggest that asymptotic command following and disturbance rejection are achieved with arbitrarily small control-rate-saturation levels. ◇

Example 36. *Measurement-rate saturation.* Let $\overline{\delta}_y > 0$ and $\underline{\delta}_y < 0$ be the positive and negative measurement-rate-saturation levels, respectively. In terms of samples, the maximum allowable increase and decrease in the sensor measurement over each sampling period are thus $\overline{\delta}_y T_\mathrm{s}$ and $\underline{\delta}_y T_\mathrm{s}$, respectively. Let $(\underline{\delta}_y, \overline{\delta}_y) = (-0.5, 0.3), (-0.7, 0.5), (-0.9, 1)$. Figure 55 shows asymptotic command following and disturbance rejection. These simulations suggest that asymptotic command following and disturbance rejection are achieved with arbitrarily small measurement-rate-saturation levels. ◇

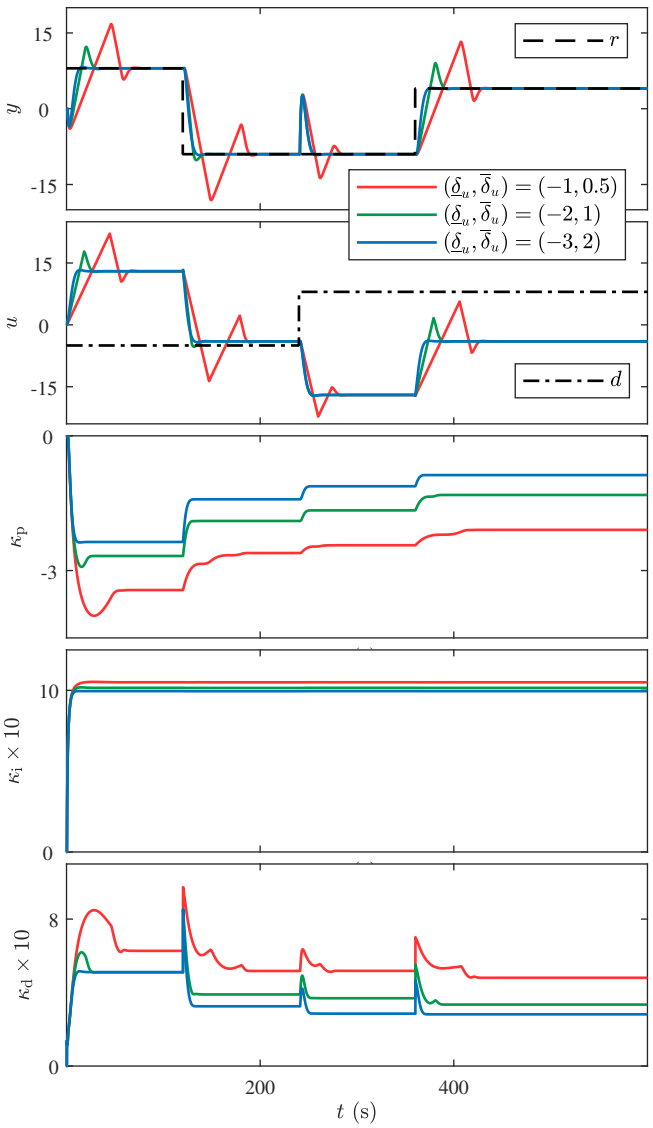

FIGURE 54 Example 35: Command following and disturbance rejection with control-rate saturation.

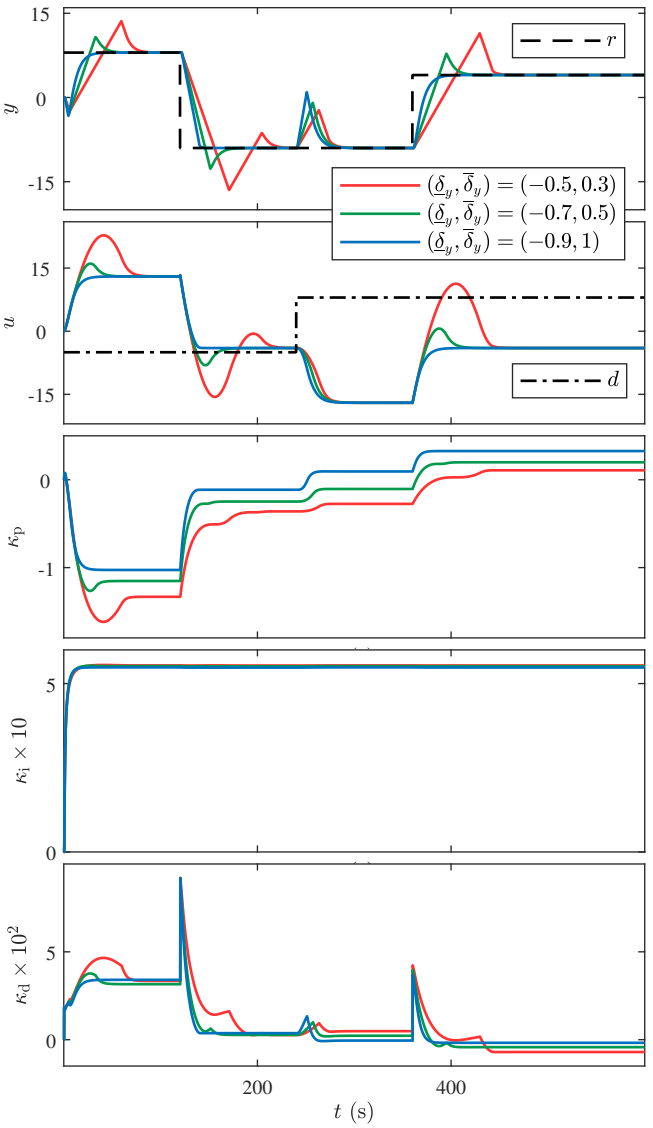

FIGURE 55 Example 36: Command following and disturbance rejection with measurement-rate saturation.

Example 37. *Infeasible r due to control-magnitude saturation $\mathcal{H}$.* Assume that $\mathcal{W}$ and $\mathcal{L}$ are absent and $\mathcal{H}$ is the control-magnitude saturation given by

$$\mathcal{H}(u) = 2 + \begin{cases} \dfrac{u}{2}, & |u| < 20, \\ 10 \operatorname{sign} u, & |u| \geq 20. \end{cases} \tag{52}$$

Let $\overline{u} = -\underline{u} = 10$ and $\tau = 10$. Figure 56 shows asymptotic command following and disturbance rejection. Figure 57 shows $\mathcal{H}$ as well as the points computed during the simulation. Note that, due to control-magnitude saturation $\mathcal{H}$, r is infeasible during some time intervals (e.g., for $t < 20$ s); therefore, integrator windup can occur. However, since the anti-windup thresholds $\overline{u}$ and $\underline{u}$ are chosen to be sufficiently small, the anti-windup technique (8) prevents integrator windup, and thus all signals remain bounded. ◇

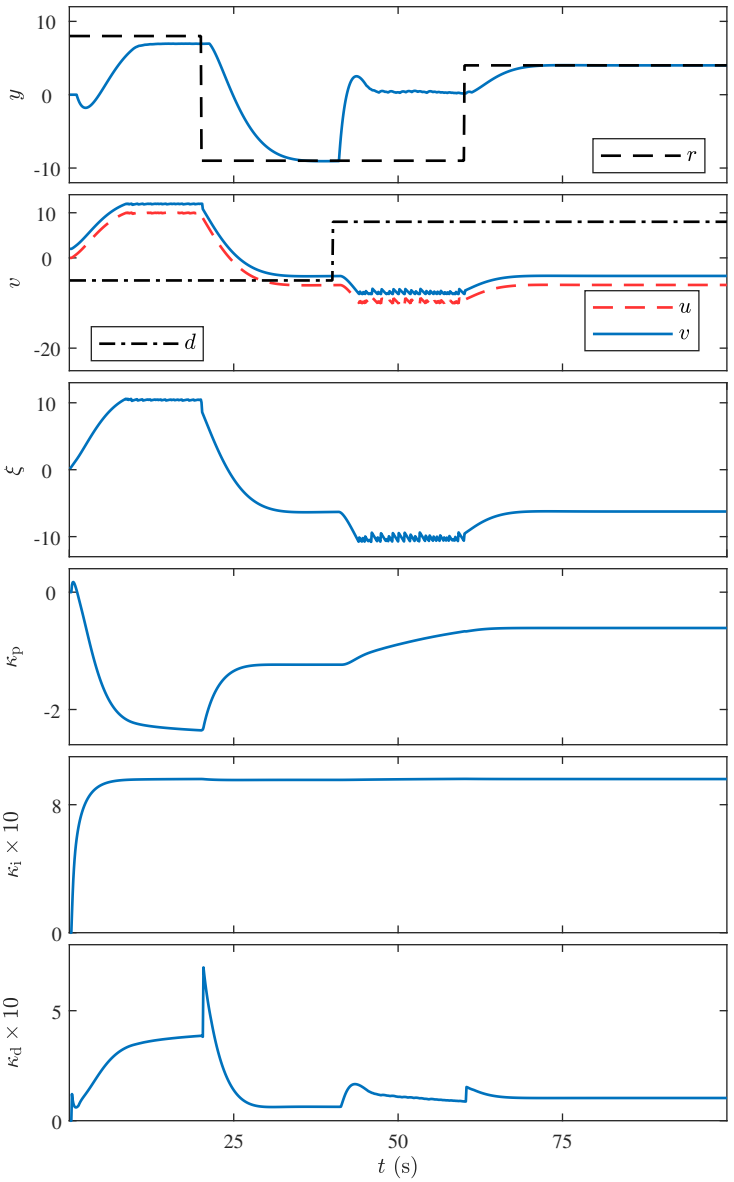

FIGURE 56 Example 37: Command following and disturbance rejection with infeasible command due to control-magnitude saturation. The anti-windup technique (8) prevents windup and all signals remain bounded.

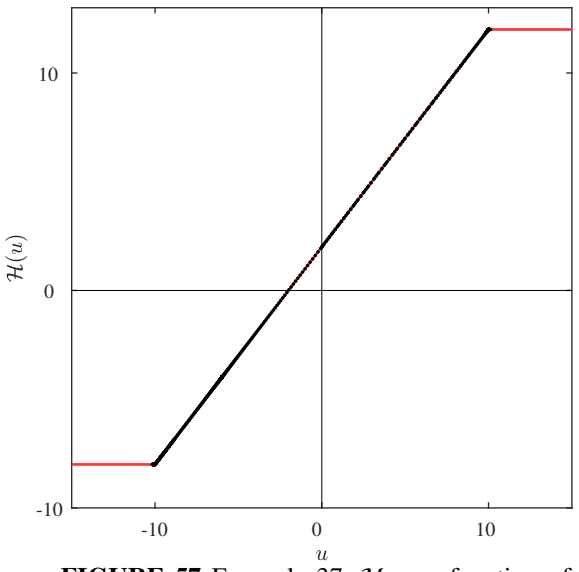

FIGURE 57 Example 37: $\mathcal{H}$ as a function of u. Each black dot denotes a point $(u(t), \mathcal{H}(u(t)))$ computed during the simulation.

Example 38. *Infeasible r due to sensor-magnitude saturation* $\mathcal{W}$. Assume that $\mathcal{H}$ and $\mathcal{L}$ are absent, and let $\mathcal{W}$ be the sensor-magnitude saturation nonlinearity

$$\mathcal{W}(y_\ell) = 4\,\mathrm{atan}(y_\ell - 2). \tag{53}$$

Let $\overline{u} = -\underline{u} = 15$. Figure 58 shows asymptotic command following and disturbance rejection. Figure 59 shows $\mathcal{W}$ and the points computed during the simulation. Note that, due to the sensor-magnitude saturation $\mathcal{W}$, r is infeasible until $t = 240$ s, and thus windup is possible. However, since the anti-windup thresholds $\overline{u}$ and $\underline{u}$ are chosen to be sufficiently small, the anti-windup technique (8) prevents windup, and thus all signals remain bounded. . ◇

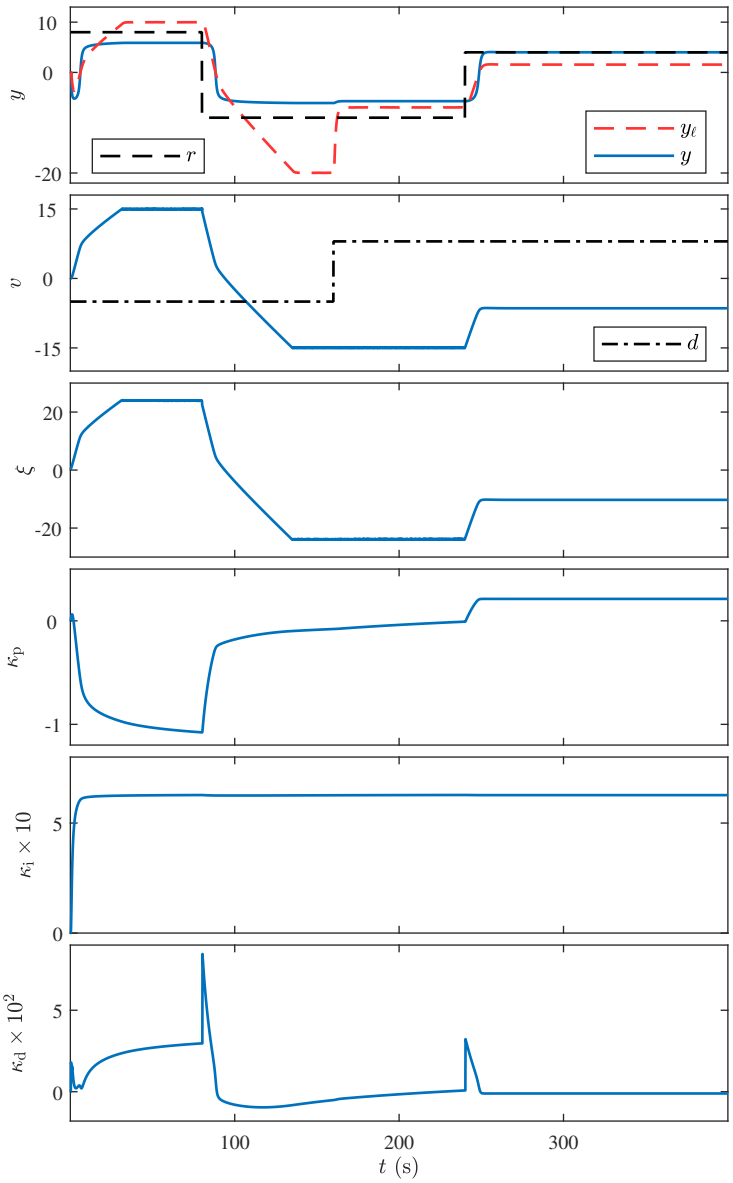

FIGURE 58 Example 38: Command following and disturbance rejection with infeasible command due to sensor-magnitude saturation. The anti-windup technique (8) prevents windup and all signals remain bounded.

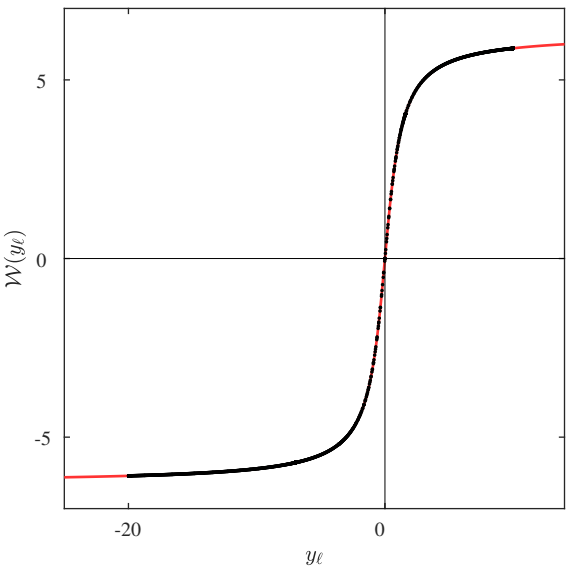

FIGURE 59 Example 38: $\mathcal{W}$ as a function of y_ℓ. Each black dot denotes a point $(y_\ell(t), \mathcal{W}(y_\ell(t)))$ computed during the simulation.

Example 39. *Infeasible r due to discontinuous $\mathcal{H}$.* Assume that $\mathcal{W}$ and $\mathcal{L}$ are absent, and consider the discontinuous actuator nonlinearity

$$\mathcal{H}(u) = 2\lceil u \rceil + 2.63, \tag{54}$$

which implies that the control input v is quantized. In this case, r is infeasible. Figure 60 shows that asymptotic command following and disturbance rejection are approximately achieved. In fact, the controller makes u_k chatter between two control values that yield the smallest and second smallest possible command following errors. ◇

Example 40. *Infeasible r due to discontinuous $\mathcal{W}$.* Assume that $\mathcal{H}$ and $\mathcal{L}$ are absent, and consider the discontinuous sensor nonlinearity

$$\mathcal{W}(y_\ell) = 2\lceil y_\ell \rceil + 2.63, \tag{55}$$

which implies that the measurement y is quantized. Figure 61 shows that asymptotic command following and disturbance rejection are approximately achieved. In fact, the controller makes u_k chatter between two control values that yield the smallest and second smallest possible command following errors. ◇

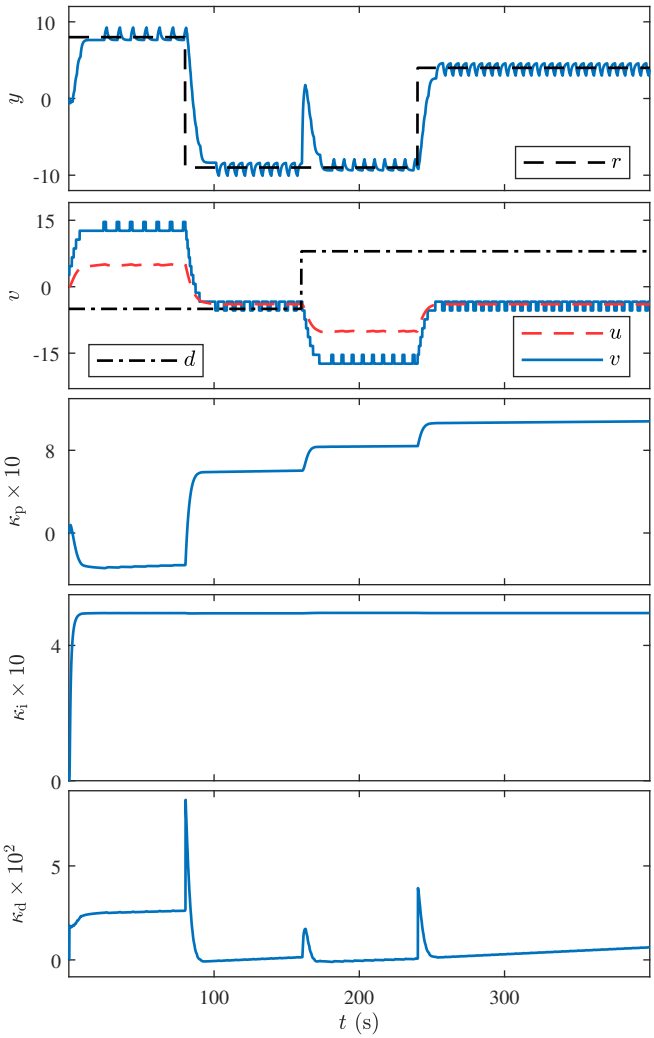

FIGURE 60 Example 39: Command following and disturbance rejection with infeasible command due to quantized actuation. The signals y_k, u_k chatter.

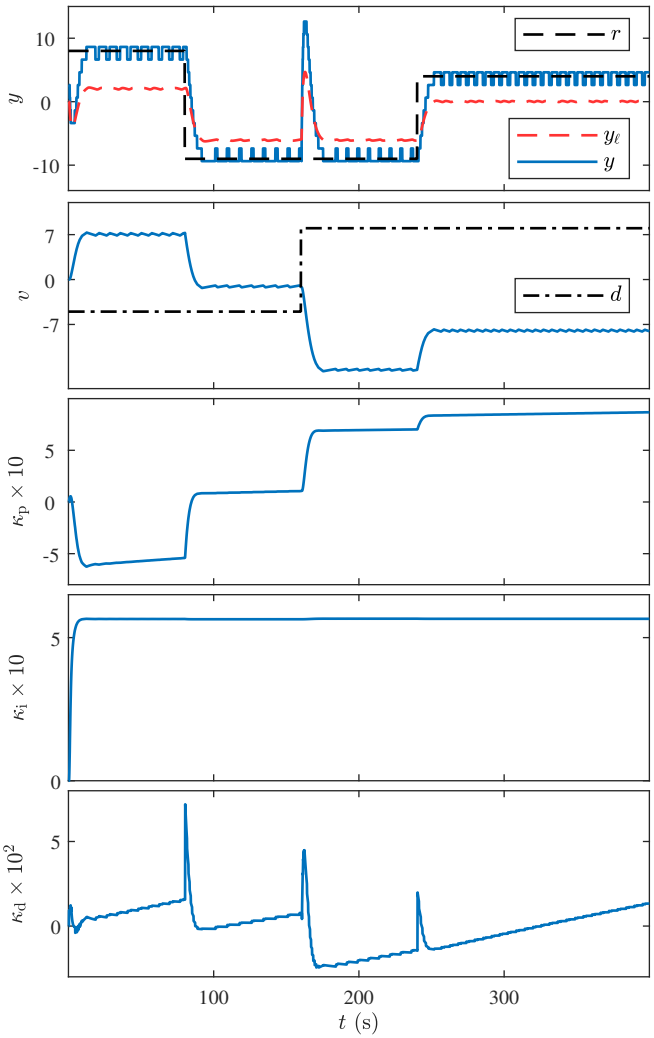

FIGURE 61 Example 40: Command following and disturbance rejection with infeasible command due to quantized measurements. The signals y_k, u_k chatter.

Example 41. *Nonmonotonic $\mathcal{H}$, $\mathcal{W}$, and $\mathcal{L}$.* Consider the nonmonotonic sensor, actuator and feedback nonlinearities

$$\mathcal{H}(u) = u + 2\sin u + 5, \qquad \mathcal{W}(y_\ell) = |y_\ell - 5| - 20, \qquad \mathcal{L}(y_\ell) = \frac{y_\ell}{1 + y_\ell^2} + 1. \tag{56}$$

which do not satisfy (A6)–(A8). Figure 62 shows that asymptotic command following and disturbance rejection are achieved despite the fact that all three nonlinearities are nonmonotonic. Figure 63 shows $\mathcal{H}$, $\mathcal{W}$, and $\mathcal{L}$ and the points computed during the simulation. ◇

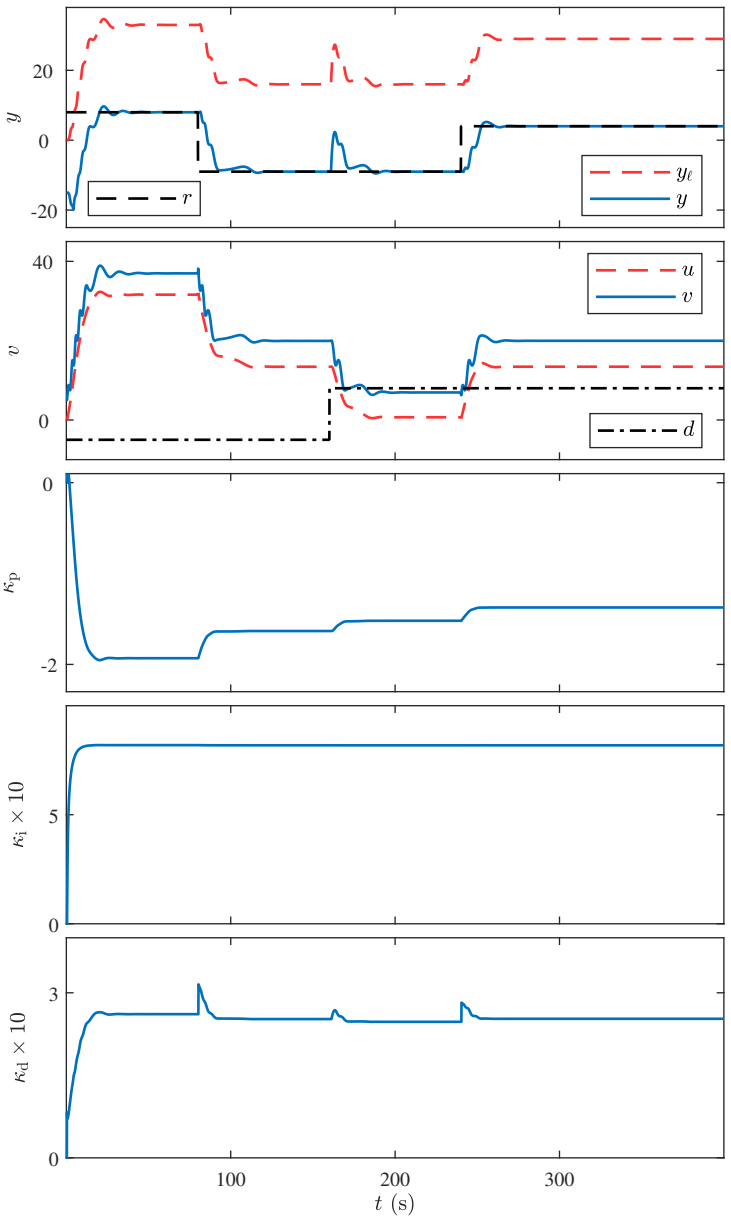

FIGURE 62 Example 41: Command following and disturbance rejection with nonmonotonic $\mathcal{H}$, $\mathcal{W}$, and $\mathcal{L}$.

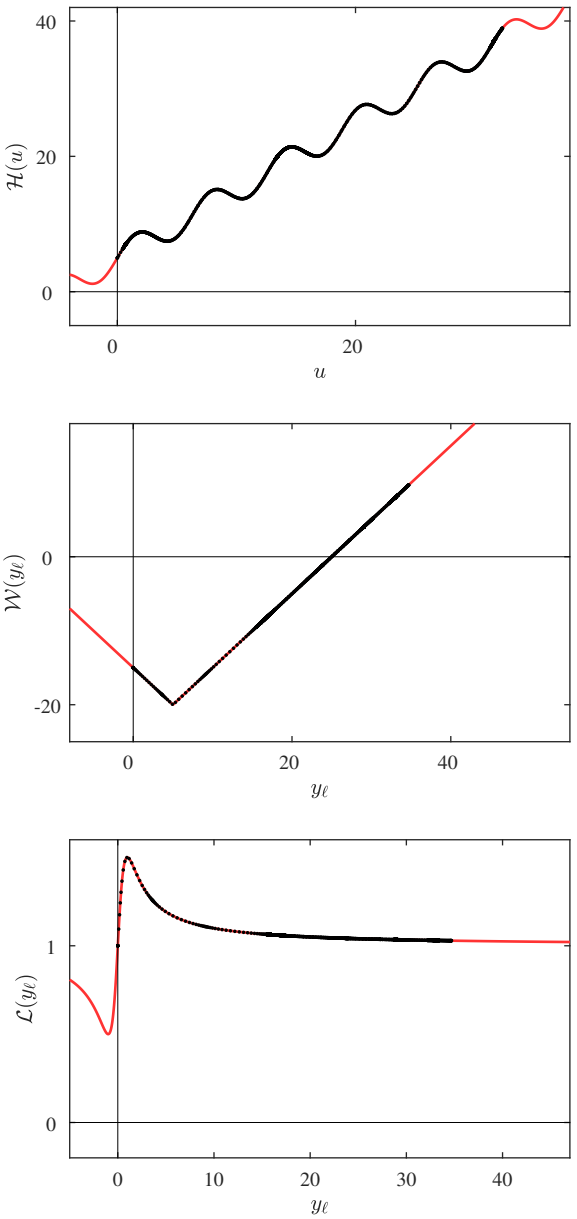

FIGURE 63 Example 41: $\mathcal{H}$ as a function of u, and $\mathcal{W}$ and $\mathcal{L}$ as functions of y_ℓ. Each black dot denotes a point $(u(t), \mathcal{H}(u(t)))$, $(y_\ell(t), \mathcal{W}(y_\ell(t)))$, and $(y_\ell(t), \mathcal{L}(y_\ell(t)))$ computed during the simulation.

Example 42. *Nonmonotonic $\mathcal{H}$, $\mathcal{W}$, and $\mathcal{L}$.* Assume that $\mathcal{W}$ and $\mathcal{L}$ are absent, and consider the nonmonotonic actuator nonlinearity $\mathcal{H}(u) = 15 \sin u$, which does not satisfy (A6). Figure 64 shows that command following and disturbance rejection are not achieved. Next, assume that $\mathcal{H}$ and $\mathcal{L}$ are absent, and consider the nonmonotonic sensor nonlinearity $\mathcal{W}(y_\ell) = 15 \cos(2y_\ell^2)$, which does not satisfy (A7). Figure 66 shows that command following and disturbance rejection are not achieved. Next, assume that $\mathcal{H}$ and $\mathcal{W}$ are absent, and consider the nonmonotonic sensor nonlinearity $\mathcal{L}(y_\ell) = 0.1y_\ell^2$, which does not satisfy (A8). Figure 68 shows that command following and disturbance rejection are not achieved. Figures 65, 67, and 69 show $\mathcal{H}$, $\mathcal{W}$, and $\mathcal{L}$ for each case. Unlike Example 41, violating (A6)–(A8) prevents asymptotic command following and disturbance rejection. ◇

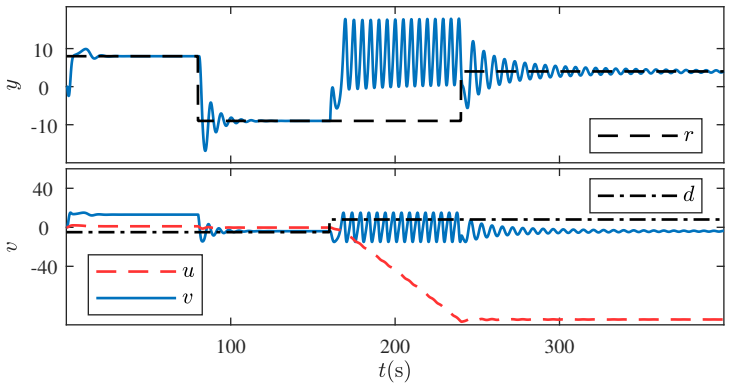

FIGURE 64 Example 42: Command following and disturbance rejection with nonmonotonic $\mathcal{H}$. The response diverges.

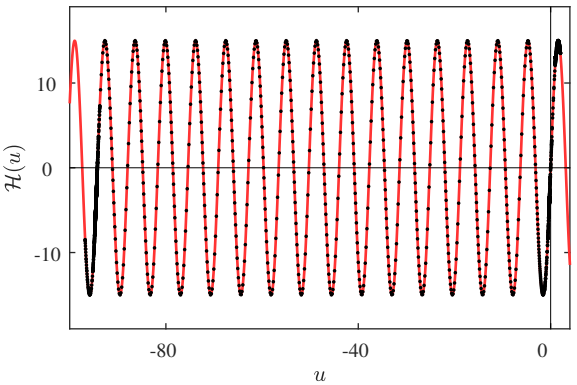

FIGURE 65 Example 42: $\mathcal{H}$ as a function of u. Black dots denote $(u(t), \mathcal{H}(u(t)))$.

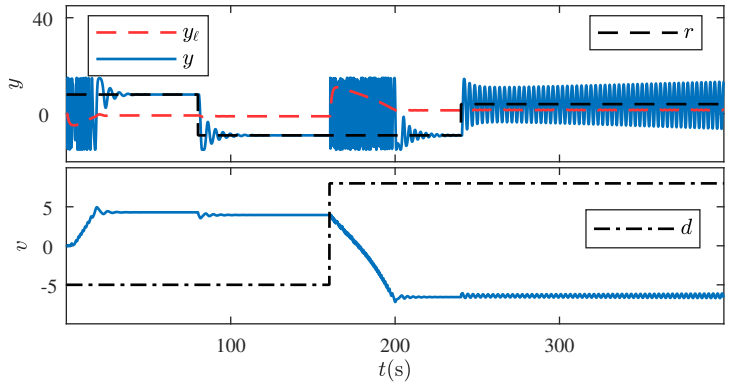

FIGURE 66 Example 42: Command following and disturbance rejection with nonmonotonic $\mathcal{W}$. The response diverges.

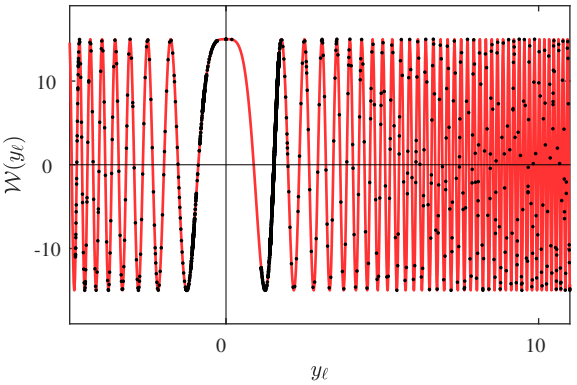

FIGURE 67 Example 42: $\mathcal{W}$ as a function of y_ℓ. Black dots denote $(y_\ell(t), \mathcal{W}(y_\ell(t)))$.

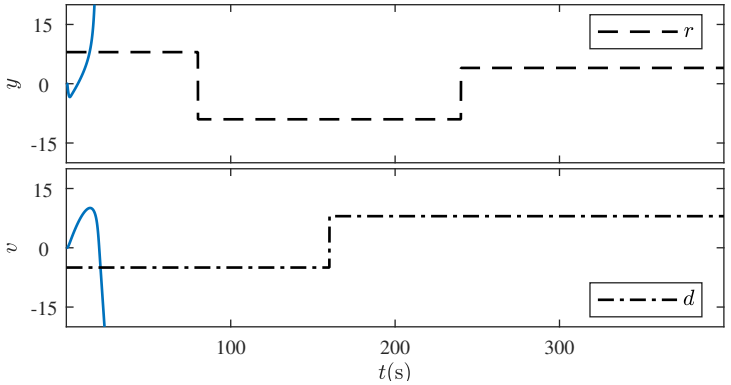

FIGURE 68 Example 42: Command following and disturbance rejection with nonmonotonic $\mathcal{L}$. The response diverges.

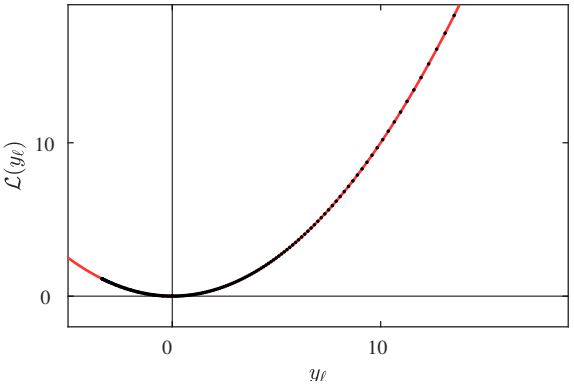

FIGURE 69 Example 42: $\mathcal{L}$ as a function of y_ℓ. Black dots denote $(y_\ell(t), \mathcal{L}(y_\ell(t)))$.

12 | ADAPTIVE DIGITAL PID CONTROL OF SECOND-ORDER SYSTEMS

This section applies the adaptive digital PID controller to second-order plants. No attempt is made to state and demonstrate a conjecture as in the case of SBC for first-order-lag-plus-dead-time dynamics. Rather, the goal is to demonstrate the feasibility of the adaptive digital PID controller for these plants while providing insight into tuning and closed-loop performance.

Consider the continuous-time, second-order plant with dead time given by

$$G(s) = \frac{e^{-\tau_d s}}{(s+a)(s+b)}, \tag{57}$$

where $\tau_d \geq 0$ is the dead time and a and b are either real numbers or complex conjugates. Assuming that $n_d = \tau_d/T_s$ is an integer, it follows that the exactly discretized dynamics are given by

$$G_d(\mathbf{z}) = \begin{cases} \dfrac{[ae^{aT_s}(e^{bT_s}-1) - be^{bT_s}(e^{aT_s}-1)]\mathbf{z} + a(e^{bT_s}-1) - b(e^{aT_s}-1)}{ab(a-b)(\mathbf{z}e^{aT_s}-1)(\mathbf{z}e^{bT_s}-1)\mathbf{z}^{n_d}}, & a \neq b, a \neq 0, b \neq 0, \\ \dfrac{[e^{bT_s}(bT_s-1)+1]\mathbf{z} + e^{bT_s} - bT_s - 1}{b^2(\mathbf{z}-1)(\mathbf{z}e^{bT_s}-1)\mathbf{z}^{n_d}}, & a = 0, b \neq 0, \\ \dfrac{[e^{2bT_s} - (bT_s+1)e^{bT_s}]\mathbf{z} + bT_s e^{bT_s} - e^{bT_s} + 1}{b^2(\mathbf{z}e^{bT_s}-1)^2\mathbf{z}^{n_d}}, & a = b \neq 0, \\ \dfrac{T_s^2(\mathbf{z}+1)}{2(\mathbf{z}-1)^2\mathbf{z}^{n_d}}, & a = b = 0. \end{cases} \tag{58}$$

These expressions show that the relative degree of the exactly discretized dynamics is $n_d + 1$. Note that poles of the continuous-time dynamics $G(s)$, which are $s = -a$ and $s = -b$, are mapped to $\mathbf{z} = e^{-aT_s}$ and $\mathbf{z} = e^{-bT_s}$, respectively, to form poles of the discrete-time dynamics $G_d(\mathbf{z})$. However, depending on the values of a and b, the sampling zero of the discrete-time dynamics $G_d(\mathbf{z})$ may lie anywhere between -1 and 0 on the real axis. In addition, in the case where a and b are not both zero, it can be shown that the sampling zero of $G_d(\mathbf{z})$ converges to zero as $T_s \to \infty$ and converges to -1 as $T_s \to 0$.

To demonstrate the performance of adaptive digital PID controller, we consider examples with dynamics given by the second-order plant (57). The properties and values considered are summarized in Table 5. For the last two examples, which are more challenging, the extended adaptive digital PID control described in the next section is used.

TABLE 5 Summary of adaptive digital PID control of second-order plants.

Example	Plant	Remarks
43	Damped oscillator with dead time	$\tau_d = 1, 5, 10$ s
44	Undamped oscillator with dead time	$\tau_d = 1, 1.5, 2$ s
45	Damped rigid body with dead time	$\tau_d = 0.5, 1$ s
46	Undamped rigid body	$\tau_d = 0$

Example 43. *Damped oscillator with dead time*. Consider the plant

$$G(s) = \frac{e^{-\tau_d s}}{2s^2 + 5s + 10}, \tag{59}$$

which represents the dynamics of a damped oscillator with dead time. Let $\tau_d = n_d T_s$, where n_d is a positive integer. It follows from (58) that the discrete-time counterpart of $G(s)$ with sample time $T_s = 0.1$ s is

$$G_d(\mathbf{z}) = \frac{0.0023\mathbf{z} + 0.0021}{(\mathbf{z}^2 - 1.735\mathbf{z} + 0.7788)\mathbf{z}^{n_d}}. \tag{60}$$

Figure 70 shows asymptotic command following and disturbance rejection for $\tau_d = 1, 5, 10$ s (i.e., $n_d = 10, 50, 100$). ◇

Example 44. *Undamped oscillator with dead time*. Consider the plant

$$G(s) = \frac{e^{-\tau_d s}}{2s^2 + 10}, \tag{61}$$

which represents an undamped oscillator with dead time. Let $\tau_d = n_d T_s$, where n_d is a positive integer. It follows from (58) that the discrete-time counterpart of $G(s)$ with sample time $T_s = 0.1$ s is

$$G_d(\mathbf{z}) = \frac{0.00249(\mathbf{z} + 1)}{(\mathbf{z}^2 - 1.95\mathbf{z} + 1)\mathbf{z}^{n_d}}. \tag{62}$$

Figure 71 shows asymptotic command following and disturbance rejection for $\tau_d = 1, 1.5, 2$ s (i.e., $n_d = 10, 15, 20$). ◇

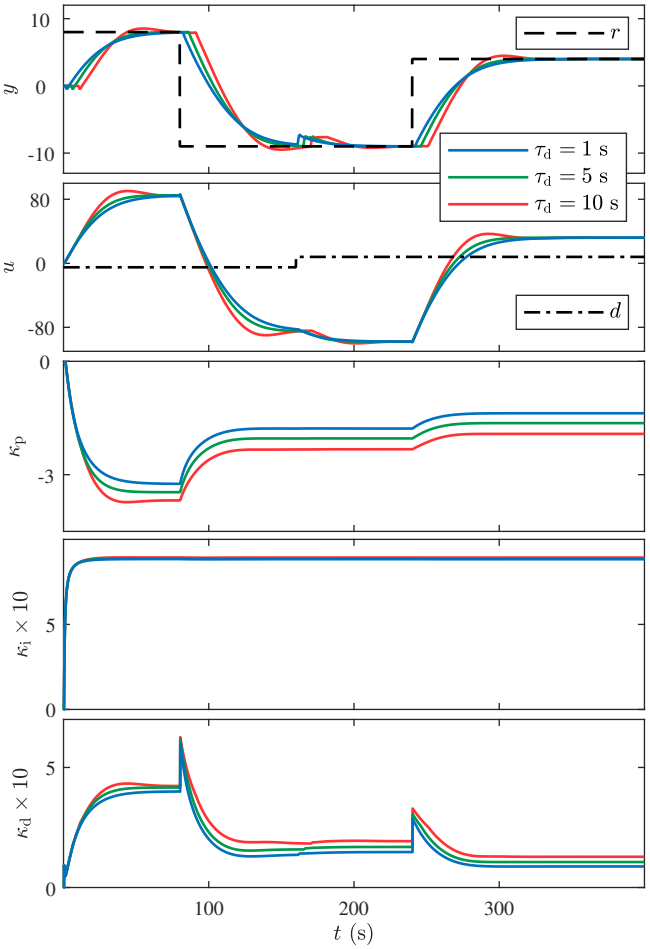

FIGURE 70 Example 43: Command following and disturbance rejection for the damped oscillator with various values of dead time.

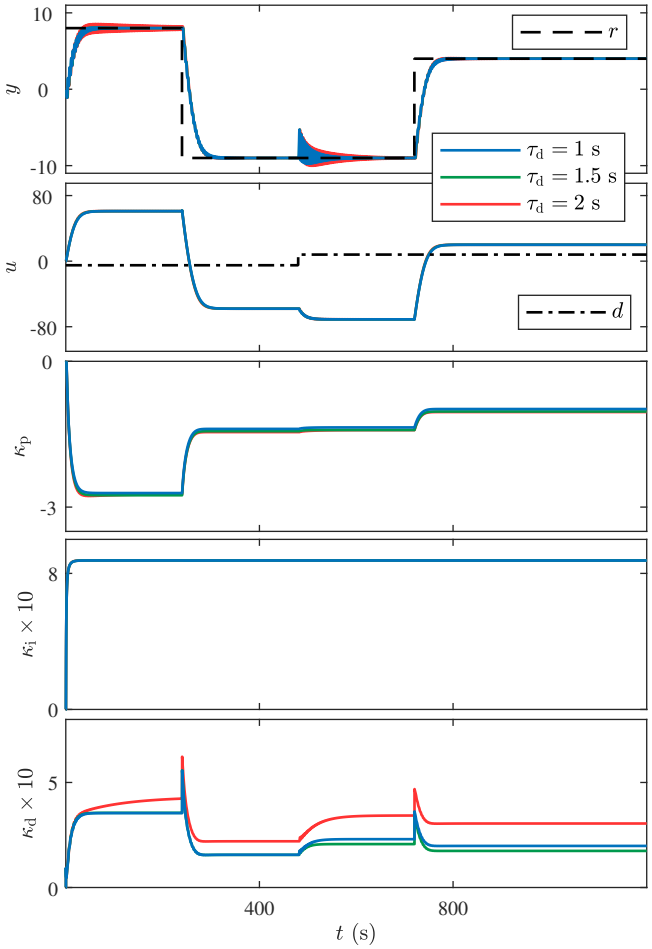

FIGURE 71 Example 44: Command following and disturbance rejection for an undamped oscillator with various values of dead time.

Example 45. *Damped rigid body with dead time*. Consider the plant

$$G(s) = \frac{e^{-\tau_d s}}{2s^2 + 20s}, \tag{63}$$

which represents the dynamics of a damped rigid body with dead time. Let $\tau_d = n_d T_s$, where n_d is a positive integer. It follows from (58) that the discrete-time counterpart of $G(s)$ with sample time $T_s = 0.1$ s is

$$G_d(\mathbf{z}) = \frac{0.0018\mathbf{z} + 0.0013}{(\mathbf{z}^2 - 1.368\mathbf{z} + 0.3679)\mathbf{z}^{n_d}}. \tag{64}$$

Let $G_f(\mathbf{q}) = \mathbf{q}^{-30}$, $p_0 = 0.1$, $\mu = 10^3$, and $\nu = 1$, and assume that the control u saturates at ± 50. The choice of G_f, which is due to the largest dead time, is implemented using the extended adaptive digital PID controller described in the next section. Figure 72 shows asymptotic command following and disturbance rejection for $\tau_d = 0.5, 1, 2$ s (i.e., $n_d = 5, 10, 20$). ◇

Example 46. *Undamped rigid body.* Consider the plant

$$G(s) = \frac{1}{s^2}, \tag{65}$$

which represents the dynamics of an undamped rigid body. Let $\tau_d = 0$. It follows from (58) that the discrete-time counterpart of $G(s)$ with sample time $T_s = 0.1$ s is

$$G_d(\mathbf{z}) = \frac{0.005(\mathbf{z} + 1)}{(\mathbf{z} - 1)^2}. \tag{66}$$

Let $G_f(\mathbf{q}) = \mathbf{q}^{-5}$, $p_0 = 10^3$, $\mu = 10^3$, and $\nu = 20$, and assume that the control u saturates at ± 50. Figure 73 shows asymptotic command following and disturbance rejection. For this example, dead time requires specialized tuning, and thus τ_d is chosen to be zero. ◇

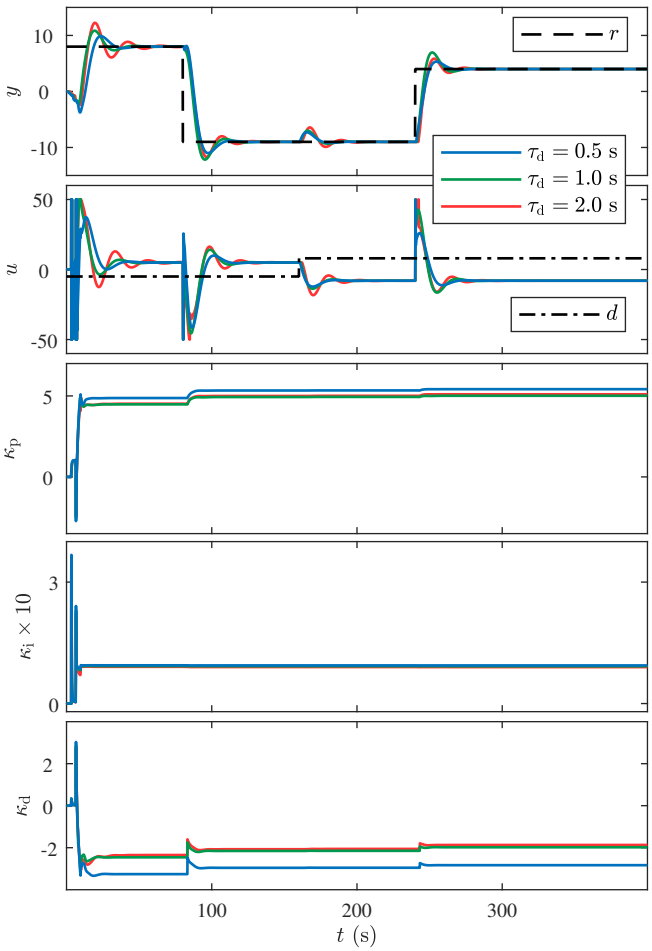

FIGURE 72 Example 45: Command following and disturbance rejection for the damped rigid body.

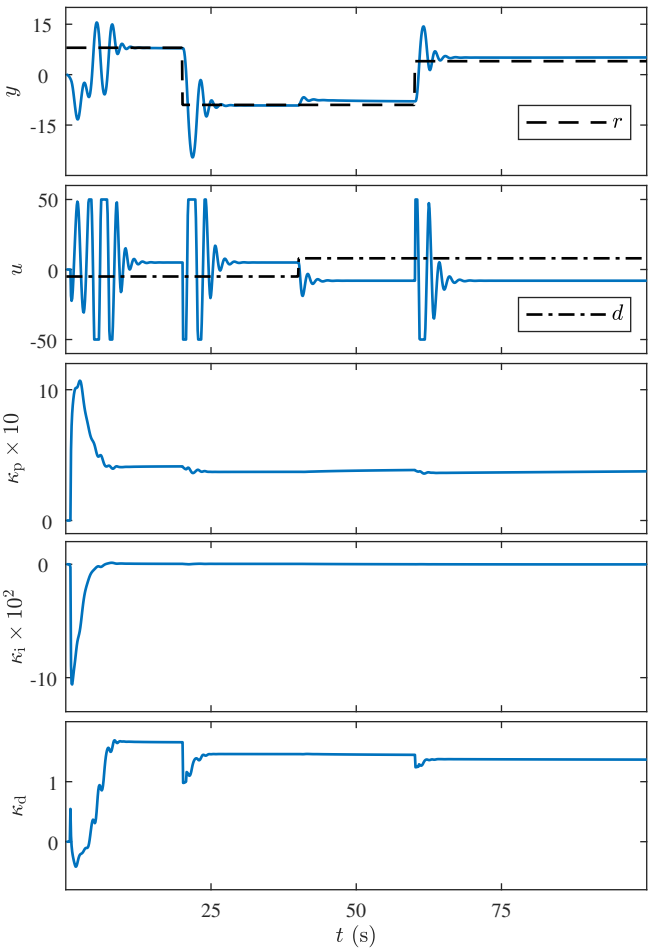

FIGURE 73 Example 46: Command following and disturbance rejection for the undamped rigid body.

13 | EXTENDED ADAPTIVE DIGITAL PID CONTROLLER

The adaptive digital PID controller given by Proposition 2 is a specialization of the adaptive controller given in[53]. A more general adaptive digital PID controller can be obtained by replacing (28) with the retrospective performance variable

$$\hat{z}_k(\theta) \triangleq \bar{e}_k - G_{\mathrm{f}}(\mathbf{q})(u_k - \phi_k\theta), \tag{67}$$

where G_{f} is a filter of order n_{f} in the forward-shift operator $\mathbf{q}$. By choosing G_{f} as

$$G_{\mathrm{f}}(\mathbf{q}) = \sum_{i=1}^{n_{\mathrm{f}}} \frac{N_i}{\mathbf{q}^i}, \tag{68}$$

(67) becomes

$$\hat{z}_k(\theta) = \bar{e}_k - N(U_k - \Phi_k\theta), \tag{69}$$

where

$$N \triangleq \begin{bmatrix} N_1 & \cdots & N_{n_{\mathrm{f}}} \end{bmatrix} \in \mathbb{R}^{1\times n_{\mathrm{f}}}, \quad U_k \triangleq \begin{bmatrix} u_{k-1} \\ \vdots \\ u_{k-n_{\mathrm{f}}} \end{bmatrix} \in \mathbb{R}^{n_{\mathrm{f}}}, \quad \Phi_k \triangleq \begin{bmatrix} \phi_{k-1} \\ \vdots \\ \phi_{k-n_{\mathrm{f}}} \end{bmatrix} \in \mathbb{R}^{n_{\mathrm{f}}\times 3}. \tag{70}$$

With this extension, (31), (30) are replaced by

$$P_{k+1} = P_k - \frac{1}{1 + N\Phi_k P_k \Phi_k^{\mathrm{T}} N^{\mathrm{T}}} P_k \Phi_k^{\mathrm{T}} N^{\mathrm{T}} N \Phi_k P_k, \tag{71}$$

$$\theta_{k+1} = \theta_k + P_{k+1}\Phi_k^{\mathrm{T}} N^{\mathrm{T}}(\bar{e}_k - NU_k + N\Phi_k\theta_k). \tag{72}$$

In the case of a known delay of n_{d} samples, the filter $G_{\mathrm{f}}(\mathbf{q}) = \frac{N_{\mathrm{d}}}{\mathbf{q}^{n_{\mathrm{d}}}}$ may be suitable. Finally, as shown in[53], including the nonminimum-phase zeros of the plant in the numerator of G_{f} helps to avoid unstable pole-zero cancellation.

14 | CONCLUSIONS AND FUTURE RESEARCH

A theoretical challenge arising from this numerical study is the need to prove the Simulation-Based Conjecture (SBC). A reasonable starting point is to assume that $\mathcal{H}$, $\mathcal{W}$, and $\mathcal{L}$ are absent and that r is feasible so that anti-windup is not needed. In this case, it may be possible to construct a discrete-time Lyapunov function to prove asymptotic command following and disturbance rejection. A proof for the case involving $\mathcal{H}$, $\mathcal{W}$, and $\mathcal{L}$ under anti-windup control is likely to be significantly more challenging.

Assuming that SBC is true, an interesting problem is to determine the class of nonmonotonic $\mathcal{H}$, $\mathcal{W}$, and $\mathcal{L}$ under which command following and disturbance rejection can be achieved. In addition, the examples suggest that some of the assumptions, such as (A14), are necessary for asymptotic command following. Furthermore, for higher order dynamics with zeros, the extension of Proposition 2 given in Section 13 provides a starting point for generalizing SBC to larger classes of SISO and MIMO plants.

As another extension of this work, variations of RLS may be useful for improving the performance and robustness of the adaptive digital PID algorithm. For example, variable-rate forgetting is a promising candidate[83,84,85,86,87].

Finally, the numerical examples given in this paper to support SBC provide a systematic numerical exploration of the robustness of the adaptive digital PID controller under a wide range of conditions that may arise in practice. The next step in this research is to experimentally apply this technique to physical systems that are subject to real-world off-nominal conditions.

ACKNOWLEDGMENTS

This research was supported by AFOSR under DDDAS grant FA9550-18-1-0171 and ONR under grants N00014-18-1-2211 and N00014-19-1-2273. The authors thank Mario Santillo for helpful suggestions and Nima Mohseni for providing (58).

References

1. Francis B, Sebakhy O, Wonham W. Synthesis of multivariable regulators: The internal model principle. *Applied Math. Optim.* 1974; 1(1): 64–86.
2. Silva GJ, Datta A, Bhattacharyya SP. New results on the synthesis of PID controllers. *IEEE Trans. Autom. Contr.* 2002; 47(2): 241–252.
3. Ang KH, Chong G, Li Y. PID control system analysis, design, and technology. *IEEE Trans. Contr. Sys. Tech.* 2005; 13(4): 559–576.
4. Yu CC. *Autotuning of PID Controllers: A Relay Feedback Approach*. Springer . 2006.
5. Visioli A. *Practical PID Control*. Springer Science & Business Media . 2006.
6. O'Dwyer A. *Handbook of PI and PID Controller Tuning Rules*. Imperial College Press. third ed. 2009.
7. Vilanova R, Visioli A. *PID Control in the Third Millennium*. Springer . 2012.
8. Díaz-Rodríguez ID, Han S, Bhattacharyya SP. *Analytical Design of PID Controllers*. Springer . 2019.
9. Maxim A, Copot D, Copot C, Ionescu CM. The 5W's for control as part of industry 4.0: Why, what, where, who, and when—A PID and MPC control perspective. *Inventions* 2019; 4(1): 10.
10. Åström KJ, Hägglund T. *PID Controllers: Theory, Design, and Tuning*. ISA Research Triangle Park, NC . 1995.
11. Keel LH, Mitra S, Bhattacharyya SP. Data driven synthesis of three term digital controllers. *SICE J. Contr. Meas. Sys. Integration* 2008; 1(2): 102–110.
12. Mizumoto I, Ikeda D, Hirahata T, Iwai Z. Design of discrete time adaptive PID control systems with parallel feedforward compensator. *Contr. Eng. Practice* 2010; 18(2): 168–176.
13. Cuoghi S, Ntogramatzidis L. Direct and exact methods for the synthesis of discrete-time proportional–integral–derivative controllers. *IET Contr. Theory Appl.* 2013; 7(18): 2164–2171.
14. Seshagiri S, Khalil HK. Robust output feedback regulation of minimum-phase nonlinear systems using conditional integrators. *Automatica* 2005; 41(1): 43–54.
15. Padula F, Visioli A. Tuning rules for optimal PID and fractional-order PID controllers. *J. Process Contr.* 2011; 21(1): 69–81.
16. Zaccarian L, Teel AR. *Modern Anti-Windup Synthesis: Control Augmentation for Actuator Saturation*. Princeton University Press . 2011.
17. Penttinen J, Koivo HN. Multivariable tuning regulators for unknown systems. *Automatica* 1980; 16(4): 393–398.
18. Nishikawa Y, Sannomiya N, Ohta T, Tanaka H. A method for auto-tuning of PID control parameters. *Automatica* 1984; 20(3): 321–332.
19. Gawthrop P. Self-tuning PID controllers: Algorithms and implementation. *IEEE Trans. Autom. Contr.* 1986; 31(3): 201–209.
20. Wellstead P, Zarrop MB. *Self-Tuning Systems: Control and Signal Processing*. John Wiley & Sons, Inc. . 1991.
21. Tomei P. Adaptive PD controller for robot manipulators. *IEEE Trans. Robotics Automation* 1991; 7(4): 565–570.
22. Åström KJ, Hägglund T, Hang CC, Ho WK. Automatic tuning and adaptation for PID controllers-a survey. In: L. Dugard MM, Landau I., eds. *Adaptive Systems in Control and Signal Processing* 1993 (pp. 371–376).
23. Schei TS. Automatic tuning of PID controllers based on transfer function estimation. *Automatica* 1994; 30(12): 1983–1989.
24. Poulin E, Pomerleau A, Desbiens A, Hodouin D. Development and evaluation of an auto-tuning and adaptive PID controller. *Automatica* 1996; 32(1): 71–82.

25. Logemann H, Ryan EP. Time-varying and adaptive integral control of infinite-dimensional regular linear systems with input nonlinearities. *SIAM J. Contr. Optim.* 2000; 38(4): 1120–1144.

26. Benaskeur AR, Desbiens A. Backstepping-based adaptive PID control. *IEE Proc. Contr. Theory Appl.* 2002; 149(1): 54–59.

27. Chang WD, Hwang RC, Hsieh JG. A self-tuning PID control for a class of nonlinear systems based on the Lyapunov approach. *J. Process Contr.* 2002; 12(2): 233–242.

28. Tan K, Huang S, Ferdous R. Robust self-tuning PID controller for nonlinear systems. *J. Process Contr.* 2002; 12(7): 753–761.

29. Parra-Vega V, Arimoto S, Liu YH, Hirzinger G, Akella P. Dynamic sliding PID control for tracking of robot manipulators: Theory and experiments. *IEEE Trans. Robotics Automation* 2003; 19(6): 967–976.

30. Chang WD, Yan JJ. Adaptive robust PID controller design based on a sliding mode for uncertain chaotic systems. *Chaos, Solitons & Fractals* 2005; 26(1): 167 - 175.

31. Monje CA, Vinagre BM, Feliu V, Chen Y. Tuning and auto-tuning of fractional order controllers for industry applications. *Contr. Eng. Practice* 2008; 16(7): 798–812.

32. Leva A, Negro S, Papadopoulos AV. PI/PID autotuning with contextual model parametrisation. *J. Process Contr.* 2010; 20(4): 452–463.

33. Romero JA, Sanchis R, Balaguer P. PI and PID auto-tuning procedure based on simplified single parameter optimization. *J. Process Contr.* 2011; 21(6): 840–851.

34. Boubakir A, Labiod S, Boudjema F. A stable self-tuning proportional-integral-derivative controller for a class of multi-input multi-output nonlinear systems. *J. Vibr. Contr.* 2012; 18(2): 228–239.

35. Shen D, Sun W, Sun Z. Adaptive PID formation control of nonholonomic robots without leader's velocity information. *ISA Trans.* 2014; 53(2): 474–480.

36. Butt WA, Yan L, Amezquita S K. Adaptive integral dynamic surface control of a hypersonic flight vehicle. *Int. J. Sys. Science* 2015; 46(10): 1717–1728.

37. Jung JW, Leu VQ, Do TD, Kim EK, Choi HH. Adaptive PID speed control design for permanent magnet synchronous motor drives. *IEEE Trans. Power Elec.* 2015; 30(2): 900–908.

38. De Keyser R, Muresan CI, Ionescu CM. A novel auto-tuning method for fractional order PI/PD controllers. *ISA Trans.* 2016; 62: 268–275.

39. Song Y, Guo J, Huang X. Smooth neuroadaptive PI tracking control of nonlinear systems with unknown and nonsmooth actuation characteristics. *IEEE Trans. Neural Networks Learning Sys.* 2017; 28(9): 2183–2195.

40. Mercader P, Åström KJ, Banos A, Hägglund T. Robust PID design based on QFT and convex–concave optimization. *IEEE Trans. Contr. Sys. Tech.* 2017; 25(2): 441–452.

41. Berner J, Soltesz K, Hägglund T, Åström KJ. An experimental comparison of PID autotuners. *Contr. Eng. Practice* 2018; 73: 124–133.

42. Habibi H, Nohooji HR, Howard I. Adaptive PID control of wind turbines for power regulation with unknown control direction and actuator faults. *IEEE Access* 2018; 6: 37464–37479.

43. De Keyser R, Muresan CI, Ionescu CM. Universal direct tuner for loop control in industry. *IEEE Access* 2019; 7: 81308–81320.

44. Åström KJ, Wittenmark B. On self-tuning regulators. *Automatica* 1973; 9(2): 185–199.

45. Clarke DW, Gawthrop PJ. Self-tuning controller. *Proc. IEE* 1975; 122(9): 929–934.

46. Isermann R. On advanced methods of process computer control for industrial processes. *IFAC Proc. Vol.* 1978; 11(1): 411–421.

47. Wellstead PE, Prager D, Zanker P. Pole assignment self-tuning regulator. *Proc. IEE* 1979; 126(8): 781–787.

48. Clarke DW. Self-tuning control of nonminimum-phase systems. *Automatica* 1984; 20(5): 501–517.

49. Radke F, Isermann R. A parameter-adaptive PID-controller with stepwise parameter optimization. *Automatica* 1987; 23(4): 449–457.

50. Chen J, Huang TC. Applying neural networks to on-line updated PID controllers for nonlinear process control. *J. Process Contr.* 2004; 14(2): 211–230.

51. Kurokawa R, Sato T, Vilanova R, Konishi Y. Closed-loop Data-driven Trade-off PID Control Design. *IFAC-PapersOnLine* 2018; 51(4): 244–249.

52. Formentin S, Campi MC, Carè A, Savaresi SM. Deterministic continuous-time Virtual Reference Feedback Tuning (VRFT) with application to PID design. *Sys. Contr. Lett.* 2019; 127: 25–34.

53. Rahman Y, Xie A, Bernstein DS. Retrospective cost adaptive control: pole placement, frequency response, and connections with LQG control. *IEEE Contr. Sys. Mag.* 2017; 37: 28-69.

54. Bloemen H, Van Den Boom T, Verbruggen H. Model-based predictive control for Hammerstein Wiener systems. *Int. J. Contr.* 2001; 74(5): 482–495.

55. O'Dwyer A. PI and PID controller tuning rules for time delay processes: a summary. Part 2: PID controller tuning rules. *Dublin Institute of Technology* 1999.

56. Åström KJ, Hägglund T. Revisiting the Ziegler–Nichols step response method for PID control. *J. Process Contr.* 2004; 14(6): 635–650.

57. Cogan B, Paor dAM, Quinn A. PI control of first-order lag plus time-delay plants: root locus design for optimal stability. *Trans. Instit. Measure. Contr.* 2009; 31(5): 365–379.

58. Gherfi K, Charef A, Abbassi HA. Proportional integral-fractional filter controller design for first order lag plus time delay system. *Int. J. Sys. Sci.* 2018: 1–20.

59. Luyben WL. Effect of derivative algorithm and tuning selection on the PID control of dead-time processes. *Indust. & Eng. Chem. Research* 2001; 40(16): 3605–3611.

60. Xiang G, Yang Y, Yang Q. Twice optimum control for a kind of first order systems with dead-time. *Information and Contr.* 1995; 4.

61. Shinskey F. PID-deadtime control of distributed processes. *Contr. Eng. Practice* 2001; 9(11): 1177–1183.

62. Roy A, Iqbal K. PID controller tuning for the first-order-plus-dead-time process model via Hermite-Biehler theorem. *ISA Trans.* 2005; 44(3): 363–378.

63. Normey-Rico J, Camacho E. *Control of Dead-Time Processes*. Springer Science & Business Media . 2007.

64. Yuan J, Chen Y, Fei S. Analysis of actuator rate limit effects on first-order plus time-delay systems under fractional-order proportional-integral control. *IFAC-PapersOnLine* 2018; 51(4): 37–42.

65. Onat C. A new design method for PI–PD control of unstable processes with dead time. *ISA Trans.* 2019; 84: 69–81.

66. Da-Silva LR, Flesch RCC, Normey-Rico JE. Controlling industrial dead-time systems: When to use a PID or an advanced controller. *ISA Trans.* 2019.

67. Sato T, Hayashi I, Horibe Y, Vilanova R, Konishi Y. Optimal robust PID control for first-and second-order plus dead-time processes. *Applied Sciences* 2019; 9(9): 1934.

68. Kurokawa R, Sato T, Vilanova R, Konishi Y. Discrete-time first-order plus dead-time model-reference trade-off PID control design. *Applied Sciences* 2019; 9(16): 3220.

69. Birs I, Muresan C, Nascu I, Ionescu C. A survey of recent advances in fractional order control for time delay systems. *IEEE Access* 2019; 7: 30951–30965.

70. Astrom KJ, Hang CC, Lim B. A new Smith predictor for controlling a process with an integrator and long dead-time. *IEEE Trans. Autom. Contr.* 1994; 39(2): 343–345.

71. Åström KJ, Hägglund T. The future of PID control. *Contr. Eng. Practice* 2001; 9(11): 1163–1175.

72. Tan F, Li HX, Shen P. Smith predictor-based multiple periodic disturbance compensation for long dead-time processes. *Int. J. Contr.* 2018; 91(5): 999–1010.

73. Porter B, Jones A. Genetic tuning of digital PID controllers. *Electronics Lett.* 1992; 28(9): 843–844.

74. Keel LH, Rego J, Bhattacharyya SP. A new approach to digital PID controller design. *IEEE Trans. Autom. Contr.* 2003; 48(4): 687–692.

75. Åström KJ, Wittenmark B. *Computer-Controlled Systems: Theory and Design, Third Edition*. Dover Publications . 2013.

76. Jury EI. *Inners and Stability of Dynamic Systems*. Kreiger . 1982.

77. Franklin G, Powell J, Workman M. *Digital Control of Dynamic Systems*. Addison Wesley Longman . 1998.

78. Islam SAU, Bernstein DS. Recursive least squares for real-time implementation. *IEEE Contr. Sys. Mag.* 2019; 39.

79. Ljung L, Soderstrom T. *Theory and Practice of Recursive Identification*. MIT Press . 1985.

80. Lennartson B, Soderstrom T. Investigation of the intersample variance in sampled-data control. *Int. J. Control* 1989; 50(5): 1587–1602.

81. Shats S, Shaked U. Exact discrete-time modelling of linear analogue systems. *Int. J. Control* 1989; 49(1): 145–160.

82. Osburn SL, Bernstein DS. An exact treatment of the achievable closed-loop H_2 performance of sampled-data controllers: from continuous-time to open-loop. *Proc. Conf. Dec. Contr.* 1993: 325–330.

83. Fortescue T, Kershenbaum L, Ydstie B. Implementation of self-tuning regulators with variable forgetting factors. *Automatica* 1981; 17(6): 831 – 835.

84. Canetti RM, Espana MD. Convergence analysis of the least-squares identification algorithm with a variable forgetting factor for time-varying linear systems. *Automatica* 1989; 25(4): 609 – 612.

85. Dayal BS, MacGregor JF. Recursive exponentially weighted PLS and its applications to adaptive control and prediction. *J. Process Contr.* 1997; 7(3): 169 – 179.

86. Leung SH, So CF. Gradient-based variable forgetting factor RLS algorithm in time-varying environments. *IEEE Trans. Sig. Proc.* 2005; 53(8): 3141–3150.

87. Paleologu C, Benesty J, Ciochina S. A robust variable forgetting factor recursive least-squares algorithm for system identification. *IEEE Sig. Proc. Let.* 2008; 15: 597–600.